Nanofiltration and hybrid sorption : ultrafiltration processes for improving water quality

Neus Pagès Hernando

DOCTORAL THESIS

Nanofiltration and Hybrid Sorption – Ultrafiltration Processes for Improving Water Quality

DOCTORAT EN ENGINYERIA DE PROCESSOS QUÍMICS

Universitat Politècnica de Catalunya, BarcelonaTech UPC

Author:

Neus Pagès Hernando

Thesis supervisors:

José Luis Cortina Pallás

Oriol Gibert Agulló

Barcelona, July 2016

Submitted to reviewers on June 2016
Final dissertation on July 2016

A la meva Família

Abstract

Reliable access to freshwater is one of the fundamental pillars for our society. Freshwater scarcity has become a major concern in many arid and semi-arid countries worldwide to such an extent that water supply for meeting current and future demands is one of our society challenges. The increasing of domestic and industrial discharges leads to increased salinity and the presence of new pollutants in freshwater sources. Different water treatment technologies including adsorption, coagulation, flotation, ozonation, ion-exchange, and pressure-driven membrane processes such as microfiltration, ultrafiltration (UF), nanofiltration (NF) and reverse osmosis (RO) have been thoroughly investigated for surface water and groundwater treatment. Nowadays, the availability to produce high quality drinking and industrial waters by removing target species is very important challenge.

NF is being promoted as a new technological solution to remove both major and minor organic and inorganic compounds from surface water. Solute transport through NF membranes is a complex process that depends on the micro hydrodynamic and interfacial events occurring at the membrane surface and within the membrane structure. Membrane structure is still one of the main challenges to be solved as some authors consider it permanent in time (e.g. nanopores structure) while others consider only a free volume structure with no permanent structure (non-pores structure). The main purpose of such models is to incorporate as much physical realism of the membrane process as possible in order to better match measurable quantities to adjustable model parameters.

NOM affects significantly many aspects of water treatment, including the performance of the unit processes, application of water treatment chemicals and biological stability of water. The fouling of membranes and decline of flux are the major problems associated to membrane techniques. Hybrid membrane processes are one potential solution. The magnetic IEX process presents a very promising method to reduce DBP formation when used upstream of chlorination.

The main objective of this thesis is to study the possible integration of separation processes based on pressure-driven membrane technologies such as NF and hybrid technologies based on IEX resins and UF membrane to reduce salinity, hardness and inorganic pollutants (NO_3^-, SO_4^{2-}) in surface and ground brackish waters and to reduce the presence of DBP precursors (DOM and Br^-) in order to improve water quality and comply with increasingly demanding regulations.

For the application of NF to reduce salinity, hardness and inorganic pollutants in brackish waters the work was devoted to characterize and identify the mechanisms of rejection of ionic species under different solution composition modifying the nature of the dominant salts. The aim of this work was to determine the reliability of the data obtained using flat sheet (FS) lab-scale configuration when NF membranes are implemented at industrial scale level using spiral wound (SW) configuration. Ions rejections in salt mixtures with the two configurations types were analysed, modelled, evaluated and compared. In both cases, the operation was carried out in cross-flow mode and with recirculation of permeate and concentrate streams into the feed tank.

Synthetic water solutions representative of surface water influenced by industrial and mining drainage (KCl, $MgCl_2$, KI, NaBr, etc) and wastewater treatment discharges of NH_4^+, NO_3^-, SO_4^{2-} were used. The ion membrane permeabilities of both NF membranes with respect to several ions (Na^+, K^+, Cl^-, Ca^{2+}, Mg^{2+}, SO_4^{2-}, NO_3^-, NH_4^+, I^- and Br^-) were determined. The different synthetic aqueous solutions were used as feed solution for the experiments. All of them were based on a dominant salt (NaCl, $MgSO_4$, Na_2SO_4, $MgCl_2$) mixed with trace ions (Na^+, Cl^-, Mg^{2+}, SO_4^{2-}, Br^-, NO_3^-, I^-, NH_4^+, K^+). The ions studied are of great interest in brackish water purification, because they are found in large quantity (Na^+, Cl^-, Mg^{2+}, SO_4^{2-}), they are precursors of THM (Br^-, I^-) or they are characteristic ions present in rivers due to the influence of agriculture and industrial discharges (NO_3^-, K^+, NH_4^+).

Hybrid technologies based on IEX resins and UF membrane to reduce salinity, hardness and inorganic pollutants in brackish waters as well as DBP precursors (DOM and Br^-) from surface brackish waters has been performed. The main objective has been to study the capacity of MIEX resin to remove targeted pollutants when used in combination with a UF membrane. In this study, the efficiency of a hybrid MIEX-UF bench-pilot (magnetic IEX resin coupled to a UF capillary membrane) to remove disinfection precursors (DOC and Br^-) and inorganic anions (SO_4^{2-} and NO_3^-) has been evaluated. During the operating time the hybrid set-up was continuously fed with sand-filtered water from a DWTP treating surface water and, occasionally, groundwater. The membrane system operated in an inside-out flow filtration mode at

variable TMP for the two different MIEX concentrations evaluated (1 and 3 ml/l). Chemical enhanced backwash cycles were regularly performed to control membrane resistance due to fouling.

The hybrid process combining magnetic IEX resins and ultrafiltration could be a promising technology after conventional clarification because it could increase the quality of water in terms of DOC and inorganic species. The use of MIEX resin allowed a rapid sorption of DOC in less than 10 min with about 40 and 60% removal yields on DOC for sand-clarified water. The reduction of DOC, for doses higher than 6 ml/l provides TOC values below 2 mg C/l. Such values are not typically achieved by conventional water potabilization treatments, using coagulation/flocculation targeting NOM and colour and particle removal. Then, for systems where coagulation/flocculation is not sufficient to achieve DOM values lower than 2 mg C/l, which is the reference guideline in the EU, the use of MIEX could provide a new solution to achieve this standard as it has been demonstrated.

The capacity of MIEX resin to reduce the levels of non-desired ions in drinking water as SO_4^{2-}, NO_3^- and Br^- under partial saturation is of mention (values from 40 to 75%) and the process implementation should consider operation criteria to avoid resin capacity saturation. If objective of the application to surface water of low quality should be not only the reduction of DOC content and the reduction of the nitrate, sulphate and bromide concentrations it should be avoided to reach the MIEX saturation on organic matter. The removal factor measured for bromide, nitrate, sulphate and TOC are similar to those obtained by EDR.

Glossary

General terms

A_{FS}	Effective membrane area of the flat sheet module
A_{SW}	Effective membrane area of the spiral wound module
A_c	Effective membrane area of the capillary module
AFM	Atomic Force Microscopy
BF	Back-Flushing
BW	Backwash
$C_E^i(t)$	concentration of the solute 'i' in the influent
$C_P^i(t)$	concentration of the solute 'i' in the permeate
CC	Chemical Cleaning
CEB	Chemical Enhanced Backwash
cfv	Cross-flow velocity
CUADLL	Water Users Community
DBP	Disinfection By-Product
DOC	Dissolved Organic Carbon
DOM	Dissolved Organic Matter
DSP-DE model	Donnan-Steric-Pore-Dielectric model
DWTP	Drinking Water Treatment Plant
EC	European Community
EDR	Electrodialysis Reversal
EPA	Environmental Protection Agency
FS	Flat Sheet

HA	Humic Acid
HAA	Haloacetic Acid
HC	Hydraulic Cleaning
HPSEC	High Performance Size Exclusion Chromatography
IC	Ionic Chromatography
IEX	Ion-Exchange
K_{v_0}	Initial Permeability
K_v	Permeability at any time
ΔK_v	Loss of Permeability
LMW	Low Molecular Weight
MCLs	Maximum Contaminant Levels
MD	Membrane Distillation
MF	Microfiltration
MIEX resin	Magnetic Ion-Exchange resin
$\frac{dm^i(t)}{dt}$	Mass flux of solute 'i' accumulated on the system at time t
$m^i_{MIEX}(t)$	Mass of solute 'i' accumulated on MIEX at time t
m_p	Permeate mass
MPD	Meta-phenylenediamine
MWCO	Molecular Weight Cut-Off
NF	Nanofiltration
NMR	Nuclear Magnetic Resonance
NOM	Natural Organic Matter
NP equation	Nernst-Planck equation
PA	Polyamide
$Q_E(t)$	flow-rate of the influent
$Q_P(t)$	Flow-rate of the permeate
$q^i_{MIEX}(t)$	Uptake of solute 'i' at time t
RAIS	Risk Assessment Information System
RO	Reverse Osmosis
R_{tot}	Total membrane resistance
SD model	Solution-Diffusion model
SEDE mechanisms	Steric, Electric and Dielectric mechanisms
SEDF model	Solution-Electro-Diffusion-Film model
SEM	Scanning Electron Microscopy
SJD-DWTP	Sant Joan Despí Drinking Water Potabilization Plant
SK model	Spiegler–Kedem model
SUVA	Specific UV Absorbance
SW	Spiral Wound
SWI	Seawater Intrusion Barrier
TDS	Total Dissolved Solids
TEM	Transmission Electron Microscopy
TFC	Thin-Film-Composite
THM	Trihalomethane
TMC	Trimesoyl Chloride

TMP	Trans-membrane pressure
TOC	Total Organic Carbon
t_p	Permeate collecting time
UF	Ultrafiltration
UNO	United Nations Organization
V_p	Permeate volume
WHO	World Health Organization

SEDF model nomenclature

b	$\equiv \frac{Z_{t^\pm} \cdot (P_+ - P_-)}{Z_+ P_+ - Z_- P_-}$, trans-membrane parameter
c_i	ion concentration in the feed solution (mol m^{-3})
$c_i^{(m)}$	ion concentration at the membrane surface (mol m^{-3})
$c_i^{"}$	ion concentration in the permeate (mol m^{-3})
c_s'	concentration of dominant salt in the feed solution (mol m^{-3})
$c_s^{(m)}$	concentration of dominant salt at the membrane surface (mol m^{-3})
$c_s^{"}$	concentration of dominant salt in the permeate (mol m^{-3})
c_t'	concentration of trace ion in the feed solution (mol m^{-3})
$c_t^{(m)}$	concentration of trace ion at the membrane surface (mol m^{-3})
$c_t^{"}$	concentration of trace ion in the permeate (mol m^{-3})
D_i	solute effective diffusion coefficient (m^2 s^{-1})
$D_s^{(\delta)}$	diffusion coefficient of dominant salt in the concentration-polarization layer (m^2 s^{-1})
$D_\pm^{(\delta)}$	diffusion coefficients to single ions of dominant salt in the concentration-polarization layer (m^2 s^{-1})
$D_{t^\pm}^{(\delta)}$	diffusion coefficients of trace ions in the concentration-polarization layer (m^2 s^{-1})
F	Faraday constant (96485.33 $C \cdot mol^{-1}$)
f_s	reciprocal trans-membrane transfer of dominant salt
f_t	reciprocal trans-membrane transfer of trace ion
j_i	ion trans-membrane flux (mol m^{-2} s^{-1})
J_v	trans-membrane flux (m s^{-1})
k_i	ion mass transfer coefficient
k_B	$\equiv \frac{R}{N_A}$, Boltzmann constant ($1.38 \cdot 10^{-23}$ $J \cdot K^{-1}$)
K	$\equiv \frac{P_s}{P_{t^\pm}}$, ratio of effective diffusion coefficients of dominant salt and trace solute in the membrane
l	membrane thickness (m)
L_i	proportionality coefficient
N_A	Avogadro's number ($6.02 \cdot 10^{23}$ mol^{-1})
P_i	ion membrane permeabilities
P_s	membrane permeability to the dominant salt (m s^{-1})

$P_s^{(\delta)}$	concentration-polarization layer permeability (m s^{-1})
$P_{\pm}$	membrane permeabilities to single ions of dominant salt (m s^{-1})
$P_{t^{\pm}}$	membrane permeability to trace ions (m s^{-1})
Pe_s	Péclet number of dominant salt
$Pe_{t^{\pm}}$	Péclet number of trace ion
r_s	Stokes radii (nm)
R	gas constant (8.314 J K^{-1}·mol^{-1})
R_s^{int}	intrinsic rejection of dominant salt
R_t^{int}	intrinsic rejection of trace ion
R_s^{obs}	observable rejection of dominant salt
R_t^{obs}	observable rejection of trace ion
T	temperature (K)
Z_i	ion charge
$Z_{\pm}$	charges to single ions of dominant salt
$Z_{t^{\pm}}$	charge of trace ion

Greek letters

δ	estimated value of concentration-polarization layer thickness (m)
λ_s^o	limiting equivalent conductivity of dominant salt (m^2 Ω^{-1} eq^{-1})
$\lambda_{\pm}^o$	ion limiting equivalent conductivity (m^2 Ω^{-1} eq^{-1})
μ	dynamic viscosity (Pa s)
μ_i	solute electrochemical potential (J mol^{-1})
φ	electrostatic potential (V)

Table of contents

List of Figures

List of Tables

Chapter 1
Introduction

Reliable access to freshwater is one of the fundamental pillars for our society. However, only a reduced fraction of planet water is directly readily available as freshwater. The shortage of potable water, as consequence of population growth, current consumption patterns and climate changing, will be a major problem in the coming decades and will have the same social impact as that of increased energy prices (Meerganz von Medeazza and Moreau, 2007; Shrivastava et al., 2008).

According to the World Bank, 9% of the world population (663 million people in 2016) lack from direct access to potable water and 2.5 billion people are supplied with untreated water (IPCC, 2014). The United Nations Organization (UNO) has warned that 60% of the Earth's population will suffer from water scarcity in 2025 if the water consumption continues growing twice as much as the population. Water availability and quality is a globally critical issue impacting human health. Improving access to clean drinking water is integrally linked to achieving all of the Millennium Development Goals (Oki and Kanae, 2006).

1.1. Water scarcity and water quality threats: salinity and natural organic matter (NOM)

Currently, freshwater scarcity has become a major concern in many arid and semi-arid countries worldwide to such an extent that water supply for meeting current and future demands is one of the main challenges (Fritzmann et al., 2007). Therefore, classic

solutions such as water conservation and water transfer or dam construction are not sufficient to cope with increasing demand any longer. Hence, one possible solution is the potabilization of the non-common and low quality water resources. In addition, the increasing of domestic and industrial discharges leads to increased salinity and the presence of new pollutants in freshwater sources. Consequently the development of efficient treatment processes is a major concern. In order to achieve the goals of Drinking Water Guidelines and Standards the treatment of low quality water sources demands alternative water treatment processes. All these effects provoke an increase of the complexity and the cost of the treatments while water quality deteriorates (Alghoul et al., 2009).

1.1.1. Salinity threats in groundwater quality

Groundwater is by far the most abundant and readily available source of freshwater followed by lakes, reservoirs, rivers and wetlands (Shiklomanov, 1993). When used for drinking water, fresh groundwater sources are preferred to other readily freshwater sources because of the absence of pathogens. However, regions with sustainable fresh groundwater resources are shrinking, throughout the world. Salinization of freshwater due to intrusion of the saline water is one of the main problems of freshwater overdrafts (Figure 1.1). Critical situation are the cases of countries such as The Netherlands, which are lying below the sea level, and where over 100 pumping stations are closed due to intruded brackish water and where it is expected that over 20% of remaining wells will suffer from salinization in coming years (Grakist et al., 2002). Negative environmental impacts of over-pumping the freshwater are a worldwide problem (e.g. Israel, United States or Spain among others (Voutchkov, 2011)).

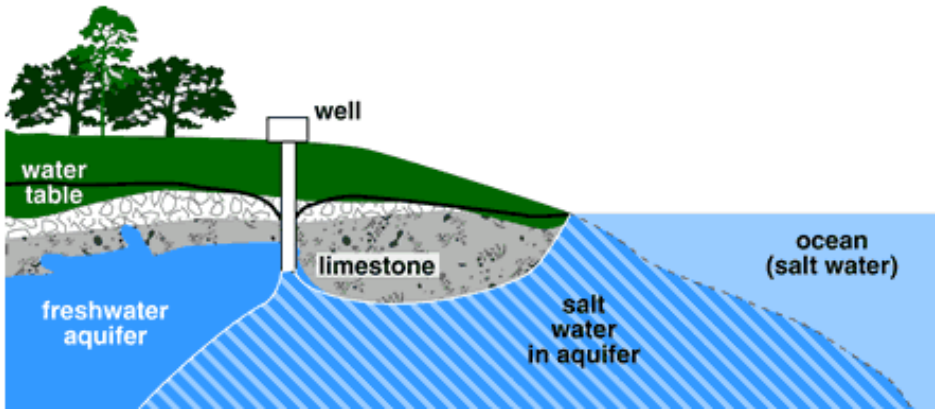

Figure 1.1. Salt water intrusion as the result of climate changing is one of the reasons of using brackish water as a new source for producing drinking water (source of picture: St. Johns River Water Management District, 2008)

In the case of Spain, one example of interest is The Llobregat Delta, located at the SW end of the densely populated area of Barcelona Metropolitan Area (NE, Spain). This area, formerly devoted to agriculture, now supports important industrial settlements

and city suburbs. The high water demand brings about an intense and continuous exploitation of surface and groundwater resources. The intensive groundwater exploitation until the late 1970s caused a significant advance of the saline intrusion interface. Saline intrusion still affects large areas of the delta. At present, the Catalonian Water Agency (ACA) together with the Water Users Community (CUADLL) are fighting to correct this situation by developing a groundwater management programme to recover groundwater quality and quantity while trying to guarantee sustainable pumping rates (Vázquez-Suñé et al., 2006).

Different actions such as reducing the pumping rates in each management area and the construction of a seawater intrusion barrier (SWI) and recharging ponds to artificially increase the recharge were implemented. Also, the use of artificial replenishment of groundwater by infiltration wells and infiltration through a dense network of ditches and canals (Rietveld et al., 2011) is used for years in The Netherlands as a solution for freshwater declination. Although the artificial groundwater recharge is an excellent alternative to natural refilling and is beneficial to environment, it has disadvantages such as considerable footprint and inapplicability of being used in the arid and semi-arid area due to high evaporation rate and operational cost. Brackish groundwater is referred as an appealing alternative to fresh groundwater for future due to its low content of suspended fines, organic pollutants and pathogenic micro-organisms (Wolthek et al., 2013). Brackish groundwater is theoretically free of xenobiotic and endocrine disruptors substances when compared to fresh groundwater due to its age and the fact that it is not affected by human activities (Olsthoorn, 2008; Stuyfzand and Raat, 2010).

Not only seawater intrusion is affecting groundwater quality, also surface water drainage from mining tailings and industrial wastes and from agriculture drainage are having direct influence. Groundwater contamination by inorganic nitrogen (in the form of NO_3^-, NO_2^- and/or NH_4^+) constitutes a major environmental concern worldwide. It usually originates from anthropogenic sources, mainly as a result of the intensive application of fertilizers and animal manure to agricultural land. The European "Directive concerning the protection of waters against pollution caused by nitrates from agricultural sources" (Nitrate Directive 91/676/EEC) emphasizes the importance of preventing pollution and decreasing existing nitrate concentration in groundwater to values under the EU limit of 50 mg/l NO_3^- (Gibert et al., 2008) and the World Health Organization (WHO) suggested a guideline maximum value of 45 mg/l. Higher concentrations of nitrate not only affect the human being but also affect the marine life.

Throughout recent decades, the wastewater treatment industry has identified the discharge of nutrients, including phosphate, and nitrate into waterways as a risk to natural environments due to the serious effects of eutrophication (Blaney et al., 2007; Wang et al., 2014). Ammonium (NH_4^+), which mainly derives from human and animal excreta, is present in water combined with unfavourable microbiological activity that is a source of contamination in sewers or animal farming sources. Currently, large amounts of ammonium are generated and released from industrial processes such as

chemical fertilizers production, agriculture, oil refining and petrochemistry, metallurgy, and wastewater treatment. Nitrite (NO_2^-) and nitrate (NO_3^-) are produced by ammonium oxidation processes, or as a consequence of using nitrogen fertilizers (Bódalo et al., 2005).

However, in areas with severe scarcity scenarios as the Mediterranean region the reduction of the river flow-rates is not accompanied by the reduction of the discharges from wastewater treatment plants or the reduction of the drainage from mining and industrial tailings and the groundwater quality decreases. An example for this scenario in Spain is the Llobregat River with a low and seasonal dependent flow-rate. It presents quality problems such as high salinity, stemming from the brines associated with the mining activities on the salt deposits located in the upper part of the basin, with a significant presence of Na^+, Ca^{2+}, K^+, Ba^{2+}, Sr^{2+}, Cl^- SO_4^{2-}, Br^-, F^- and I^-.

The potash mine industry has been exploiting potassium chloride since 1920s generating important volumes of salt and clays rejection tailing from the mineral flotation processing stages. The drainage of these areas contributes to increase the saline content of the pristine headwaters. As a result, not only the surface water shows large concentrations of those parameters and also groundwater at the upper part of the basin is affected with high salinity contents (López-Roldán et al., 2016).

As a consequence of the described scenarios, water quality of the natural bodies is affected by the incorporation of major, minor and trace compounds from both natural geological origin and external anthropogenic agents such as industrial and urban wastewater discharges that can be harmful to human health according to their concentrations in water. The main associated species with this increase of salinity, due to the described problems (e.g. seawater intrusion, industrial discharges from mining or industries, agriculture and farming drainage) are sodium, ammonium, magnesium and calcium, sulphate, nitrate, bicarbonate and halide. According to WHO and EC a freshwater threshold of 250 mg/l for chloride is defined whereas the U.S Environmental Protection Agency (EPA) has secondary standards of 250 mg/l chloride and 500 mg/l of total dissolved solids (TDS). The consumption of water exceeding the recommended concentration cause several disorders. For example sodium and magnesium sulphates levels above 250 mg/l in drinking water may produce a laxative effect. Excess sodium may affect those restricted to low sodium diets and pregnant women suffering from toxaemia (El-Manharawy and Hafez, 2001).

Moreover, organoleptic properties must be taken into consideration: high levels of TDS may cause an objectionable taste to drinking water. The levels of the reported inorganic compounds in drinking water are rarely high enough to cause acute health effects but, in some cases, they can be associated with chronic illnesses. Health risk organizations set the different thresholds according to the risks and the available technologies to avoid them. For instance, major compounds in brackish water sources such as sulphate and carbonate, as well as alkaline earths (Ca^{2+}, Mg^{2+}, Ba^{2+}) could be present in considerable concentrations. Hard water is considered by WHO as not harmful for human health as there is not any convincing evidence that water hardness

causes adverse health effects in humans. However, some of these compounds such as calcium and magnesium have a defined threshold, because studies have shown a weak inverse relationship between water hardness and cardiovascular disease in men (Marque et al., 2003). Sulphate may give water a bitter taste and have a laxative effect and increasing its intake is a likely causative factor in certain respiratory problems (Bódalo et al., 2004) and a maximum concentration of 500 mg/l is recommended (WHO, 2008).

The use of brackish groundwater is especially interesting for inland and coastal areas with seawater intrusion problems, as it provides an added value. Its utilization protects unaffected groundwater and reduces the risk of brackish water intrusion on the freshwater bodies. The latter becomes very attractive considering the current trends of climate change predictions where increase of seawater level as the consequence of climate changing causes seawater intrusion leakage of seawater as the final result (Kooiman et al., 2004; Post, 2004).

However, brackish groundwater is not directly used as consumable for human, industrial or agriculture uses and needs to be treated. Agriculture, especially at areas of highly intensive greenhouses demands (e.g. Spain, Australia, Israel, The Netherlands) large amounts of freshwater with the minimum salt content are needed (Yermiyahu et al., 2007). Water with the minimum salt content is favourable to greenhouses because it does not damage the soil, stunt the plant growth, and the environment. The Netherlands with an area of about 9500 ha of greenhouses was one of the biggest international exporters of greenhouses products in 2014 and in the case of Spain about 53800 ha have been reported (Martínez Beltrán and Koo-Oshima, 2006).

Treatment of brackish water can be done by desalination and, among the desalination processes, membrane processes are becoming more attractive through cheaper material and system development. Reverse osmosis (RO), Electrodialysis Reversal (EDR), Nanofiltration (NF) and Ion-Exchange (IEX) resins are commonly used as the main technologies of producing low salinity content from saline water. This makes brackish groundwater the perfect feed water for membrane desalination technologies (e.g. RO, EDR, NF, membrane distillation (MD)) considering the operation and fouling prevention (Pérez-González et al., 2012).

1.1.2. Organic matter threats in surface waters quality

Natural organic matter (NOM) is defined as a complex matrix of organic materials present in all natural waters. NOM is often found in soil and all water resources, especially in surface water, for example in rivers and lakes. As a result of the interactions between the hydrological, the biosphere and geosphere cycles, the water sources used for drinking water purposes generally contain NOM. Thus the amount, character and properties of NOM differ considerably in waters of different origins and depend on the biogeochemical cycles of the surrounding environments (Fabris et al., 2008). NOM contains a variety of compounds that also have a variety in size, chemical composition, structure and functional groups depending on the origin and

age of the material, such as humic substances, hydrophobic compounds, hydrophilic compounds, small organic acids, aromatic compounds, proteins and aminosugars (Chen et al., 2007; Dong et al., 2007; Her et al., 2008; Kitis et al., 2001).

NOM changes seasonally both quantitatively and qualitatively. Moreover, the range of organic components of NOM might vary also on the same location seasonally (Sharp et al., 2006a, 2006b; Smith and Kamal, 2009), due to for instance rainfall event, snowmelt runoff, floods or droughts. Floods and droughts are the main impacts of climate change on water availability and quality. It has been suggested that these changes might be the reason for an increase in the total amount of NOM (Delpla et al., 2009; Smith, 2001), which has been noted to occur on several areas around the world during the past 20 years (Evans et al., 2005; Korth et al., 2004; Worrall and Burt, 2007). Besides the quantity of NOM, the quality of NOM has been noted to alter as well, since other important characteristics of NOM, e.g. specific UV absorbance (SUVA), have also increased (Eikebrokk et al., 2004). The changes in NOM quantity and quality have a significant influence on selection, design and operation of water treatment processes (Worrall and Burt, 2009).

NOM both in dissolved or particulate forms may be toxic in different degrees to living organisms, including humans. It can be the origin of serious problems such as taste and odour alteration and bio-instability. Moreover, it is accompanied by the presence of anthropogenic organic compounds incorporated to natural resources due to the discharge of treated wastewater from urban and industrial origin.

According to the classification established by the WHO (WHO, 2008) under the organic chemical contaminants category are included*:* hydrocarbons, chloroform and methane halogenates, halogenated solvents (trichloroethylene, tetrachloroethylene among others) and generic organic solvents (e.g. benzene, acetone, phenols among others). This group also contains the so-called organic micropollutants such as pesticides, hormones, pharmaceuticals and industrial chemicals whose presence in surface water has grown because of their increased production and consumption. The attention for this compounds increases due to the continuous improvement of analytical methods to allow micropollutants detection even at low concentrations.

The most common process to remove microbiological contaminants is dosing biocides as chlorine, chloramine and chlorine dioxide. Generally, disinfection of surface water lead to greater disinfection by-products (DBPs) concentration than groundwater due to the higher NOM content and levels typically vary seasonally with the organic content of the source water supply. The principal ones are trihalomethans (THMs), haloacetic acids (HAAs), BrO_3^- and ClO_2^-, with maximum concentration of 1 mg/l. Br^- and dissolved organic carbon (DOC) are the two main precursors in the formation of halogenated DBPs resulting from chlorination of drinking water. Br^- is easily oxidized to hypobromous acid (HBrO) by free chlorine (HClO and ClO^- or NaClO). HBrO and HClO are both strong oxidants which react with NOM to form halogenated DBPs including THMs and HAAs, which currently are regulated, for example at United States, by the EPA under the Stage 1 Disinfectants and Disinfection By-Products

(D/DBP) Rule (EPA, 1998).
The intake of drinking water with excess of these compounds over many years may cause in liver, kidneys, or central nervous systems, disorders, including cancer (WHO, 2008). The EPA assessed the hazard of over 85000 chemicals for an effective removal of organic compounds in potable water production (EPA, 1998) and the Maximum Contaminant Levels (MCLs) of each contaminant were defined. Besides, the Risk Assessment Information System (RAIS) contains an updated database of concentration limits for each pollutant in drinking water.

A common strategy to control DBP formation is to remove the precursors prior to chlorination. However, these efforts, using processes such as enhanced coagulation, activated carbon adsorption, and NF, have been directed at the removal of DOC which tends to increase the Br^-/DOC ratio and the corresponding Br/Cl_2 dose ratio, leading to preferential formation of brominated DBPs. Bromide can be removed by membrane processes, such as RO or by IEX but both have associated high cost (Hsu and Singer, 2010). The effectiveness of DOC removal is affected by NOM characteristics and the presence of other anions which compete with DOC for the anion exchange sites on the resin. In general, DOC is more effectively removed from waters with higher SUVA values (Boyer and Singer, 2005; Singer and Bilyk, 2002). Waters with high TDS exhibit poor removal of DOC by IEX resins such as the magnetic IEX (MIEX) resins (Hsu and Singer, 2010; Singer et al., 2007).

1.2. Advanced processes based on membrane and hybrid IEX-membrane technologies for removal of inorganic pollutants and disinfection by-products precursors

Different water treatment technologies including adsorption, coagulation, flotation, ozonation, IEX, and pressure-driven membrane processes such as microfiltration (MF), ultrafiltration (UF), NF and RO have been thoroughly investigated for surface water and groundwater treatment (Edzwald, 2011). Nowadays, the availability to produce high quality drinking and industrial waters by removing target species is very important challenge.

Integrating IEX and membrane technologies represents alternative processes to improve organic and inorganic contents from process and natural waters. Water treatment should provide water quality standards to fulfil requirements for human consumption (e.g. health risk standards) or industrial requirements (Litter et al., 2010). Membrane technologies have become an important part of the separation processes during the last decades. Their use has increased significantly in the water industry compared to other water treatment technologies. In particular, RO and NF are widely used to produce water with low salinity content and to improve the quality of process waters (Yoon and Lueptow, 2005). While RO and UF were well established in several applications, there was a lack of available membranes with cut-offs between 400 and 4000 g/mol. For this reason, increasing interest in NF membranes developed in the last decade. An extensive review on principles and industrial applications of NF has been

published recently (Van der Bruggen et al., 2008; Voutchkov, 2011). NF is important for water softening, removal of organics, concentration of juice and demineralization of whey. The improvement of solvent stability of available NF membranes opens a wide range of potential applications in the chemical and pharmaceutical industry as well as in metal and acid recovery (Pereira and Peinemann, 2006).

However, in most of the cases the requirements on TDS contents is not a critical objective and the improvement of quality is directed to the specific removal of given target species. In this case, the alternative separation process (materials or technologies) are directed to the use of approaches where only a given component or group of components are specifically removed. When the selected or target group of species are charged species (anions and cations) IEX materials and processes are one of the most appropriate option.

IEX resins have been widely used for water softening and production of ultrapure water. IEX resins consist of solid matrixes carrying functional groups that can exchange cations or anions with the electrolyte solution. The reaction of the dissolved ions with functional groups results in the creation of coordinating or electrostatic bonding. The solid-phase can be a resin which is usually made of a complex crosslinked polymer matrix (Helfferich, 1962). Advantages of IEX resins include simplicity of operation and the fact that there is no energy need for the exchange phenomenon to occur, while the limitations of IEX resins are restricted to the resin exchange capacity and consumption of chemicals for regeneration (Edzwald, 2011).

The idea to use IEX resins for tap water remediation was suggested recently. This usage is characterized by the low regulable concentration limit (below even to mg/l or to μg/l) of contaminants that could be achieved even in the presence of water microelements (e.g. calcium, magnesium, sodium, potassium, and chloride) thanks to the selectivity of the IEX resin selective groups (Becker et al., 2004; Bolto et al., 2004). However, two obstacles limit their further application: a) the difficulty to operate with mixed beads due to the problem associated to different IEX particle size and b) the lower adsorption efficiency due to the longer time for adsorption equilibrium (Nassar, 2010).

In parallel to the growth of the development of IEX membranes, both cationic and anionic ones; initially devoted for applications on the production of chlor-alkali or in the energy application in fuel cells, has promoted the development of electrodialysis as a solution for water desalination of brackish water for potable consumption by removing harmful anions from surface water and groundwater as NO_3^- as an alternative to biological treatments such as denitrification (Bae et al., 2002).

1.2.1. Nanofiltration (NF) membranes for salinity removal

NF is being promoted as a new technological solution to remove both major and minor organic and inorganic compounds from surface water (Darvishmanesh et al., 2011; Sotto et al., 2013). NF membranes have relatively large rejections of double-charged

ions (up to 99%) and moderate rejections of single-charged ones in the range of 20-70%. Because of this performance, NF membranes are considered between RO membranes, which offer salt rejections higher than 95%, and UF membranes, which have salt rejections lower than 10% (Baker, 2012). In comparison with RO, NF takes the benefit of working at less operational pressure by producing the same flux. Thus, NF is pointed out useful for the potable water production, since using this technique, the remineralisation process can be reduced.

NF membranes exhibit properties in between UF and RO. Their free volume distribution is typically below 1 nm, which corresponds to molecular weight cut-off (MWCO) of 300–500 Da (Kim et al., 2005). NF membranes were designed, after a request from the oil companies to remove sulphate from the process waters extracted from oil wells, by modification of RO membranes to achieve higher rejection of multi-charged species. Polymeric NF membranes contain ionizable groups such as carboxylic, sulfonic and amine groups among others which may be ionized depending on the feed solution pH (Coronell et al., 2011, 2010). Then, as RO membranes, NF membranes provide separation factors for inorganic and low molecular weight (LMW) organic compounds (Van Der Bruggen et al., 2004, 2001). Distinguishing characteristics are low rejection of single-charged ions, high rejection of multi-charged ions and higher flux compared to RO membranes.

Recently, Mohammad et al. (Mohammad et al., 2015) provided a thorough review on commercial membranes, together with their properties and top layer composition (Table 1.1). However, a wide review of the state of the art is collected by a series of relevant publications covering from fundamentals aspects (Hilal et al., 2004; Schäfer et al., 2005), membranes modification (Van der Bruggen, 2009), fouling (Al-Amoudi, 2010; Tang et al., 2011), effect of aqueous solution composition (Luo and Wan, 2013), applications (Lau and Ismail, 2009), and NF modelling (Oatley-Radcliffe et al., 2014; Wang et al., 2014).

Table 1.1. Specifications of commercial NF membranes by manufacturer (Mohammad et al., 2015)

Membrane	Manufacturer	MWCO (Da)	Maximum temperature (°C)	pH range	Stabilized salt rejection (%)	Composition on top layer
NF270	Dow Filmtec[a]	200–400	45	2–11	>97%	Polyamide thin-film composite
NF200	Dow Filmtec[a]	200–400	45	3–10	50–65% $CaCl_2$ 3% $MgSO_4$ 5% Altrazine	Polyamide thin-film composite
NF90	Dow Filmtec[a]	200–400	45	3–10	85–95% NaCl >97% $CaCl_2$	Polyamide thin-film composite
TS80	TriSep[b]	150	45	2–11	99%	Polyamide
TS40	TriSep[b]	200	50	3–10	99%	Polypiperazineamide
XN45	TriSep[b]	500	45	2–11	95%	Polyamide
UTC20	Toray[c]	180	35	3–10	60%	Polypiperazineamide
TR60	Toray[c]	400	35	3–8	55%	Cross-linked polyamide composite
CK	GE Osmonics[d]	2000	30	5–6.5	94% $MgSO_4$	Cellulose acetate
DK	GE Osmonics[d]	200	50	3–9	98% $MgSO_4$	Polyamide
DL	GE Osmonics[d]	150–300	90	1–11	96% $MgSO_4$	Cross-linked aromatic polyamide
HL	GE Osmonics[d]	150–300	50	3–9	98% $MgSO_4$	Cross-linked aromatic polyamide
NFX	Synder[e]	150–300	50	3–10.5	99% $MgSO_4$ 40% NaCl	Proprietary polyamide thin-film composite
NFW	Synder[e]	300–500	50	3–10.5	97% $MgSO_4$40% 20% NaCl	Proprietary polyamide thin-film composite
NFG	Synder[e]	600–800	50	4–10	50% $MgSO_4$ 10% NaCl	Proprietary polyamide thin-film composite
TFC SR100	Koch[f]	200	50	4–10	>99%	Proprietary thin-film composite polyamide
SR3D	Koch[f]	200	50	4–10	>99%	Proprietary thin-film composite polyamide
SPIRAPRO	Koch[f]	200	50	3–10	99%	Proprietary thin-film composite polyamide
ESNA1	Nitto-Denko[g]	100–300	45	2–10	89%	Composite polyamide
NTR7450	Nitto–Denko[g]	600–800	40	2–14	50%	Sulfonated polyethersulfone

NF membranes, like the majority of membranes currently employed in the industry, are asymmetric porous membranes (Loeb and Sourirajan, 1964) whose structure and transport properties vary across the thickness. An asymmetric membrane commonly consists of a 0.1–1 μm thick dense layer supported by a highly porous, 100–200 μm thick support layer (Kesting, 1990; Mulder, 1996). The dense layer provides the majority of selectivity for the membrane. Separation properties are determined by the chemical nature, polymer structure and layer thickness. The porous structure of the other two layers is assumed to provide mechanical support for the fragile thin selective layer and thought to have little effect on the separation performance of the membrane. In thin-film-composite (TFC) membranes, the porous support layer is generally an integrally skinned membrane formed through the non-solvent induced phase separation process, while the dense layer is typically formed through either interfacial polymerization or dip coating followed by cross-linking (Pendergast and Hoek, 2011; Pendergast et al., 2010).

The most common thin film chemistry for RO membranes is based on a fully aromatic polyamide (PA) formed by interfacial polymerization of meta-phenylenediamine (MPD) and trimesoyl chloride (TMC), while semi-aromatic PA NF membranes are formed by interfacial polymerization of piperazine and TMC (Ramon et al., 2012; Van der Bruggen and Kim, 2012). It is assumed that the dense selective layer formed by interfacial polymerization is heterogeneous throughout its thickness (20–200 nm) and highly cross-linked. The surface properties of a PA film are different from the properties within the PA dense layer because the polymer density is not uniformly distributed (Freger, 2003).

The PA dense layer was initially characterized as highly negatively charged since acyl chloride groups are not fully converted to amide in the formation process; however, it was recently reported that direct titration experiments revealed the simultaneous presence of both positive and negative fixed charges in the dense layer of composite PA NF membranes (Coronell et al., 2011). Freger and Srebnik (Freger and Srebnik, 2003) proposed that the fixed charge is not uniform on the film but it is actually a "sandwich" comprising two oppositely charged layers.

The dense coating layer has historically been treated as a non-porous film. Recently more advanced characterization techniques, such as atomic force microscopy (AFM), scanning electron microscopy (SEM), transmission electron microscopy (TEM), X-ray photoelectron spectroscopy, electron spin resonance, nuclear magnetic resonance (NMR), small angle X-ray scattering, and molecular dynamics simulation have been employed to reveal the dense layer structure (Bowen et al., 1997; Hilal et al., 2005a; Tung et al., 2009). A highly cross-linked PA dense layer structure with sub-nanoscale pores (0.2–1 nm) and low porosity has been reported in literature (Boussu et al., 2007; Hung et al., 2010; Pacheco et al., 2010; Stawikowska and Livingston, 2012).

Then, NF membranes contain functional groups that could be charged, depending on the pH of the solution in contact with the membrane. At neutral pH, NF membranes can be slightly negative-charged as their isoelectric points are around pH 3–4.5

(Childress and Elimelech, 1996; Coronell et al., 2010, 2007; Mouhoumed et al., 2014; Oatley et al., 2012; Richards et al., 2010). Determining the functional membrane composition is still an important challenge to better explain the different ion rejections using the various kinds of NF membranes (Coronell et al., 2011, 2010; Schäfer et al., 1998).

1.2.2. Solute transport on NF membranes: transport models

Solute transport through NF membranes is a complex process that depends on the micro hydrodynamic and interfacial events occurring at the membrane surface and within the membrane structure. Membrane structure is still one of the main challenges to be solved as some authors consider it permanent in time (e.g. nanopores structure) while others consider only a free volume structure with no permanent structure (non-pores structure).

Rejection by NF membranes may be attributed to a combination of steric, Donnan, dielectric and transport effects. The classical Donnan effect describes the equilibria and membrane potential interactions between charged species and the interface of the charged membrane (Donnan, 1995). The membrane charge originates from the dissociation of ionizable groups at the membrane surface and from within the membrane pore structure (Ernst et al., 2000; Hagmeyer and Gimbel, 1998; Hall et al., 1997). These groups may be acidic or basic in nature or indeed a combination of both depending on the specific materials used during the fabrication process. The dissociation of these surface groups is strongly influenced by the pH of the contacting solution and where the membrane surface chemistry is amphoteric in nature, the membrane may exhibit an isoelectric point at a specific pH (Childress and Elimelech, 1996).

In addition to the ionizable surface groups, NF membranes have a weak IEX capacity and in some cases ions from the contacting solution might be exchanged into the membrane surface causing a slight modification of the membrane charge (Afonso et al., 2001; Schaep and Vandecasteele, 2001). Electrostatic repulsion or attraction takes place according to the ion valence and the fixed charge of the membrane that may vary depending on the localized ionic environment as a result of the aforementioned phenomena.

The phenomena of dielectric exclusion are much less understood and there are two main competing hypotheses as to the exact nature of the interaction. These are the so called ‘image forces’ phenomenon (Yaroshchuk, 1998) and the ‘solvation energy barrier’ mechanism (Bowen and Welfoot, 2002). Both exclusion mechanisms arise as a result of the extreme spatial confinement and nano-length scales that are present in NF membrane separations which are effectively charge-based exclusion phenomena. These interactions have been reviewed in detail (Oatley et al., 2012). Solutes moving in free solution experience drag forces exerted by the solvent flowing through the confined pore structure. The movement of solutes in this confined space is greatly affected by the local environment and the transport of the solute is considered as

hindered.

Hindered transport can be expressed in terms of both a convective and diffusive element which contributes to the overall transport effect. The fact that the dimensions of the NF active layer are at near atomic-length scales, coupled with limitations in current measurement technologies, has delayed a detailed knowledge of the physical structure and electrical properties of NF membranes. This has resulted in uncertainty and significant debate over the true nature of the separation mechanisms (Schäfer et al., 2005) and the role of dielectric exclusion is particularly contested (Oatley et al., 2012).

1.2.3. Predictive modelling

The prediction of membrane performance has been an intensive active area of research over the last two decades. During this time, the emphasis has shifted from empirical black box models based on irreversible thermodynamics (Levenstein et al., 1996) to models based on the extended Nernst–Planck equation (Tsuru et al., 1991) due to the ability of the latter to provide information related to properties of both the membrane and the process stream.

The main purpose of such models is to incorporate as much physical realism of the membrane process as possible in order to better match measurable quantities to adjustable model parameters. One should always be mindful that the major limitation of NF modelling is the requirement for characteristic model parameters, such as pore radius and membrane charge, that are not readily measured at the near atomic length scales encountered. The nano-scale phenomena involved in neutral solute and charged electrolyte separations by NF membranes are extremely complex and, as such, are likely to be a rigorous test of any macroscopic continuum description of ion transport and partitioning. Similarly, the development of rigorous physical descriptions (such as molecular dynamics simulations) has been limited due to the lack of detailed knowledge of the physical structure and electrical properties of real NF membranes and process streams.

As a direct consequence, developments in modelling have moved in parallel with improvements in the measurement techniques employed for the characterization of NF membranes and process streams, as only then a check of the appropriateness of model parameters will be possible. The application of the extended Nernst–Planck equation was originally proposed by Schlögl (Schlögl and Helfferich, 1952) for the description of transport of electrolytes in RO through IEX membranes and is arguably the most commonly used model. The equation is particularly useful for NF as consideration is given to the mechanisms of transport and the adjustable fitting parameters required are based upon real measurable membrane properties.

A good engineering model should employ a limited number of adjustable parameters obtainable from a well-defined set of experiments. At the same time, such a model should take into account the principal physico-chemical phenomena, at least semi-

quantitatively. Recently, Yaroshchuk et al. (Yaroshchuk et al., 2013, 2011) developed the Solution-Electro-Diffusion-Film (SEDF) model to describe the transport of multiple ions through NF membranes with high rejections for at least some of the ions. Only two adjustable parameters are needed to quantify the membrane permeabilities of all ions present on the feed solution. At the same time, the use of ion (rather than salt) membrane permeabilities, accounts for the important coupling between trans-membrane ion fluxes via spontaneously-arising electric fields (Figure 1.2).

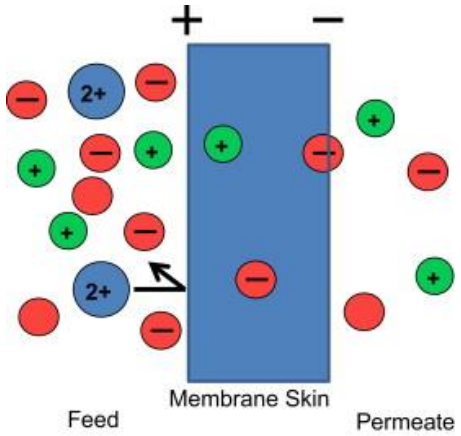

Figure 1.2. Cartoon of NF with a 3-ion system. In this case, high rejection of the divalent cation leads to an electric field that enhances transport of the monovalent cation. At low monovalent ion concentrations, negative rejection may occur. (Yaroshchuk et al., 2013)

The dense layers of commercial TFC membranes (especially, those for NF) have thicknesses well below 100 nm (Bason et al., 2011, 2007; Freger, 2004). Despite the nanometer-scale barrier-layer thicknesses, NF membranes noticeably reject ions at moderate trans-membrane fluxes, indicating that the effective diffusion coefficients of ions inside such layers are several orders of magnitude lower than those in bulk electrolyte solutions. These strongly-reduced diffusivities are hardly compatible with the popular view of NF membranes as nano-porous (Bowen et al., 2004, 2002; Oatley et al., 2012). As a first approximation, whether a medium is essentially non-porous, one can neglect the convective coupling between the trans-membrane volume flux and solute transfer. Then, the solution-electro-diffusion phenomenon should only be taken into account to describe the trans-membrane ion transport in NF.

Recent theoretical and experimental studies demonstrate that these fields essentially control the trans-membrane transfer of trace amounts of “rapid” ionic solutes (primarily small monovalent cations and anions) (Yaroshchuk et al., 2011). Multi-ionic solutions occur in virtually all practical applications of membrane processes. Additionally, measurements of ion rejection from electrolyte mixtures provide much richer information about the membrane transport properties than conventional measurements with single salts (Déon et al., 2012; Yaroshchuk and Ribitsch, 2002; Yaroshchuk, 2008).

An analytical solution for ion transport in solutions containing ions with up to 4 different charges for ion flux during pressure-driven solvent transport through membrane barrier layers was developed. For systems of most practical interest with 4 different ion charges a single ordinary differential equation, easy to solve numerically, including the formulation of a numerical sub-routine for the external concentration polarization within the scope of the Nernst model of the unstirred layer, was also formulated. The model developed is a natural extension of the classical Solution-Diffusion (SD) model to include electrolyte mixtures.

Previously, the SD model (applicable to non-electrolytes and single salts) was mainly used to describe RO (Bódalo et al., 2004; Malek et al., 1994; Oh et al., 2009; Wijmans and Baker, 1995; Wijmans, 2004). However, recently, several studies, demonstrated that the SD model also describes solute and solvent transport across NF membranes (Bason and Freger, 2010; Bason et al., 2010, 2009; Hung et al., 2009; Kedem and Freger, 2008; Yaroshchuk et al., 2009).

Most previous studies that interpreted ion rejections in electrolyte mixtures used numerical approaches to the solution of the corresponding system of ordinary differential equations, as it is commonly believed that such systems of equations do not have analytical solutions. However, an analytical solution in the limiting case of one dominant salt and trace ions was developed (Yaroshchuk et al., 2011). Analytical solutions are also available for the limiting cases of small and large trans-membrane fluxes (Vonk and Smit, 1984, 1983). However, both of these limiting cases are typically experimentally inaccessible because of impractically low permeate fluxes or high concentration polarization at high permeate fluxes.

1.2.4. Ion-exchange resins for disinfection by-products (DBPs) precursors removal and integration on hybrid systems.

NOM affects significantly many aspects of water treatment, including the performance of the unit processes, application of water treatment chemicals and biological stability of water. Recently, Matilainen, et al. (Matilainen et al., 2010), critically reviewed the fundamentals and drawbacks on the coagulation and flocculation on NOM removal from drinking water. According to this extensive evaluation the presence of NOM causes as main problems in drinking water and drinking water treatment processes the following: (a) negative effect on water quality indicators by causing colour, taste and odour nuisance problems, (b) increased coagulant and flocculants and disinfectant doses (which in turn results in increased sludge volumes), (c) production of harmful DBPs, (d) promotion of biological growth in drinking water distribution networks and (e) increased levels of complexed transition metals (e.g. Fe, Al, Zn, Cu, ..) and adsorbed organic micro-pollutants.

NOM can be removed from drinking water by several treatment options, of which the most common and economically feasible processes are considered to be coagulation and flocculation followed by sedimentation/flotation and sand filtration. Most of the NOM can be removed by coagulation, although, the hydrophobic fraction and high

molar mass compounds of NOM are removed more efficiently than hydrophilic fraction and the low molar mass compounds (Gibert et al., 2015). Thus, enhanced and/or optimized coagulation, as well as new process alternatives for the better removal of NOM by coagulation processes need to be investigated. Among them, the combination or integration of IEX with coagulation or the integration of IEX with membrane filtration processes.

Anion exchange resins, non-ionic resins (Anderson and Maier, 1979) and activated carbon (Boening et al., 1980; Weber and Van Vliet, 1981) have also been applied. However, in very recent years, IEX processes have received considerable attention with the use of a new MIEX resin developed by Orica Co. (Abdulgader et al., 2013; Allpike et al., 2005; Drikas et al., 2003; Fearing et al., 2004; Humbert et al., 2005; Singer and Bilyk, 2002). MIEX is similar to conventional resins, however in comparison it uses microsized resin particles dispersed as a slurry on a stirred contactor, thus allowing maximum surface area for sorption. The MIEX resin is a strong-base resin ($R_4N^+Cl^-$) with iron oxide integrated into a macroporous, polyacrylic matrix, and is typically used with chloride as the counterion. The average MIEX resin particles are 180 μm in diameter, 2–5 times smaller than traditional resins. The increased surface area-to-volume ratio allows for faster IEX kinetics and decreased resin fouling due to shorter NOM diffusion paths within the resin (Bourke et al., 2001; Hsu and Singer, 2010; Rouquerol et al., 1994; Shuang et al., 2012).

The magnetic component allows the fluidization of MIEX beads at high hydraulic loading rates and also their agglomeration and subsequent quick settling when the regeneration is needed (Kim and Dempsey, 2010; Wang et al., 2012). It removes both organic and inorganic contaminants like sulphate, nitrate or phosphate (Singer et al., 2007). Specifically, effective DOC removal was achieved at MIEX resin concentrations between 0.5 - 1 ml/l of treated water (Ding et al., 2012a; Singer et al., 2009).

MIEX resin has been used as pretreatment method prior to coagulation to enhance the efficiency of coagulation and reduce the coagulant dose (up to 60%), with reduced sludge formation and turbidity load (Humbert et al., 2007). In the MIEX process, the NOM compounds with higher charge density are more kindly removed than the aromatic ones (Mergen et al., 2008). Moreover, MIEX resin also removes hydrophilic, LMW NOM, thus being able to remove a fraction of NOM recalcitrant to coagulation (Mergen et al., 2009, 2008). The flocs formed after pretreatment with MIEX have been larger and more resistant to shearing effects than those formed by conventional process (Jarvis et al., 2008; Sani et al., 2008). Hence, MIEX in combination with coagulation has increased the DOC and DBP precursor reduction, although this has not been evident in all cases (Bond et al., 2010). According to the literature, an addition of 8–63% and about 10–30% of DOC removal has been observed in jar (Mergen et al., 2008) and pilot tests (Shorrock and Drage, 2006), respectively.

The MIEX process presents a very promising method to reduce DBP formation when used upstream of chlorination. Several studies have shown very effective NOM

removal using the MIEX resin (Allpike et al., 2005; Boyer and Singer, 2005; Drikas et al., 2003; Fearing et al., 2004; Morran et al., 2004; Singer and Bilyk, 2002). Reduction of THM and HAA formation potential from MIEX treatment has also been shown to be greater than that achieved through enhanced coagulation (Boyer and Singer, 2006; Hsu and Singer, 2010). The high density and magnetic properties of the resin provide rapid clarification following the contact stage (Morran et al., 2004). MIEX resin can be easily regenerated and even after several regenerations it gives almost the same organic matter removal efficiency. Moreover, it is suitable for both small and large plants and complements other water treatment technologies like coagulation or membrane filtration.

MIEX process has been used at bench-scale, pilot and full scale to rapidly remove NOM and trace organics in combination with either conventional coagulation, sorption on activated carbon or low-pressure membrane filtration (Drikas et al., 2011; Humbert et al., 2008, 2007; Mergen et al., 2008). Unlike larger, traditional IEX resins that tend to be used in packed beds downstream of solid-liquid separation processes, the MIEX resin is used either in a slurry contactor or in a fluidized bed at the head of the treatment train.

From the findings of these studies, the MIEX resin provides a potentially effective technology for controlling the formation of chlorinated and brominated DBPs because it can remove appreciable amounts of DOC and can lower bromide concentrations, but its effectiveness for the latter will be limited by the presence of other anions in the water (Boyer and Singer, 2008; Hsu and Singer, 2010). In addition to DOC removal, bromide has also been observed to be removed to a significant extent by the MIEX resin (Humbert et al., 2005; Johnson and Singer, 2004) but the effectiveness of bromide removal strongly depends on water quality. High alkalinities (bicarbonate concentrations) and, especially, high sulphate concentrations (>50 mg/l) have been shown to inhibit bromide removal (Boyer and Singer, 2006; Johnson and Singer, 2004; Singer and Bilyk, 2002; Singer et al., 2007).

1.2.5. Integration of hybrid IEX-membrane ultrafiltration (MIEX-UF)

Currently MF, UF, NF and RO are widely used for treatment of surface and waste water, including desalination of brackish and seawater. However, one of the main problems arising upon the operation of membrane units is membrane fouling, which seriously hinders the application of this technology (Edzwald, 2011). Moreover, RO, which is regarded as one of the most attractive methods for water desalination, is hampered by a high energy consumption (Fritzmann et al., 2007).

The fouling of membranes and decline of flux are the major problems associated to membrane techniques (Zularisam et al., 2006). Several studies have indicated that NOM, and especially the hydrophobic fraction of NOM and high molecular weight compounds, have great impact on the fouling and decline of flux (Chen et al., 2007; Dong et al., 2007). Thus the pretreatment with coagulation is an effective method to prevent these adverse effects (Howe et al., 2006; Jung et al., 2006; Xiangli et al.,

2008), and combination of coagulation and membrane filtration is also reducing the amount of coagulant needed while improving turbidity and DOC reductions (Blankert et al., 2007).

Moreover, coagulation has been observed to provide an effective hygienic barrier in combination with membranes (Leiknes, 2009). However, also contradictory results have been obtained, and the removal of NOM has been significantly affected by the type of coagulant, coagulation conditions, the type of membrane, filtration conditions, and the characteristics of the water to be treated (Cai et al., 2008; Cho et al., 2006; Choi et al., 2008; Kim et al., 2006; Tran et al., 2006; Zularisam et al., 2009). The way of combining coagulation with ultrafiltration (Konieczny et al., 2009) or MF (Loi-Brügger et al., 2006) has been the "inline" hybrid process. The coagulant dose and the duration of water treatment are reduced by batching the coagulant to the feed immediately before the membrane (Tian et al., 2008).

Therefore a search for new solutions to overcome or at least minimize these drawbacks is needed. Among these approaches hybrid membrane processes are one potential solution. Hybrid membrane processes were described as processes where "one or more membrane process is coupled with another unit process such as adsorption, IEX, coagulation and bioconversion (Edzwald, 2011). In the last years, the interest on hybrid processes has increased substantially and is derived by the need for overall process optimization and/or cost reduction. Often a combination of various water treatment technologies is required to provide high level of water treatment and purification.

The recent tendencies focused on the combination of low pressure membrane processes such as MF and UF with adsorption have been reviewed by Stoquart et al. (Stoquart et al., 2012). An hybrid adsorption–membrane process, where metal oxide particles are deposited on membrane surface to enhance the membrane NOM removal, has been described (Stylianou et al., 2015). Also the use of IEX resins combined with membranes has shown advantages over systems based on activated carbon combined with membranes in terms of selective removal of targeted species and prevention of inorganic scaling.

The first studies on hybrid IEX-RO processes for water softening prior to RO membranes and then to use the RO retentate to regenerate an IEX resin column were published back to the 1970s (Zagorodni, 2007), however they were not widely adopted at that time. Nowadays, interest on hybrid IEX-pressure driven membrane processes of water treatment is greatly recognized at industry level. The main factors responsible for that include: (i) the current very strict regulations of water quality, (ii) the problems of membrane brine management, (iii) the increased attention given to emerging pollutants, which have been identified in surface water and in drinking water and are poorly removed by conventional methods of water treatment, (iv) the development of new efficient IEX resins, and (v) new challenges on waste waters produced from unconventional gas resources (e.g. fracking).

1.3. Objectives

The main objective of this thesis is to study the possible integration of separation processes based on pressure-driven membrane technologies such as NF and hybrid technologies based on IEX resins and membrane UF to reduce salinity, hardness and inorganic pollutants (NO_3^-, SO_4^{2-}) in surface and ground brackish waters and to reduce the presence of DBP precursors (DOM and Br^-) in order to improve water quality and comply with increasingly demanding regulations.

For the application of NF to reduce salinity, hardness and inorganic pollutants in brackish waters the work will be devoted to characterize and identify the mechanisms of rejection of ionic species under different solution composition modifying the nature of the dominant salts. The aim of this work was to determine the reliability of the data obtained using flat sheet (FS) lab-scale configuration when NF membranes are implemented at industrial scale level using spiral wound (SW) configuration. Ions rejections in salt mixtures with the two configurations types were analysed, modelled, evaluated and compared. In both cases, the operation was carried out in cross-flow mode and with recirculation of permeate and concentrate streams into the feed tank. More specifically the following research questions will be addressed:

- to validate the extended SEDF model via comparison with experimental data on the rejection of several dominant salts and trace ions using the NF270 membrane in a cross-flow experimental set-up.

- to study the influence of dominant Mg-based salts ($MgCl_2$, $MgSO_4$) and Na-based salts (NaCl, Na_2SO_4) on the removal of both dominant and trace salts.

- to determine simultaneously both trace ions rejections using the same dominant-salt-controlled parameters of the SEDF model, in this way the ion permeabilities to the membrane with respect to several ions (Na^+, Cl^-, Mg^{2+}, SO_4^{2-}) will be determined.

Synthetic water solutions representative of surface water influenced by industrial and mining drainage (KCl, $MgCl_2$, KI, NaBr, etc) and wastewater treatment discharges of NH_4^+, NO_3^-, SO_4^{2-} will be used. The ion membrane permeabilities of both NF membranes with respect to several ions (Na^+, K^+, Cl^-, Ca^{2+}, Mg^{2+}, SO_4^{2-}, NO_3^-, NH_4^+, I^- and Br^-) will be determined. The different synthetic aqueous solutions will be used as feed solution for the experiments. All of them will be based on a dominant salt (NaCl, $MgSO_4$, Na_2SO_4, $MgCl_2$) mixed with trace ions (Na^+, Cl^-, Mg^{2+}, SO_4^{2-}, Br^-, NO_3^-, I^-, NH_4^+, K^+). The ions studied are of great interest in brackish water purification, because they are found in large quantity (Na^+, Cl^-, Mg^{2+}, SO_4^{2-}), they are precursors of THM (Br^-, I^-) or they are characteristic ions present in rivers due to the influence of agriculture and industrial discharges (NO_3^-, K^+, NH_4^+).

The nature of the experiments conducted within this thesis will follow a progressive approach from conceptual and logistic perspectives. For the part of the thesis devoted to NF, initial bench scale tests aiming at evaluating the feasibility of NF membranes

for the removal of inorganic solutes will be performed by FS membrane module scale experiments focusing on the evaluation of different solutions composition where different dominant salts will be employed. Finally, laboratory based assays will be carried out to explore further impacts when using SW NF modules complementing the study.

Hybrid technologies based on IEX resins and UF membrane to reduce salinity, hardness and inorganic pollutants in brackish waters as well as DBP precursors (DOM and Br^-) from surface brackish waters will be performed. The main objective will be to study the capacity of MIEX resin to remove targeted pollutants when used in combination with a UF membrane. To solve this research question the following objectives will be addressed:

- Evaluation of the IEX capacity on DOM removal and determination of the kinetic performance.

- To determine rejection ratios of dissolved ions involved, as well as to determine the optimal hydrodynamic parameters to allow the maximum effectiveness of the hybrid process (MIEX-UF).

- Evaluation of the hydraulic performance on the hybrid system incorporating MIEX with a capillary UF membrane.

- Evaluation of the capacity for the removal of inorganic pollutants as nitrate, sulphate and bromide.

Chapter 2
Modelling of ion mass transfer of multi-ion solutions with NF membranes

2.1. Evolution of NF modelling

Nowadays, ion removal by NF under different water matrices is still not well understood. Predictive modelling of ion rejection in aqueous solutions using NF membranes is crucial for the optimization and scale-up of water treatment processes, and enormous effort on this field has been expended in the last decade.

Ion transport in NF membranes has been widely described by either the non-equilibrium thermodynamic model and their modifications (Bason et al., 2010; Spiegler and Kedem, 1966; Yaroshchuk, 2002) or with the extended Nernst–Planck equations (Bowen and Mukhtar, 1996).

By using the non-equilibrium thermodynamic model (Kedem and Katchalsky, 1958) to non-electrolytes, the Spiegler–Kedem (SK) equation was developed (Spiegler and Kedem, 1966) to electrolytes by assuming the membrane as a black box. This assumption explains the mass transport by means of the coupling between the convective solvent and the diffusive solute fluxes that lead to one electrolyte permeates through the membrane. Then, water and solute are described by two membrane permeability coefficients.

Later, SK equation was accordingly modified taking into account the influence of membrane structural parameters (Jagur-Grodzinski and Kedem, 1966; Jonsson, 1983) and the concentration dependence (Bason et al., 2009) on the phenomenological transport coefficients. Then, the number of fitting parameters was needed to be increased up to six (X. L. Wang et al., 2012).

Simultaneously, the pore flow-film phase model was developed including up to three ion exclusion mechanisms, steric, electric (Donnan equilibrium) (Afonso and Pinho, 2000; Bruni and Bandini, 2009; Wang et al., 1995) and dielectric (SEDE) (Szymczyk et al., 2007; Szymczyk and Fievet, 2005), and using the description of the solute transport in the membrane phase by the extended Nernst-Planck (NP) equation. In this case, several structural membrane parameters such as pore size, fixed charge and dielectric properties, and size and charge of the ions involved needs to be determined. These complex equations systems also required a large number of fitting structural parameters that makes difficult the solution of the inverse problem of unambiguous determination of these from experimental data.

An alternative approach is the use of the SD model, widely applied originally in RO (Paul, 2004). Unlike the established extended NP or Donnan-Steric-Pore-Dielectric (DSP-DE) model and the SK equation, the SD model has satisfactorily explained the high SO_4^{2-}/Cl^- selectivity of NF or the weak convective coupling between the solute and solvent transfers in the membrane phase (Bason et al., 2010; Yaroshchuk et al., 2009).

In this direction, Yaroshchuk et al. demonstrated that for single salts, the simple version SD model coupled with the film model theory, the SEDF model is applicable (Yaroshchuk et al., 2009). However, for electrolyte mixtures the SEDF model was needed to be extended by consider the coupling between the electro-diffusion fluxes of different ions via the electric field of membrane potential (Pages et al., 2013; Yaroshchuk et al., 2013, 2011).

Integrating the membrane phase, the electric coupling between the fluxes of different ions also occurs within the concentration-polarization layer, which is the transition zone of the unstirred layer between the homogeneous well-stirred bulk solution and the dense thin-film membrane active layer. Taking into account the ion electro-diffusion fluxes in the whole membrane phase and the coupling phenomenon, the good description of ion rejection dependence on the trans-membrane flux from different electrolyte mixtures was provided (Pages et al., 2013; Yaroshchuk et al., 2011). In this approach it is assumed that the ion mass transfer occurs via electro-diffusion through the membrane as well as in the concentration-polarization layer where it also occurs via convection by the solvent transfer.

This new description of the trans-membrane mass transfer by the SEDF model allows the development of efficient procedures to characterize NF membranes by their own ion mass transfer coefficients (k_i), based on the determination not only of single salts permeabilities but also of membrane permeabilities to the ions (P_i) from experimental

data.

2.2. Ion mass transport phenomena by NF with electrolyte mixtures

Modelling NF membrane performance in electrolyte mixtures requires the knowledge of membrane transport properties with respect to single ions. When NF membrane properties are obtained from the measurements of single salt rejections, the membrane transport properties with respect to cations and anions are entangled due to the spontaneously arising electric fields.

When using trace ions the effect of these fields on the trans-membrane transfer of these trace ions is more visible than in single salts rejections. On the other hand, when the trace ion concentrations are sufficiently low, the membrane properties are unaffected by the presence of such traces. Therefore, they can be considered a kind of non-interfering probes for the study of the transfer mechanism of dominant ions (Yaroshchuk and Ribitsch, 2002).

As a result, the ion rejection dependence on the trans-membrane flux from different dominant single salts as well as the electrolyte mixture with trace ions can be quite well described by the SEDF model. Essentially, it assumes that not only the solute transfer occurs via diffusion and electric migration through the membrane, but also in the concentration-polarization layer where it also occurs via convection. A scheme of ion transport processes through the concentration-polarization and the membrane layers is provided by Figure 2.1.

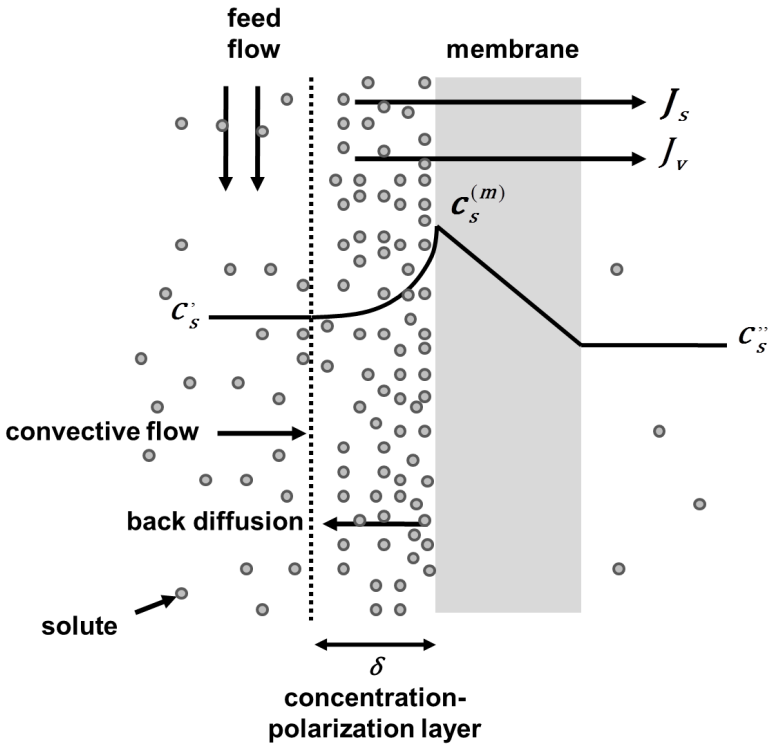

Figure 2.1. Schematic description of ion transport processes through both concentration-polarization and membrane layers ($\boldsymbol{j_i}$ is the trans-membrane solute flux (mol m^{-2} s^{-1}), $\boldsymbol{J_v}$ is the trans-membrane flux (m s^{-1}), $\boldsymbol{c_i'}$ is the ion concentration in the feed solution (mol m^{-3}), $\boldsymbol{c_i^{(m)}}$ is the ion concentration at the membrane surface (mol m^{-3}), $\boldsymbol{c_i''}$ is the ion concentration in the permeate (mol m^{-3}), $\boldsymbol{\delta}$ is the concentration-polarization layer thickness (m)).

2.3. Solution-Electro-Diffusion-Film (SEDF) model

In pressure-driven NF/RO membrane processes the electrochemical potential driving force is the main responsible for ion mass transport across the membrane. The ion trans-membrane fluxes (j_i) are related to the electrochemical potential gradient $\left(\frac{d\mu_i}{dx}\right)$ by a proportionality coefficient (L_i) not necessarily constant (Wijmans and Baker, 1995) as Eq.(1) shows in Table 2.1.

Specifically, the electrochemical potential gradient is defined by both ion concentration $\left(\frac{dc_i}{dx}\right)$ and electrostatic potential $\left(\frac{d\varphi}{dx}\right)$ gradients. Particularly, the electrostatic potential gradient located between both sides of membrane, results in an electric field that accelerates or slows down the ions across the membrane, and concentrates them on both feed and permeate interfaces depending on their own ion charge. The extent of the electric field and consequently, its effect on the ions over the membrane thickness (l) is higher as the concentration gradient increases. Hence, the

ion trans-membrane fluxes should be related to the concentration and electrostatic gradients by means of ion effective diffusion coefficients (D_i) that intrinsically characterize the membranes employed. Although, a steady-state membrane process might be assumed due to the global net ion mass transport, a quasi-steady state process would be better considered as ions and water molecules are not in equilibrium on the membrane phase.

This approach is used in the so-called SEDF model developed by Yaroshchuk (Yaroshchuk et al., 2011) as Eq.(2) and Eq.(3) from Table 2.1 describe. In addition of taking into account the ion electrochemical gradients within the membrane, the SEDF model also considers them across the concentration-polarization layer. However, the equilibrium between ions and water molecules on the concentration-polarization layer has to be also considered as Eq.(3) shows on its third term.

A summary of the mass transport equations used to modelling NF membrane performance with multi-ion solutions is provided in Table 2.1.

Table 2.1. Summary of mass transport equations of the Solution-Electro-Diffusion-Film (SEDF) model to fit experimental data (Pages et al., 2013; Yaroshchuk et al., 2011, 2009)

Ion mass transfer in the membrane phase
$j_i = -L_i\left(\frac{d\mu_i}{dx}\right)$ (1)
Ion mass transfer in the membrane
$j_i = -D_i\left(\frac{dc_i}{dx} + Z_i c_i \frac{d\varphi}{dx}\right)$ (2)
where $D_i = \frac{RTL_i}{c_i}$ and $\varphi = \frac{F\tilde{\varphi}}{RT}$
Ion mass transfer in the concentration-polarization layer
$j_i = -D_i^{(\delta)}\left(\frac{dc_i}{dx} + Z_i c_i \frac{d\varphi}{dx}\right) + c_i J_v$ (3)
Mass balance transfer of quasi-steady state filtration
$j_i = c_i^{"} J_v$ (4)
Observable salt rejections
$R_s^{obs} \equiv 1 - \frac{c_s^{"}}{c_s'} = \frac{\frac{J_v}{P_s} exp\left(-\frac{J_v}{P_s^{(\delta)}}\right)}{1+\frac{J_v}{P_s} exp\left(-\frac{J_v}{P_s^{(\delta)}}\right)}$ (5)
where $P_s^{(\delta)} = \frac{D_s^{(\delta)}}{\delta}$, $D_s^{(\delta)} = \frac{(Z_+ - Z_-)D_+^{(\delta)}D_-^{(\delta)}}{Z_+ D_+^{(\delta)} - Z_- D_-^{(\delta)}}$ and $P_s = \frac{D_s}{l}$
Intrinsic salt rejections
$R_s^{int} \equiv 1 - \frac{c_s^{"}}{c_s^{(m)}} = \frac{\frac{J_v}{P_s}}{1+\frac{J_v}{P_s}}$ (6)
Trace ion concentration at the membrane surface
$\frac{c_{t^\pm}^{(m)}}{c'_{t^\pm}} =$ (7)
$exp\left(Pe_{t^\pm}\right)\left[1 + R_s^{obs}(exp(Pe_s) - 1)\right]^{b^{(\delta)}} \cdot$
$\left\{1 - \left(1 - R_{t^\pm}^{obs}\right)\int_{exp\left(-Pe_{t^\pm}\right)}^{1} \frac{dy}{\left[1+R_s^{obs}(y^{-\alpha}-1)\right]^{b^{(\delta)}}}\right\}$
where $Pe_s = \frac{J_v \cdot \delta}{D_s^{(\delta)}}$, $Pe_{t^\pm} = \frac{J_v \cdot \delta}{D_{t^\pm}^{(\delta)}}$, $b^\delta \equiv \frac{Z_{t^\pm} \cdot (D_+^{(\delta)} - D_-^{(\delta)})}{Z_+ D_+^{(\delta)} - Z_- D_-^{(\delta)}}$, $\alpha = \frac{D_{t^\pm}^{(\delta)}}{D_s^{(\delta)}}$
Reciprocal trans-membrane trace ion transfer
$f_{t^\pm} = (f_s)^b + K \cdot \left(\frac{f_s - (f_s)^b}{1-b}\right)$ (8)
where $f_s \equiv \frac{c_s^{(m)}}{c_s^{"}} \equiv \frac{1}{1-R_s^{int}}$, $b \equiv \frac{Z_{t^\pm} \cdot (P_+ - P_-)}{Z_+ P_+ - Z_- P_-}$, $K \equiv \frac{P_s}{P_{t^\pm}}$
Membrane permeabilities to dominant ions
$P_\pm = \frac{P_s}{1-\left(\frac{Z_\pm}{Z_{t^\pm}}\right)\cdot b}$ (9)

2.4. Data Analysis. Determination of Ion Membrane Permeabilities

Prior to start the modelling, raw data from the experimental tests performed by FS and SW set-ups were selected to introduce them into the SEDF model. Such trans-membrane flux (J_v) and observable rejections of both dominant and trace ions $\left(R_s^{obs}, R_t^{obs}\right)$ were therefore calculated before their use as an input data. The J_v was determined by weighting the mass $\left(m_p\right)$ of a specific permeate volume $\left(V_p\right)$ approached as water at 25ºC ($\rho = 997.1\ Kg\ m^{-3}$), which had crossed through the effective membrane area ($A_{FS} = 0.014\ m^2, A_{SW} = 2.6\ m^2$) during certain time $\left(t_p\right)$ as it can be depicted by Eq.(10).

$$J_v = \frac{1}{A}\frac{V_p}{t_p} = \frac{1}{A}\frac{m_p/\rho}{t_p} \tag{10}$$

In general terms for all solutes involved on the multi-ion solution either for dominant or trace ions, the corresponding R_s^{obs} and R_t^{obs} are calculated by the c_i and $c_i^{"}$ from the feed and permeate streams respectively, obtained by ion chromatography as Eq.(11) describes.

$$R_i^{obs} = 1 - \frac{c_i^{"}}{c_i} \tag{11}$$

The data treatment procedure to apply the SEDF model (Pages et al., 2013; Yaroshchuk et al., 2011) consist of relating the observable rejections to the intrinsic ones $\left(R_s^{int}, R_t^{int}\right)$ by taking into account the extent of the concentration-polarization layer at the membrane surface.

Initially, the dominant salt rejections are fitted by Eq.(5) as a function of the flux produced by means of two characteristic membrane parameters, which are obtained towards the dominant salt involved on the multi-ion solution: the membrane and the concentration-polarization layer permeabilities to the dominant salt $\left(P_s,\ P_s^{(\delta)}\right)$. Then, the intrinsic rejections of the dominant salts $\left(R_s^{int}\right)$ can be calculated by Eq.(6), and so that their reciprocal trans-membrane transfers (f_s) and the corresponding concentrations $\left(c_s^{(m)}\right)$ at the membrane surface can be determined.

Subsequently, trace ion concentrations at the membrane surface $\left(c_t^{(m)}\right)$ are calculated by Eq.(7), where the effect of concentration-polarization magnitude over the trace ions is taken into account according to the estimated value of the concentration-polarization thickness (δ) and literature data of diffusion coefficients of ions $\left(D_{\pm}^{(\delta)}\right)$ listed in Table 2.2.

Table 2.2. Limiting equivalent conductivities ($\boldsymbol{\lambda^{o}_{\pm,s}}$) and diffusion coefficients ($\boldsymbol{D^{(\delta)}_{\pm,s}}$) of ions and salts at the concentration-polarization layer, the charges ($\boldsymbol{Z_{\pm}}$) and the Stokes radius of ions ($\boldsymbol{r_s}$)

Ion/Salt	$Z_{\pm}$	$\lambda^{o}_{\pm,s} \cdot 10^{-4}$ ($m^2\ \Omega^{-1}\ eq^{-1}$)	$D^{(\delta)}_{\pm,s} \cdot 10^{-9}$ ($m^2\ s^{-1}$)	Stokes radii (r_s) (nm)
Na^+	1	50.10	1.34	0.185
K^+	1	73.50	1.96	0.126
NH_4^+	1	73.50	1.96	0.126
Mg^{2+}	2	53.00	0.71	0.350
Ca^{2+}	2	59.50	0.79	0.312
Cl^-	-1	76.35	2.04	0.121
Br^-	-1	78.14	2.09	0.119
I^-	-1	76.80	2.05	0.121
NO_3^-	-1	71.46	1.91	0.130
SO_4^{2-}	-2	80.00	1.07	0.232
KCl	-	149.85	2.00	-
NaCl	-	126.45	1.62	-
$MgCl_2$	-	129.35	1.25	-
$CaCl_2$	-	135.85	1.34	-
Na_2SO_4	-	130.10	1.23	-
$MgSO_4$	-	133.00	0.85	-

(Robinson and Stokes, 2002)

where

$D^{(\delta)}_{\pm} = k \cdot \frac{\lambda^{o}_{\pm}}{|Z_{\pm}|}$ $\quad k = D^{(\delta)}_{s(KCl)} \cdot \frac{Z_+\lambda^{o}_{+} - Z_-\lambda^{o}_{-}}{(Z_+ - Z_-)\lambda^{o}_{+}\cdot\lambda^{o}_{-}} = 2.67 \cdot 10^{-7}\ \left(\Omega\ eq\ s^{-1}\right)$

$\lambda^{o}_{s} = \lambda^{o}_{+} + \lambda^{o}_{-}$

$r_s = \frac{k_B \cdot T}{6 \cdot \pi \cdot \mu \cdot D^{(\delta)}_{\pm}} \cdot 10^9$ (Einstein-Stokes relation)

Hence, once $c_t^{(m)}$ was determined the intrinsic rejections $\left(R_t^{int}\right)$ and their reciprocal trans-membrane transfers to the trace ions $\left(f_t \equiv \frac{c_t^{(m)}}{c_t^{"}} \equiv \frac{1}{1-R_t^{int}}\right)$ can be obtained.

Finally, the modelling of the trace ions is carried out by Eq.(8) using two trans-membrane parameters, b and K, to adjust the $f_{t^{\pm}}$with respect to f_s, the trace ion and the dominant salt reciprocal intrinsic transfers. Then, intrinsic and observable rejections of any trace ion contained on the multi-ion solution as a function of the measured J_v can be depicted.

All possible fitting is optimized by minimizing the sum of the square relative or absolute errors with respect to the real values. As a result, not only the P_s and the $P_s^{(\delta)}$ can be determined, but also the membrane permeabilities to the dominant and the trace ions $\left(P_{\pm}, P_{t^{\pm}}\right)$ are obtained by Eq.(9) and from the estimated K parameter, respectively.

Chapter 3
Rejection of multi-ion solutions in NF process. Influence of aqueous phase composition

The use of NF process in water treatment has been proposed to improve the quality of the produced water and extend the options of concentrate valorization, taking the benefit of its different ions selectivity patterns. However, there is a need to understand and optimise the rejection not only of major components (e.g. NaCl or $MgSO_4$) but also of minor components especially in brackish waters.

The selectivity of ion rejection by NF membranes has been studied experimentally and theoretically. In this chapter, experimental ion rejection data of common cation and anion species (Na^+, Cl^-, Mg^{2+}, SO_4^{2-}) present in natural waters at various trans-membrane pressures (TMP) and cross-flow velocities (cfv) have been obtained with a NF membrane (NF270). Theoretical analysis has been performed by the SEDF model which has been recently extended to multi-ion solutions (Chapter 2).

3.1. Materials and methods

3.1.1. NF rejection experiments with brackish waters

The selected system reproduces common scenarios of low quality river surface waters receiving industrial and mining brine discharges with high contents of inorganic salts (Mg^{2+}, SO_4^{2-}, Na^+, Cl^-). Synthetic aqueous solutions of different salts were used as feed solutions for the rejection experiments. They are based on a dominant salt (NaCl, Na_2SO_4, $MgSO_4$, $MgCl_2$) mixed with trace ions (Na^+, Cl^-, Mg^{2+}, SO_4^{2-}). The concentration of dominant salt was maintained at 0.1 mol L^{-1} for all the experiments carried out while the molar concentrations of trace ions were at about 0.5-2% of dominant salt concentrations. All reagents used were of analysis quality (PA-ACS-ISO reagent, PANREAC). A summary of the performed NF experiments can be found in Table 3.1.

Table 3.1. NF experiments with brackish waters (Na^+, Cl^-, Mg^{2+}, SO_4^{2-})

Dominant salts	Trace salt	Feed concentration		Cross-flow velocity	Trans-membrane pressure	Nanofiltration Membrane
		Dominant salt (mol L^{-1})	Trace salt (mol L^{-1})	(m s^{-1})	(bar)	
NaCl	$MgSO_4$	0.1	0.002	0.35; 0.7; 1	4.5 - 20	NF270
Na_2SO_4	NaCl	0.1	0.0005	0.35; 0.7; 1	7 - 20	
$MgSO_4$	NaCl	0.1	0.0005	0.35; 0.7; 1	4.5 - 20	
$MgCl_2$	NaCl	0.1	0.0005	0.35; 0.7; 1	7 - 20	

3.1.2. FS membrane cross-flow set-up

Experimental data have been obtained with a PA-based thin-film composite NF membrane NF270 (Dow Chemical) in a cross-flow set-up equipped by a FS membrane module (GE SEPA^{TM} CF II) with a spacer-filled feed channel and the possibility of independent variation of TMP and cfv. An effective membrane area of 0.014 m^2 was provided. The schematic configuration of the membrane filtration unit is shown in Table 3.1.

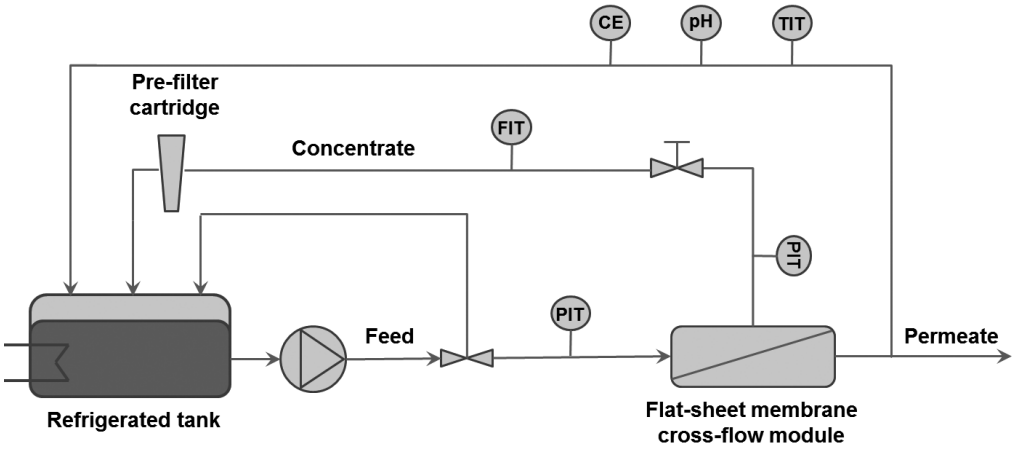

Figure 3.1. Membrane cross-flow set-up

3.1.3. Operating procedure. Monitoring of hydrodynamic and chemical parameters

Membranes were firstly cut into appropriately-sized pieces (19 cm x 14 cm) and wetted overnight in distilled water to wash-out potential storage products. Then, they were compacted with distilled water during one hour and with the working feed solution over one hour and a half at the maximum working cfv (1 m s^{-1}) and TMP (22 bar). As a result, the membranes had constant water permeabilities in all experiments.

Feed solutions were kept at constant temperature (22 ± 1ºC) in a thermostated feed tank (30 L) and pumped into the cross-flow module with a high-pressure water diaphragm pump (Hydra-Cell, USA) at a prefixed flow rate and pressure. The two output streams from the membrane module, the permeate and the concentrate, were recirculated into the feed tank, providing thus a fairly constant concentration in the feed water.

The set-points of cfv and TMP were therefore fixed by the needle valve located in the concentrate stream. So the permeate flux could be determined by collecting a permeate volume during certain period of time at specific cfv and TMP when its conductivity remained constant. The first set of membrane experiments was performed at different cfv and the TMP was varied between the osmotic pressure of the feed solution and 20 bars (Table 3.1).

A pre-filter cartridge had been also installed in the concentrate stream to protect the membrane from fouling by erosion products from the pump. The system had been also provided by flow-meters, pressure-meters, a conductivity cell, a pH-meter and a temperature sensor to control and monitor the hydrodynamic and chemical parameters. Furthermore, a data acquisition system programmed in Labview was developed to ensure the robustness of the system and obtain reproducible data. Sensor calibration was also performed under the hydrodynamic conditions used in the experimental work.

3.1.4. Analytical methodologies and chemical analysis off-line

Salt rejections were determined by using the online conductivity measurements of the feed and permeate samples as first approximation. After that, ion concentrations of feed and permeate samples were measured by ion chromatography (Dionex ICS-1000) and were used to calculate the ions rejections. The cation and anion analyses were performed by the IONPAC® CS16 cation-exchange column that uses 0.03 mol L^{-1} methane sulphonic acid eluent and the IONPAC® AS23 anion-exchange column which uses a mixture of 0.0045 mol L^{-1} Na_2CO_3 and 0.0008 mol L^{-1} $NaHCO_3$ as eluent.

3.2. Results and discussion

3.2.1. Rejection of single salts

Both the intrinsic and the observable rejections of dominant salts and the fits obtained by the SEDF model are depicted by Figure 3.2. In Table 3.2 are shown the fitted values of P_s and $P_s^{(\delta)}$ obtained by Eq.(5).

As it can be seen the measured salt rejection (R) sequence was: $R(Na_2SO_4) \approx R(MgSO_4) > R(MgCl_2) > R(NaCl)$ in accordance with (Mohammad et al., 2007; Peeters et al., 1998; Schaep et al., 1998; Zhu et al., 2011). According to Donnan exclusion mechanism, negatively charged membranes are expected to follow as retention sequence: $R(Na_2SO_4) > R(NaCl) \approx R(MgSO_4) > R(MgCl_2)$, while positively charged membranes are expected to follow: $R(MgCl_2) > R(NaCl) \approx R(MgSO_4) > R(Na_2SO_4)$. These differences in salt rejection have been mainly explained, as a preliminary hypothesis, by the electrostatic membrane surface properties associated to the presence, on the PA layer, of functional groups with acid-base properties (e.g. carboxylic, amine) (Coronell et al., 2010; Zhu et al., 2011).

As it is seen in Figure 3.2, the concentration polarization is quite noticeable especially at higher TMPs as the R_s^{int} are clearly different from the R_s^{obs} values.

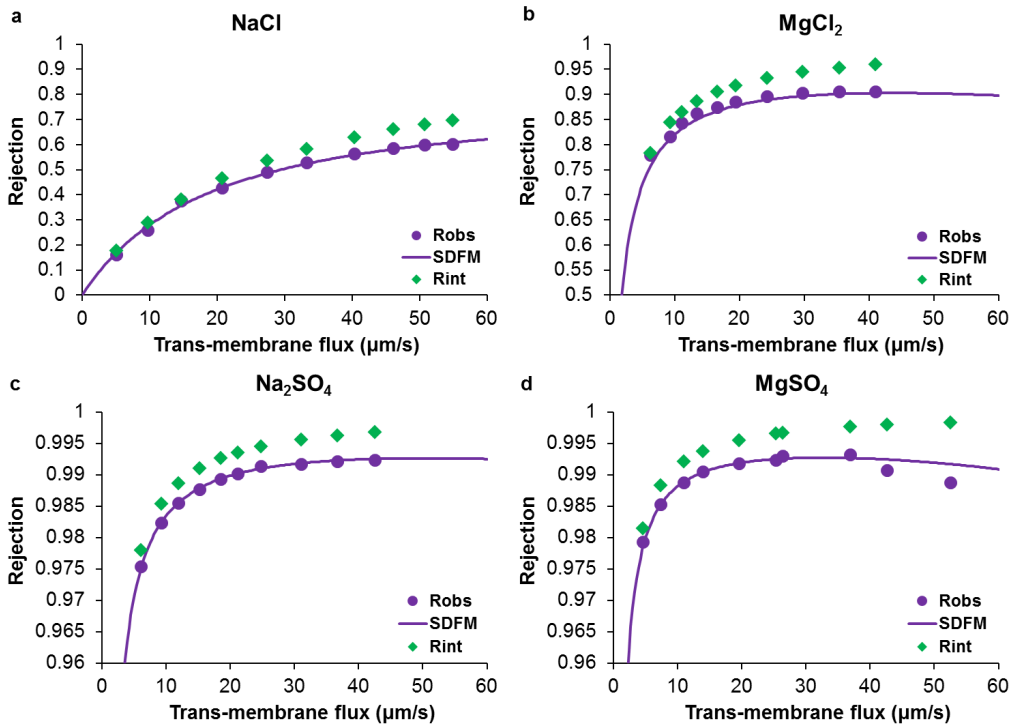

Figure 3.2. Observed rejections $\left(\boldsymbol{R_s^{obs}}\right)$ and intrinsic rejections $\left(\boldsymbol{R_s^{int}}\right)$ of dominant salts at cross-flow velocity1 m s^{-1}. Solid lines were obtained by the SEDF model.

The concentration-polarization layer permeability values obtained $\left(P_s^{(\delta)}\right)$ for the different dominant salts (Table 3.2) are correlated with their diffusion coefficients $\left(D_s^{(\delta)}\right)$ listed in Table 2.2. As it can be observed in Table 3.2, the concentration-polarization layer permeabilities $\left(P_s^{(\delta)}\right)$ to Na_2SO_4, $MgSO_4$, $MgCl_2$ are somewhat disproportionally lower than that for NaCl possibly due to the non-ideality of the solutions of these electrolytes or the effects of the ion complexation disregarded both in this model.

Analysis of the complexation constants of Na and Mg cations with chloride and sulphate ions indicate that for the dominant salt solutions (at 0.1 mol dm^{-3}) at the pH of the experiments between 5 to 6.5, salt ions are partially complexed (Puigdomènech, 2001). In the case of $MgSO_4$ solutions Mg and SO_4 ions are partially complexed as a non-charged species ($MgSO4_{aq}$), in the case of Na_2SO_4 solutions Na and SO_4 ions are partially complexed as an anionic species ($NaSO_4^-$) and in the case of $MgCl_2$ solutions Mg and Cl ions are partially complexed as a cationic complex ($MgCl^+$). For the case of NaCl the complexation effect of Cl ions to Na ions is very weak and both ions remain as monocharged species (Na^+ and Cl^-).

Table 3.2. Membrane permeabilities (P_s) and concentration-polarization layer permeabilities $\left(P_s^{(\delta)}\right)$ for the dominant salts at cross-flow velocity 1 m s^{-1}

Dominant salt	P_s (μms^{-1})	$P_s^{(\delta)}$ (μms^{-1})
NaCl	24	139
Na_2SO_4	0.16	54
$MgSO_4$	0.09	33
$MgCl_2$	2	44

Both Figure 3.2 and Table 3.2 show that salts such as Na_2SO_4 and $MgSO_4$ are much better rejected than NaCl or $MgCl_2$, respectively, despite having the same cations. Most probably, this is due to the much lower membrane permeability to the sulphates than to the chlorides. This means that (at least in sulphate-containing dominant salts) the membrane permeabilities with respect to cations and anions are different.

As expected an increase in the cfv brings about higher single-salt rejections (see Figure 3.3).

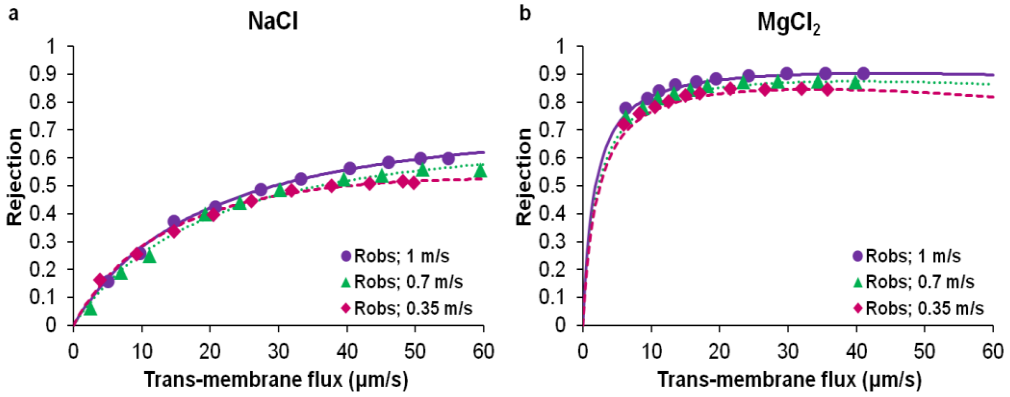

Figure 3.3. Observed rejections of NaCl and $MgCl_2$ and their fits with SEDF model at variable cross-flow velocity of 1, 0.7 and 0.35 m s^{-1}

In Table 3.3, it can be also seen that at higher cfv the concentration-polarization layer permeability $\left(P_s^{(\delta)}\right)$ is increased and the concentration-polarization layer thickness (δ) decreased. However, the membrane permeabilities (P_s) are almost constant at variable cfv. The membrane permeabilities sequence obtained by different authors for NF200 and NF270 to different salts follows P(NaCl) > P($MgCl_2$) > P(Na_2SO_4) ≈ P($MgSO_4$).

Table 3.3. Rejections of NaCl, Na_2SO_4, $MgCl_2$ and $MgSO_4$ $\left(\boldsymbol{R_s^{obs}}\right)$ and their membrane permeabilities $(\boldsymbol{P_s})$ and concentration-polarization layer permeabilities $\left(\boldsymbol{P_s^{(\delta)}}\right)$ estimated by means of SEDF model by NF270/NF200

Polyamide NF membrane	Feed composition		cfv	TMP	J_v	R_s^{obs}	P_s	$P_s^{(\delta)}$	Reference
	Salt	C_S' (mol L^{-1})	(m s^{-1})	(bar)	(μm s^{-1})	(%)	(μm s^{-1})	(μm s^{-1})	
NF270	NaCl	0.45	[1]	-	[8,90]	[7,25]	21.8*/86.5	[86.5]	(Yaroshchuk et al., 2009)
NF270	NaCl	0.17	-	[2,9]	[5,25]	[6,21]	18.5*	-	(Hilal et al., 2005b)
NF270	NaCl	0.085	-	[2,9]	[6,30]	[11,29]	13.9*	-	(Hilal et al., 2005b)
NF270	NaCl	0.085	[0.3;0.7;1.2]	-	[10,130]	[15,55]	46.5	[96;125;150]	(Yaroshchuk et al., 2009)
NF270	NaCl	0.088	[1]	-	[13,128]	[39,67]	18	[102]	(Yaroshchuk et al., 2011)
NF200	NaCl	0.085	[0.3;0.7;1.2]	-	[4,60]	[27,80]	12	[75;110;128]	(Yaroshchuk et al., 2009)
NF270	NaCl	0.1	[0.35;0.7;1]	[4.5,20]	[2.5,60]	[16,60]	24	[65;119;139]	this work
NF270	Na_2SO_4	0.22	[1]	-	[0.5,62]	[40,98]	0.76*/0.69	[85]	(Yaroshchuk et al., 2009)
NF270	Na_2SO_4	0.07	-	[2,9]	[0.1,5]	[28,95]	0.25*	-	(Al-Zoubi et al., 2007)
NF200	Na_2SO_4	0.1	[0.47]	[1,20]	[0.4,15]	[80,99]	0.05*	-	(Bason and Freger, 2010)
NF200	Na_2SO_4	0.001	[0.47]	[1,20]	[2,28]	[99]	0.01*	-	(Bason and Freger, 2010)
NF270	Na_2SO_4	0.044	[1]	-	[7,93]	[97,99]	0.2	[63]	(Yaroshchuk et al., 2011)
NF270	Na_2SO_4	0.1	[0.35;0.7;1]	[7,20]	[6,47]	[97,99]	0.14	[56;51;54]	this work
NF270	$MgSO_4$	0.125	-	[2,9]	[0.5,14]	[65,96]	0.29*	-	(Al-Zoubi et al., 2007)
NF270	$MgSO_4$	0.083	-	[2,9]	[1,16]	[83,98]	0.19*	-	(Al-Zoubi et al., 2007)
NF270	$MgSO_4$	0.1	[0.35;0.7;1]	[4.5,20]	[4.5,52]	[98,99]	0.1	[28;29;33]	this work
NF200	$MgCl_2$	0.1	[0.47]	[1,20]	[0.4,14]	[50,95]	0.42*	-	(Bason and Freger, 2010)
NF200	$MgCl_2$	0.001	[0.47]	[1,20]	[3,30]	[50,86]	1.6*	-	(Bason and Freger, 2010)
NF270	$MgCl_2$	0.1	[0.35;0.7;1]	[7.5,20]	[6,41]	[78,90]	2	[34;40;44]	this work

*Salt membrane permeabilities estimated by the Spiegler-Kedem (SK) model.

3.2.2. Ion rejections and ion membrane permeabilities

NF is carried out under conditions of zero electric current, hence the trans-membrane fluxes of cations and anions must be stoichiometric. If the intrinsic membrane permeabilities to cations and anions are different the stoichiometry of trans-membrane ion transfer can be assured only due to the appearance of trans-membrane electric fields. In electrolyte mixtures, the effect of these fields is especially visible. They give

rise to negative rejections of "rapidly-permeating" ions present as relatively small additions to well-rejected dominant salts. This is most pronounced in the limiting case of trace feed concentrations of single-charged inorganic ions illustrated by Figure 3.4.

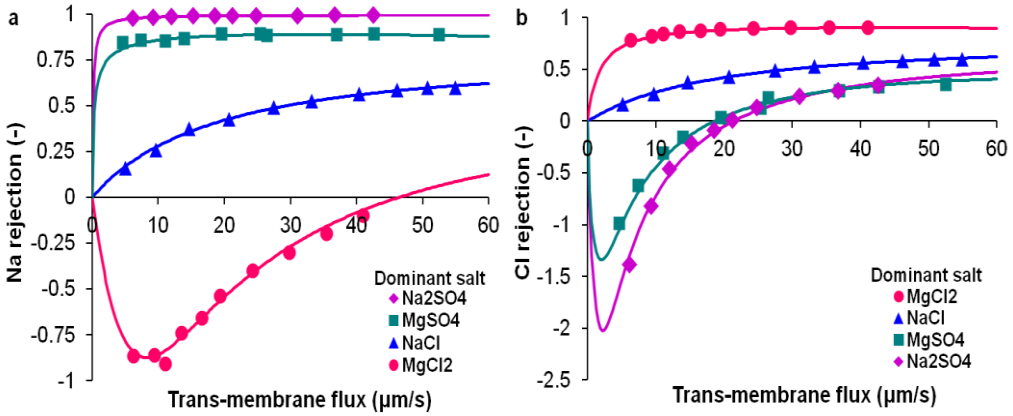

Figure 3.4. Observed rejections of Na^+ and Cl^- at cross-flow velocity 1 m s^{-1}. Solid lines were obtained by the SEDF model

Figure 3.4a shows the rejections of Na^+ as a part of NaCl and Na_2SO_4 dominant salts and as traces added to $MgCl_2$ and $MgSO_4$. In the case of dominant $MgCl_2$ the rejection of Na^+ is negative because the membrane permeability to Mg^{2+} is lower than to Cl^- as it is seen from Table 3.4. Therefore, the electric field accelerates cations such as Na^+ and makes their rejections negative. At the same time, the membrane permeability to SO_4^{2-} is still much lower than to Mg^{2+}. Accordingly, with the dominant $MgSO_4$, the trans-membrane electric field retards cations (including trace Na^+) and makes the rejections of the latter positive and relatively high (ca.90%). The dramatic difference in the rejection of sodium ions in those two cases (dominant $MgCl_2$ and $MgSO_4$) clearly demonstrates that the rejection of "rapid" ions is primarily controlled by the trans-membrane electric fields.

Table 3.4. Membrane permeabilities with respect to single ions

Dominant salt/ ion permeability (µm s^{-1})	NaCl	$MgCl_2$	Na_2SO_4	$MgSO_4$
P_{Na^+}	95.4	> 100*	> 100*	63.1
P_{Cl^-}	13.6	11.6	16.8	12.9
$P_{Mg^{2+}}$	7.95	0.65	-	0.55
$P_{SO_4^{2-}}$	0.16	-	0.05	0.05

*Value not specified as modelling becomes insensitive to the exact value at high ionic permeabilities.

Figure 3.4b shows the rejections of Cl^- as a part of dominant NaCl and $MgCl_2$, and as traces added to $MgSO_4$ and Na_2SO_4. In both sulphate-containing dominant salts ($MgSO_4$ and Na_2SO_4) the rejections of Cl^- are negative because the membrane permeability to SO_4^{2-} is lower than to both Mg^{2+} and Na^+, as it can be seen from Table

3.4. Therefore, the electric field accelerates anions such as Cl^- and makes their rejection negative at small trans-membrane fluxes. However, the double-charge dominant magnesium cations make this field weaker.

Accordingly, the negative rejections of chloride ions in dominant $MgSO_4$ are noticeably less pronounced than in dominant Na_2SO_4. For both dominant salts ($MgSO_4$ and Na_2SO_4) $P_+ \gg P_-$. The definition of parameter b shows that in this limiting case $b \to Z_t/Z_+$, which means that for single-charge anionic traces this parameter tends to -1 in Na_2SO_4 but it tends to only -1/2 in $MgSO_4$. The rejections of these two dominant salts are similar (because they are controlled by the membrane permeability to sulphates), which means that both parameter K and f_s are similar, too. Therefore, according to Eq.(8), smaller negative values of b lead to smaller negative rejections of chloride.

Thus it can be seen that the rejection of trace ions crucially depends on their "environment" namely the nature of dominant salt. The extent of asymmetry of membrane permeabilities with respect to ions of dominant salt is important for the electric fields magnitude. For example, the intrinsic membrane permeability to SO_4^{2-} is very low in dominant Na_2SO_4 and $MgSO_4$. The electric field strongly retards the cations and makes the rejection of Na^+ very high. At the same time, in dominant NaCl the direction of electric field is the same but its magnitude is essentially smaller due to the much higher membrane permeability to Cl^-.

Figure 3.5 shows the rejections of Mg^{2+} and SO_4^{2-} as traces added to dominant salts and as parts of dominant salts.

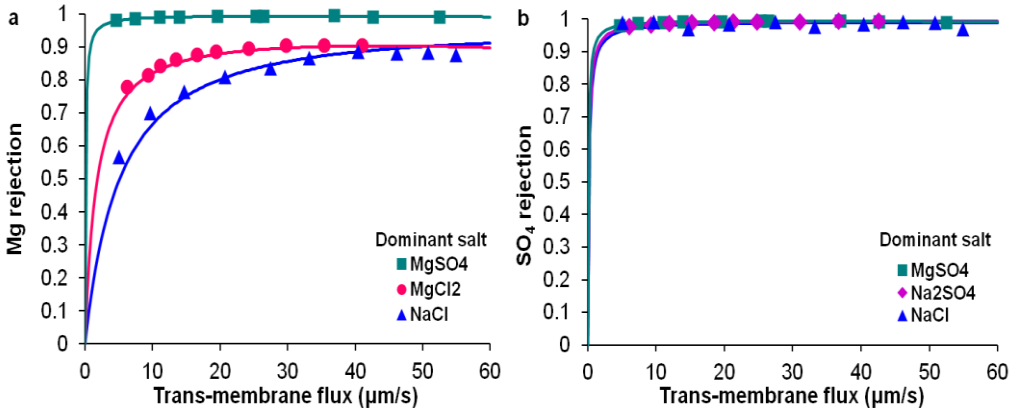

Figure 3.5. Observed rejections of Mg^{2+} and SO_4^{2-} at cross-flow velocity 1 m s^{-1}. Solid lines were obtained by the SEDF model

It is seen in Figure 3.5 that SO_4^{2-} is better rejected than Mg^{2+}. Since the membrane permeability to cations is lower than to anions in dominant $MgCl_2$, the cations are accelerated by the electric field and the rejection of Mg^{2+} is lower than in dominant $MgSO_4$ where the cations are electrically slowed down.

In dominant NaCl, cations are also slowed down electrically, and at the same intrinsic membrane permeability to magnesium ions one could expect higher Mg^{2+} rejections than from dominant $MgCl_2$. However, the experimental data show that the rejection of traces of Mg^{2+} actually was lower. This can occur only if the membrane permeability to the trace Mg^{2+} is essentially higher than to dominant magnesium ions as reflected in Table 3.4. For the moment, the mechanism of this strong dependence of ion permeability on the ion status (trace vs. dominant) is not quite clear and it is under study. Table 3.5 compares the experimental results of this work with similar studies.

As it can be seen in Table 3.4 and Table 3.5 , the divalent ions are better rejected than monovalent ones in accordance with the ionic membrane permeabilities following the sequence $P_{Na^+} > P_{Cl^-} > P_{Mg^{2+}} > P_{SO_4^{2-}}$. Typically, the rejections of divalent ions such as sulphate always reach 99% while the permeabilities to magnesium and calcium are somewhat higher.

Table 3.5. Experimental data of solutes rejections and ion membrane permeabilities from electrolyte mixtures of Na^+, Cl^-, Mg^{2+}, Ca^{2+} and SO_4^{2-} by NF270

Polyamide NF membrane	Feed composition	cfv ($m\ s^{-1}$)	TMP (bar)	J_v ($\mu m\ s^{-1}$)	Solute rejection* (%)	Ion permeability** ($\mu m\ s^{-1}$)	Reference
NF270	0.1 mol L^{-1} NaCl 0.002 mol L^{-1} $MgSO_4$	[0.35;0.7;1]	[4.5,20]	[2.5,60]	SO_4^{2-}: [97,99] Mg^{2+}: [57,88] NaCl: [16,60]	SO_4^{2-}: 0.16 Mg^{2+}: 7.95 Cl^-: 13.6 Na^+: 95.4	this work
NF270	0.088 mol L^{-1} NaCl 0.00027 mol L^{-1} Na_2SO_4	[1]	-	[13,128]	SO_4^{2-}: [98,99] NaCl: [39,67]	SO_4^{2-}: 0.13 Cl^-: 10.1 Na^+: 80.0	(Yaroshchuk et al., 2011)
NF270	0.088 mol L^{-1} NaCl 0.00038 mol L^{-1} $CaCl_2$	[1]	-	[13,128]	Ca^{2+}: [52,81] NaCl: [39,67]	Cl^-: 10.1 Ca^{2+}: 56.4 Na^+: 80.0	(Yaroshchuk et al., 2011)
NF270	0.1 mol L^{-1} Na_2SO_4 0.0005 mol L^{-1} NaCl	[0.35;0.7;1]	[7,20]	[6,47]	Na_2SO_4: [97,99] Cl^-: [-139,34]	SO_4^{2-}: 0.07 Cl^-: 19.5 Na^+: > 100	this work
NF270	0.044 mol L^{-1} Na_2SO_4 0.00022 mol L^{-1} NaCl	[1]	-	[7,93]	Na_2SO_4: [97,99] Cl^-: [-120,55]	SO_4^{2-}: 0.07 Cl^-: 10.5 Na^+: > 100	(Yaroshchuk et al., 2011)
NF270	0.1 mol L^{-1} $MgSO_4$ 0.0005 mol L^{-1} NaCl	[0.35;0.7;1]	[4.5,20]	[4.5,52]	$MgSO_4$: [98,99] Na^+: [84,89] Cl^-: [-99,36]	SO_4^{2-}: 0.05 Mg^{2+}: 0.33 Cl^-: 14.7 Na^+: 62.7	this work
NF270	0.1 mol L^{-1} $MgCl_2$ 0.0005 mol L^{-1} NaCl	[0.35;0.7;1]	[7.5,20]	[6,41]	$MgCl_2$: [78,90] Na^+: [-90,-10]	Mg^{2+}: 0.65 Cl^-: 11.6 Na^+: > 100	this work
NF270	0.044 mol L^{-1} $CaCl_2$ 0.00023 mol L^{-1} NaCl	[1]	-	[10,110]	$CaCl_2$: [67,87] Na^+: [-80,30]	Ca^{2+}: 1.8 Cl^-: 26.7 Na^+: 50.5	(Yaroshchuk et al., 2011)

*Rejection of dominant salt (R_s^{obs}) as well as of trace ion $\left(R_t^{obs}\right)$.

**Ion membrane permeabilities to single ions of dominant salt (P_+, P_- ($m\ s^{-1}$)) and to trace ions ($P_{t^\pm}$ ($m\ s^{-1}$)).

However, the rejection of monovalent ions is much more conditioned by the dominant feed composition especially at the lower trans-membrane fluxes (Figure 3.4). For instance, sodium is much more rejected in sulphate-containing (as a part of Na_2SO_4 dominant salt or as a trace ion added to $MgSO_4$) than in chloride dominant environment (as a part of NaCl dominant salt or as a trace ion added to $MgCl_2$) where negative rejections can be obtained at the lower trans-membrane fluxes (Figure 3.4a). At the same time, chloride is much more rejected in chloride dominant environment (as a part of NaCl or $MgCl_2$ dominant salts) than in sulphate dominant environment (as a trace ion added to Na_2SO_4 or $MgSO_4$ dominant solutions) where chloride negative rejections are obtained using NF270 at the lower trans-membrane fluxes (Figure 3.4b).

Negative rejections of sodium have been also reported by (Déon et al., 2011) and (Escoda et al., 2011) with electrolyte mixtures experiments performed using NF membranes as Desal DK and AFC 40. As reported by (Vonk and Smit, 1983) hydrogen negative rejections were observed with mixtures of HCl-$Ca(NO_3)_2$, HCl-$CaCl_2$ and HCl-NaCl as well as sodium negative rejections were observed with mixtures of NaCl-$CaCl_2$ using cellulose acetate RO membranes (KP90, KP96, KP98).

3.3. Conclusions

The rejections of easily-permeating ions such as single-charged inorganic ions are controlled to a larger extent by the electric field rather than by the membrane permeability to them. The experimental data with various trace ions and dominant salts confirm this hypothesis and can be qualitatively interpreted within the scope of extended SEDF model in the case of feed solutions consisting of one dominant salt and (any number of) trace ions.

The novelties of this study are the use of two trace ions at the same time (e.g. NaCl added to $MgSO_4$) and the demonstration that their rejections can be simultaneously be fitted by using the same dominant-salt-controlled parameters of the model.

This also enabled us to demonstrate that the rejection of a trace ion (e.g. Na^+) depends decisively on its environment (dominant salt: e.g. either $MgCl_2$ or $MgSO_4$). This dependence has been explained by the spontaneously arising electric fields generated in the membrane phase. The electric field gives rise to negative rejections of singly charged inorganic ions present as small additions to well-rejected dominant salts.

The application of the SEDF model to relate the intrinsic rejections to the observable ones has provided a theoretical interpretation of the intrinsic membrane permeabilities. This approach allowed determining the membrane permeabilities to cations (Mg^{2+} and Na^+) and to anions (Cl^- and SO_4^{2-}) of dominant salts as well as to the trace ions, in comparison to conventional measurements with single salts where only the salt permeability could be determined.

The selected model system reproduces common scenarios of low quality river surface waters receiving industrial and mining brine discharges with high contents of inorganic salts (Mg^{2+}, SO_4^{2-}, Na^+, Cl^-) and the measured ion membrane permeabilities will provide a better description and prediction of ions rejections in NF based membrane processes.

Further studies will need to be performed with different water matrices representing other scenarios of low quality surface waters comprising other trace ions such as ammonia, nitrate, bromide, iodide, etc.

Chapter 4

Trace ions rejection tunning in NF by selecting solution composition: ion permeabilities estimation

NF is being promoted as a new technological solution to remove both major and minor organic and inorganic compounds from aqueous solutions (Darvishmanesh et al., 2011; Sotto et al., 2013). In comparison with RO, NF needs less pressure requirements to provide the same flux (but with lower quality) and offers higher ion selectivities. Typically, NF are thin-film composites made by different polymers such as (aromatic) polyamides, polysulfone/poly(ether sulfone)/sulfonated polysulfone, polyimide and poly(piperazine amide) (Van der Bruggen and Kim, 2012).

As RO, NF membranes contain functional groups (not fully cross-linking of the carboxylic and amine groups), resulting during she synthesis stages, that can be charged, depending on the pH of the solution in contact with the membrane. At neutral pH, NF membranes can be slightly negative-charged (e.g. deprotonated forms of the carboxylic groups) as their isoelectric points are around pH 3–4.5 (Childress and Elimelech, 1996; Coronell et al., 2010, 2007; Mouhoumed et al., 2014; Oatley et al., 2012; Richards et al., 2010). Determining the functional membrane composition is still an important challenge to better explain the different ion rejections using the various kinds of NF membranes (Coronell et al., 2011, 2010; Schäfer et al., 1998).

Additionally, multi-ionic solutions occur in virtually all practical applications of membrane processes, and then the solution composition, in terms of chemical nature of the ions, especially in terms of charge (sign and number) and the relative molar

compositions, has been demonstrated to play a critical role. Rejection for a given ion does not depend only on ion properties, but also on the solution environment. As an example, recently, Umpuch et al. (Umpuch et al., 2010), investigated how the addition of strong electrolytes (e.g. NaCl or Na_2SO_4) affected the selectivity of the sodium lactate/glucose separation by NF. The addition of Na_2SO_4 (0.25 M) compared to NaCl (0.25 M) provided a maximum separation factor of 1.9 for sodium glucose (0.1 M)/sodium lactate (0.1 M) solutions whereas the separation was impossible without the addition of salt.

The predictive modelling of ion rejection in aqueous solutions using NF membranes is crucial for the optimization and scale-up of water treatment processes, and enormous effort on this field has been expended in the last decade. Ion transport through NF membranes has been widely described by either the non-equilibrium thermodynamic model and their modifications (Bason et alt. 2010; Spiegler and Kedem 1966; Yaroshchuk 2002) or with the extended Nernst–Planck equations (Bowen and Mukhtar 1996).

Among the former, the SK model equation (Spiegler and Kedem, 1966) explained the mass transport by means of the coupling between the convective solvent and the diffusive solute fluxes that lead to an electrolyte to permeate through the membrane. In order to include the interactions of solute-solvent, solute-membrane and solvent-membrane when electrolytes mixtures were employed, the SK equation was accordingly modified taking into account the influence of membrane structural parameters (Jonsson 1983) and the concentration dependence (Bason, 2009) on the phenomenological transport coefficients. Then, the number of fitting parameters was needed to be increased up to six (X. L. Wang et al., 2012). It was shown how the permeability coefficients to the water and the solutes might be derived from the experimental data and how to choose suitable electroneutrality conditions to obtain the membrane permeabilities with respect to all the ions involved in the feed solution compositions.

Simultaneously, considering up to three ion exclusion mechanisms, i.e. steric, electric (Donnan equilibrium) (Afonso and Pinho 2000; Bruni and Bandini 2009) and dielectric (Szymczyk et al. 2007), and the description of the solute transport in the membrane phase by the extended NP equation, several parameters of the membrane (such as pore size, fixed charge and dielectric properties) and the ions involved (such as size and charge) were determined. In addition, several extensions of the NP equations included macroscopic hydrodynamic and electrostatic equations to describe the equilibrium, partitioning and transport of the ions involved through a pore-flow thin-film phase. These complex equations systems also required a large number of fitting structural parameters that makes difficult the solution of the inverse problem of unambiguous determination of these from experimental data.

An alternative approach is the use of the SD model, widely applied originally in RO (Paul, 2004). Unlike the established extended NP or DSP-DE model and the SK equation, the SD model has satisfactorily explained the high SO_4^{2-}/Cl^- selectivity of

NF or the weak convective coupling between the solute and solvent transfers in the membrane phase (Bason et al. 2010; Yaroshchuk et al. 2009).

In this direction, Yaroshchuk et al. demonstrated that for single salts, the same simple version of SD model coupled with the film model theory, the SEDF model is applicable (Yaroshchuk et al., 2009). However, for electrolyte mixtures the SEDF model was needed to be extended in order to consider the coupling between the electro-diffusion fluxes of different ions via the electric field of membrane potential (Pages et al., 2013; Yaroshchuk et al., 2013, 2011). Taking into account the ion electro-diffusion fluxes in the whole membrane phase and the coupling phenomenon, a good description of ion rejection dependence on the trans-membrane flux for different electrolyte mixtures was provided (Pages et al., 2013; Yaroshchuk et al., 2011).

In this approach it is assumed that the ion mass transfer occurs via electro-diffusion through the membrane as well as in the concentration-polarization layer where it also occurs via convection by the solvent transfer. This new description of the trans-membrane mass transfer by the SEDF model allows the development of efficient procedures to characterize NF membranes by their own ion mass transfer coefficients (k_i) based on the determination not only of single salts (P_s) but also of ion membrane permeabilities (P_i) from experimental data.

The main target of this work was to extend the validation of the SEDF model by comparing experimental and theoretical data on the rejection of several dominant salts and trace ions using the NF270 membrane in a cross-flow experimental set-up. Synthetic water solutions representative of natural waters influenced by industrial and mining drainage (Na^+, K^+, Mg^{2+}, Cl^-, Br^-, I^-) and industrial wastewaters (NH_4^+, NO_3^-, SO_4^{2-}) have been used. Three different major dominant electrolyte types were used (NaCl, $MgCl_2$, $MgSO_4$). The membrane permeability with respect to several ions (Na^+, K^+, Cl^-, Ca^{2+}, Mg^{2+}, SO_4^{2-}, NO_3^-, NH_4^+, I^- and Br^-) was calculated.

4.1. Materials and methods

4.1.1. Membrane cross-flow set-up

Experiments were performed with a NF270 membrane in a cross-flow set-up equipped with a test cell (GE SEPA^{TM} CF II) with a spacer-filled feed channel and the possibility of independent variation of cfv and TMP (Pages et al., 2013). An effective filtration surface of 0.014 m^2 was provided by the FS membrane test cell. Feed solutions were kept at constant temperature (23 ± 2ºC) in a thermostated feed tank (30 L) and pumped into the cross-flow filtration system with a high-pressure water diaphragm pump (Hydra-Cell, USA) at a prefixed flow rate and pressure. The two output streams from the test cell, permeate and concentrate, were recirculated into the feed tank providing thus a fairly constant concentration in the feed water. The set-points of cfv and TMP were fixed by a needle valve located in the concentrate stream.

The system was also provided by flow-meters, pressure-meters, a conductivity cell, a pH-meter and a temperature sensor to control and monitor the hydrodynamic and chemical parameters. Furthermore, a data acquisition system programmed in Labview was developed to ensure the robustness of the system and obtain reproducible data. Sensor calibration was also performed under the hydrodynamic conditions used in the experimental work.

4.1.2. Ion rejection experimental tests of multi-ion electrolyte solutions

Several multi-ion water solutions consisting of a dominant single salt (NaCl, $MgCl_2$ and $MgSO_4$) mixed with trace ions such as Na^+, Cl^-, Ca^{2+}, Mg^{2+}, SO_4^{2-}, K^+, NO_3^-, NH_4^+, I^- and Br^- were used as feed solutions. Common scenarios of low quality surface waters influenced by industrial and mining drainage containing KCl, $MgCl_2$, KI, NaBr, etc and industrial wastewater containing NH_4^+, NO_3^-, SO_4^{2-} (Raich-Montiu et al. 2014) were reproduced by these selected model systems.

Before performing any rejection experiments, membranes were wetted overnight in distilled water to wash-out potential storage products. Then, they were compacted with distilled water for one hour and with the working solution over one hour and a half at maximum working cfv and TMP to ensure constant trans-membrane flux in all the experiments at the same pressure requirements.

The experimental tests were carried out at a fixed cfv of 0.7 m s^{-1} and the TMP was varied between osmotic pressure of feed solution (4.5-7 bar) and 20 bar. Concentrations of dominant salts in feed solutions were maintained at 0.1 mol L^{-1} while concentrations for trace ions were at about 0.5-2% dominant salt concentrations. All reagents used were of analysis quality (PA-ACS-ISO reagent, PANREAC). The rejection experiments performed with multi-ion solutions by NF270 are summarized in Table 4.1.

Table 4.1. Experimental conditions for the filtration of multi-ion solutions of Na^+, Cl^-, K^+, Ca^{2+}, Mg^{2+}, SO_4^{2-}, NO_3^-, NH_4^+, I^- and Br^- by the membrane NF270

Dominant salts	Trace salt	Feed concentration		Cross-flow velocity	Trans-membrane pressure
		Dominant salt (mol L^{-1})	Trace salt (mol L^{-1})	(m s^{-1})	(bar)
NaCl	$MgSO_4$	0.1	0.002	0.7	4.5 - 20
NaCl	$MgCl_2$	0.1	0.002	0.7	4.5 - 20
NaCl	$CaCl_2$	0.1	0.002	0.7	4.5 - 20
NaCl	KCl	0.1	0.002	0.7	4.5 - 20
NaCl	NH_4Cl	0.1	0.002	0.7	4.5 - 20
NaCl	$NaNO_3$	0.1	0.002	0.7	4.5 - 20
NaCl	NaBr	0.1	0.002	0.7	4.5 - 20
NaCl	NaI	0.1	0.002	0.7	4.5 - 20
$MgCl_2$	KCl	0.1	0.0005	0.7	7 - 20
$MgCl_2$	NH_4Cl	0.1	0.0005	0.7	7 - 20
$MgCl_2$	Na_2SO_4	0.1	0.0005	0.7	7 - 20
$MgCl_2$	$NaNO_3$	0.1	0.0005	0.7	7 - 20
$MgCl_2$	NaBr	0.1	0.0005	0.7	7 - 20
$MgCl_2$	NaI	0.1	0.0005	0.7	7 - 20
$MgSO_4$	NaCl	0.1	0.0005	0.7	4.5 - 20
$MgSO_4$	NH_4Cl	0.1	0.0005	0.7	4.5 - 20
$MgSO_4$	$NaNO_3$	0.1	0.0005	0.7	4.5 - 20
$MgSO_4$	NaBr	0.1	0.0005	0.7	4.5 - 20
$MgSO_4$	NaI	0.1	0.0005	0.7	4.5 - 20

The J_v was determined collecting permeate volume during a certain period of time at specific cfv and TMP. Ion concentrations of feed and permeate samples were measured by ion chromatography (Dionex ICS-1000). The cation and anion analyses were performed by using the IONPAC® CS16 cation-exchange that uses 0.03 mol L^{-1} methane sulphonic acid eluent and the IONPAC® AS23 anion-exchange columns. A mixture of 0.0045 mol L^{-1} Na_2CO_3 and 0.0008 mol L^{-1} $NaHCO_3$ was used as eluent. The pH of the feed and permeate solutions were measured with a pH electrode. Overall the experimental tests, pH ranged between 4.76 and 6.26 with NF270.

4.1.3. NF270 properties

NF270 (Dow Chemical) membrane was used to perform the experimental tests. Its active layers is semi-aromatic poly(piperazine) amide whose chemical structure is shown in Figure 4.1.

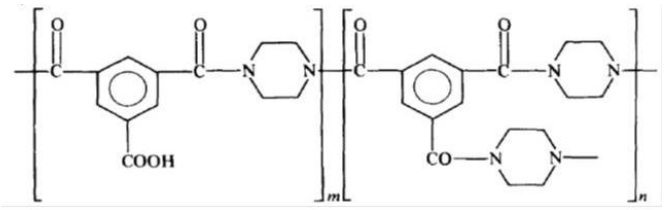

Figure 4.1. Chemical polymeric structure of NF270 membrane active layer (Koros et al. 1998)

Salt and ion permeabilities are correlated to the total dominant salt content in the membrane and to changes in the membrane effective fixed charge. The latter could be related to specific ion adsorption and competitive complexing counter-ions to the fixed charge sites of the polymer membrane structure that diminishes effective fixed charge via ion interaction.

Recently aromatic PA active layers produced by interfacial polymerization (e.g. NF270) were characterized by a concentration of ionizable functional groups (carboxylic (RCOOH/R-COO^-) and amine (R-NH_3^+/R-NH_2)) related to the degree of polymer cross-linking (Coronell et al., 2010; Kim et al., 2005).

For the case of NF270, although no data on the determination of acidity constants of the carboxylic groups have been published, most of the characterization studies of the pH indicated that at neutral pH values 6-7, carboxylic groups will be deprotonated (R-COO^-). Then, in the present study where experiments were performed at pH around 6.6 the carboxylic groups were assumed to be deprotonated (R-COO^-). Ionizable functional groups affect water and solute permeation not only because they produce pH-dependent charges in the active layer, but also because they affect the active layer structure (Coronell et al., 2011; Mi et al., 2006).

4.2. Results and discussion

4.2.1. NaCl as dominant salt

Figure 4.2 shows the observable rejection for the dominant salt (NaCl) in the presence of a trace salt (referred to as NaCl_CA, where CA is the trace salt) (Figure 4.2a) and for the trace ions (referred to as C^+ (NaCl_CA) for the cations and A^- (NaCl_CA) for the anions) (Figure 4.2b) as a function of trans-membrane flux. The symbols represent the experimental points and the lines were derived with the SEDF model equations (Table 2.1). Calculated membrane permeabilities to dominant and trace ions are

collected in Table 4.2.

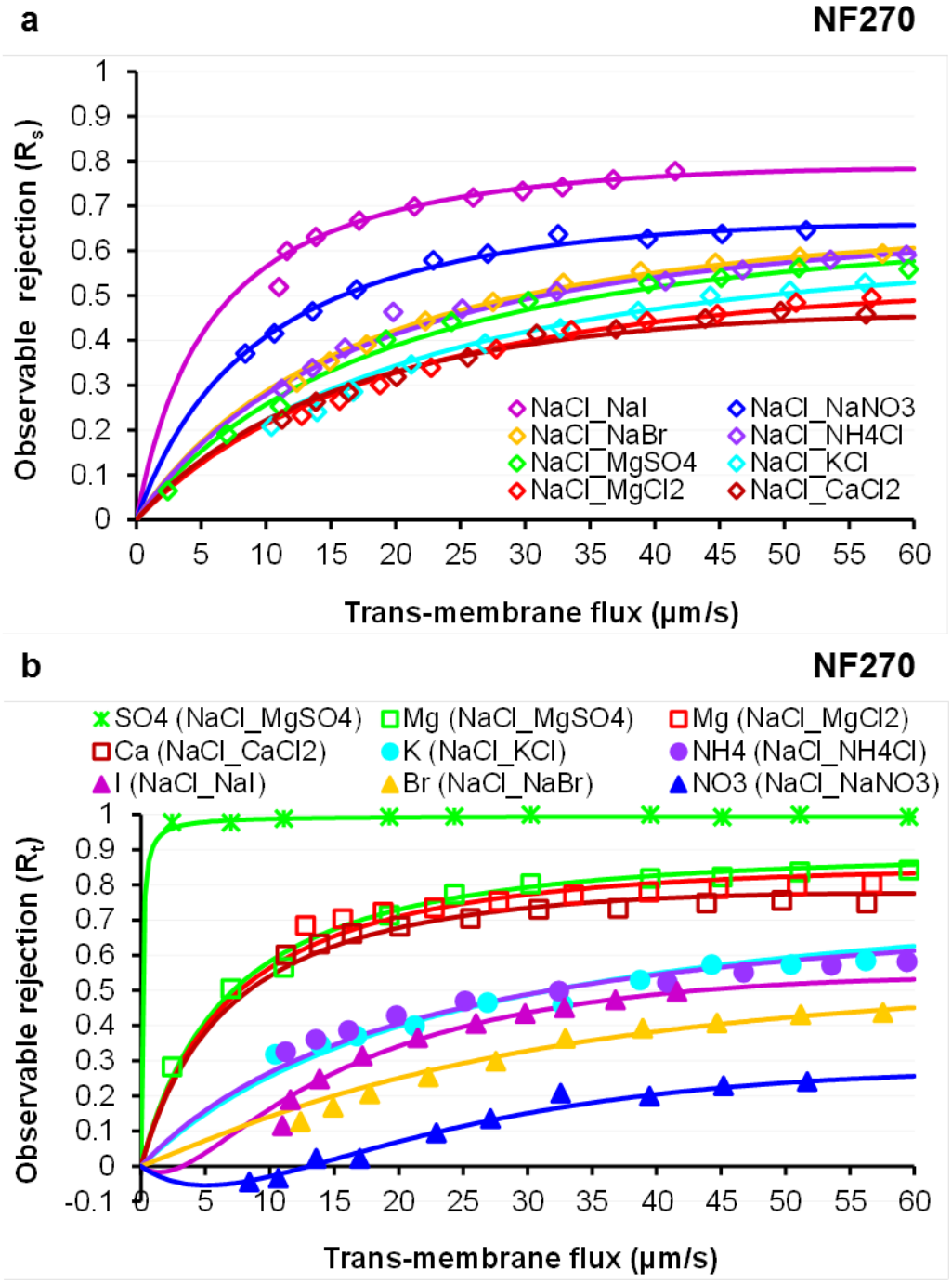

Figure 4.2. Observable rejections for the dominant salt NaCl in the presence of trace ions (Figure 4.2a) and for the trace ions (Mg^{2+}, Ca^{2+}, K^{+}, NH_4^{+}, SO_4^{2-}, NO_3^{-}, Br^{-}, I^{-}) accompanying the dominant salt (Figure 4.2b) as a function of trans-membrane flux. Lines were obtained by the SEDF model.

Table 4.2. Concentration-polarization layer and membrane permeabilities to the dominant salt $\left(\boldsymbol{P_s^{(\delta)}}, \boldsymbol{P_s}, \text{respectively}\right)$ as well as ionic membrane permeabilities $\left(\boldsymbol{P_{\pm}}, \boldsymbol{P_{t^{\pm}}}\right)$ of Na^+, Cl^-, K^+, Ca^{2+}, Mg^{2+}, SO_4^{2-}, NO_3^-, Br^-, I^- and NH_4^+ from NaCl, $MgCl_2$ and $MgSO_4$ based multi-ion solutions by using NF270 membrane.

Dominant and trace salts	**Salt permeability (μm s^{-1})**		**Ion membrane permeability (μm s^{-1})**									
	$P_s^{(\delta)}$	P_s	$P_{NH_4^+}$	P_{K^+}	P_{Na^+}	$P_{Mg^{2+}}$	$P_{Ca^{2+}}$	P_{Cl^-}	P_{Br^-}	$P_{NO_3^-}$	P_{I^-}	$P_{SO_4^{2-}}$
NaCl $MgSO_4$	119	27	-	-	106	12	-	15	-	-	-	0.09
NaCl M gCl_2	94	33	-	-	662	13	-	17	-	-	-	-
NaCl $CaCl_2$	69	30	-	-	203	-	14	16	-	-	-	-
NaCl KCl	120	32	-	202	3236	-	-	16	-	-	-	-
NaCl NH_4Cl	110	24	2358	-	298	-	-	12	-	-	-	-
NaCl NaI	65	23	-	-	96	-	-	10	-	-	9	-
NaCl NaBr	112	23	-	-	151	-	-	12	19	-	-	-
NaCl $NaNO_3$	65	21	-	-	1242	-	-	11	-	18	-	-
Dominant and trace salts	**Salt permeability (μm s^{-1})**		**Ion membrane permeability (μm s^{-1})**									
	$P_s^{(\delta)}$	P_s	$P_{NH_4^+}$	P_{K^+}	P_{Na^+}	$P_{Mg^{2+}}$	$P_{Ca^{2+}}$	P_{Cl^-}	P_{Br^-}	$P_{NO_3^-}$	P_{I^-}	$P_{SO_4^{2-}}$
$MgCl_2$ Na_2SO_4	40	2.1	-	-	2116	0.8	-	18	-	-	-	0.9
$MgCl_2$ KCl	38	2.1	-	99	-	0.8	-	9	-	-	-	-
$MgCl_2$ NH_4Cl	45	2.1	427	-	-	0.8	-	21	-	-	-	-
$MgCl_2$ NaI	50	1.9	-	-	27	0.8	-	10	-	-	12	-
$MgCl_2$ NaBr	47	2.8	-	-	63	1.1	-	14	17	-	-	-
$MgCl_2$ $NaNO_3$	38	2.2	-	-	2177	1.0	-	10	-	5	-	-
Dominant and trace salts	**Salt permeability (μm s^{-1})**		**Ion membrane permeability (μm s^{-1})**									
	$P_s^{(\delta)}$	P_s	$P_{NH_4^+}$	P_{Na^+}	$P_{Mg^{2+}}$	$P_{Ca^{2+}}$	P_{Cl^-}	P_{Br^-}	$P_{NO_3^-}$	P_{I^-}	$P_{SO_4^{2-}}$	
$MgSO_4$ NaCl	27	0.1	-	769	1	-	13	-	-	-	0.04	
$MgSO_4$ NH_4Cl	22	0.2	54	-	2	-	9	-	-	-	0.1	
$MgSO_4$ NaI	21	0.1	-	50	1	-	-	-	-	19	0.03	
$MgSO_4$ NaBr	25	0.6	-	57	5	-	-	26	-	-	0.3	
$MgSO_4$ $NaNO_3$	23	0.2	-	62	5	-	-	-	41	-	0.1	

For NF270, the rejections of the dominant salt varied between 50-60% (Figure 4.2a). Trace ions exhibited different selectivity patterns clearly depending on feed solution composition. A priori uncertain which ions, cations (C^{n+}) or anions (A^{n-}), would be the faster. The electrostatic potential gradient located between both sides of membrane, results in an electric field that accelerates or slows down the ions across the membrane, and concentrates them on both feed and permeate interfaces depending on their own ion charge.

Double-charged trace ions (SO_4^{2-}, Mg^{2+}, Ca^{2+}), were mostly better rejected than the dominant salt (NaCl) itself and the single-charged trace ions (Figure 4.2b). Particularly, the double-charged anion SO_4^{2-} was the best rejected trace ion, exhibiting a percentage removal >98% over the whole range of trans-membrane fluxes tested, followed by the double-charged cations Mg^{2+} and Ca^{2+} (with rejection percentages of 80-85% and 75% at the highest fluxes tested, respectively). This finding is consistent with the fact that the experiments were performed at pH around 6.6±0.2, whereby the carboxylic groups of the PA membrane were assumed to be deprotonated (R-COO^-) so the permeability to C^{n+} was expected to be significantly higher than that to A^{n-}.

With regards to single-charged trace ions, cations (K^+ and NH_4^+) were better rejected than anions (I^-, Br^-, NO_3^-) just in opposite way of double-charged trace ions (Figure 4.2b). Although, K^+ and NH_4^+ rejections showed both a very similar pattern increased up to 60%, anions were rejected up to 50% (for I^-), 45% (Br^-) and 20% (NO_3^-) at largest trans-membrane fluxes. Besides that, negative rejections of NO_3^- (-5%) were observed at smallest trans-membrane flux (Figure 4.2b). Indeed, NO_3^- was more quickly transported to the permeate than Cl^- as their ion membrane permeability values show (Table 4.2).

4.2.2. $MgCl_2$ as dominant salt

The observable rejections of the dominant salt $MgCl_2$ and the trace ions over the trans-membrane fluxes are shown in Figure 4.3a and Figure 4.3b respectively, and following the notation described above in section 4.2.1. Experimental data are represented with symbols whereas their modelling by the SEDF model is shown by lines. The calculated membrane permeabilities towards the dominant salt and the trace ions by the SEDF model are presented also in Table 4.2.

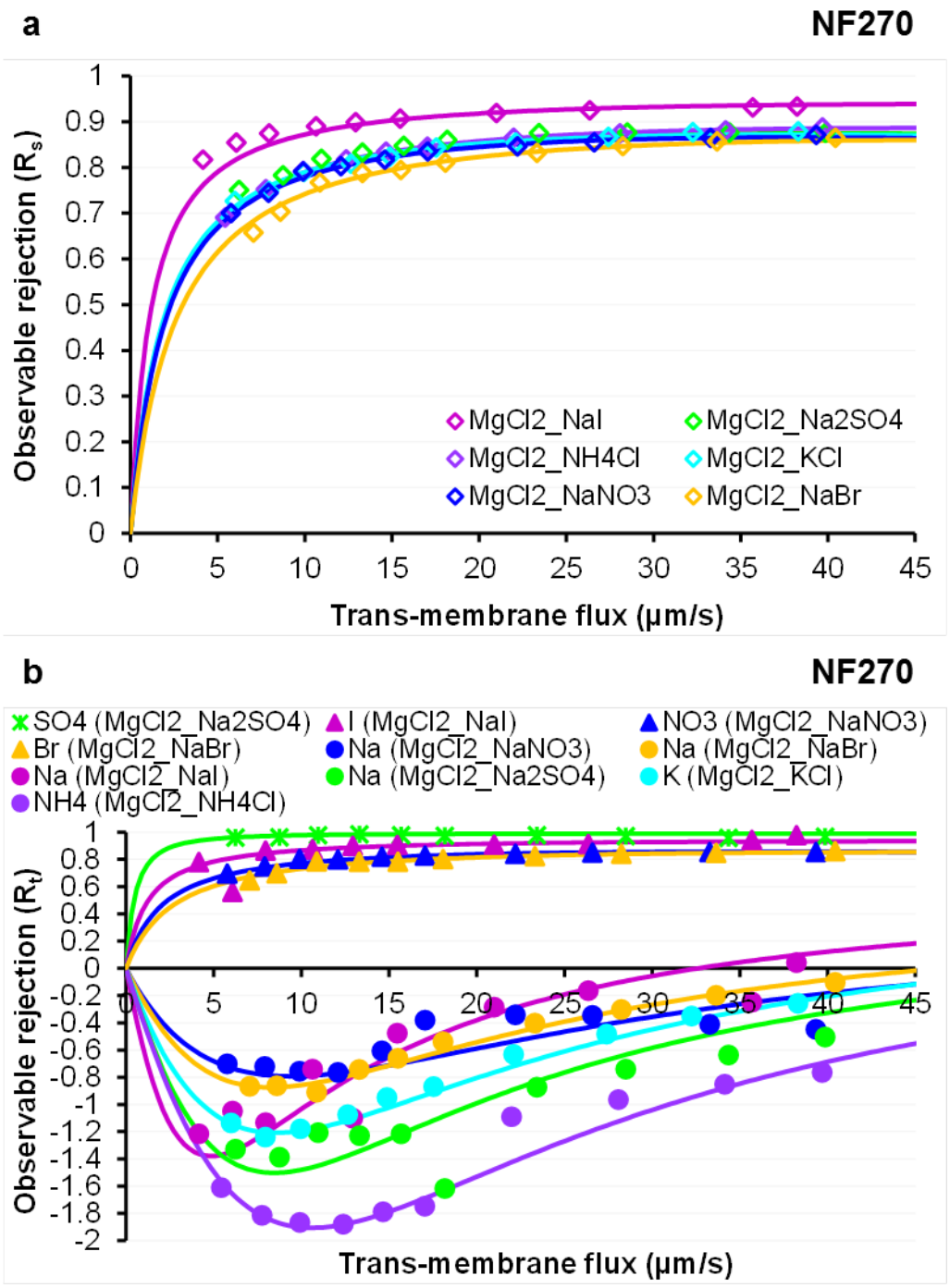

Figure 4.3. Observable rejections for the dominant salt $MgCl_2$ in the presence of trace ions (Figure 4.3a) and for the trace ions (Na^+, K^+, NH_4^+, SO_4^{2-}, NO_3^-, Br^-, I^-) accompanying the dominant salt (Figure 4.3b) as a function of trans-membrane flux. Lines were obtained by the SEDF model.

It can be observed that the dominant salt and the trace anions were fairly well-rejected (with removal percentages between 60% and 100%) (Figure 4.3a and Figure 4.3b) while the trace cations were poorly rejected showing even negative values (with removal percentages between (-10% and -190%) almost over all trans-membrane

fluxes (Figure 4.3b)).

Compared to NaCl-dominant salt, dominant $MgCl_2$ exhibited higher rejections (85-95%) at the highest trans-membrane fluxes (Figure 4.3a). Similarly to the dominant salt $MgCl_2$, high rejections were also observed for double-charged (SO_4^{2-}) and single-charged (I^-, NO_3^-, Br^-) trace anions (97-99% and between 85-95%, respectively, from intermediate to largest trans-membrane fluxes).

On the other hand, single-charged trace cations exhibited very different rejection patterns, with most of them showing negative rejections over the whole trans-membrane fluxes (Figure 4.3b). The observed rejections at maximum trans-membrane fluxes were mostly in the range of -55% and 5% for Na^+ (depending upon the trace salt involved), -25% for K^+ and -75% for NH_4^+. At lower trans-membrane fluxes, these ions exhibited even lower (i.e. more negative) rejection values, with minima at -75% for Na^+ at a trans-membrane flux of 7 µm/s or -190% for NH_4^+ at a trans-membrane flux of 12 µm/s. Although, the highest negative rejections of K^+ and NH_4^+ being -125% and -190% respectively, were larger than the highest of Na^+ having negative single-charged counterions (Cl^- or Br^-). In addition, the highest negative rejection of Na^+ with SO_4^{2-} as a counterion was larger than this of K^+ but smaller than this of NH_4^+.

To sum up, the negative rejection (i.e. permeation through the NF membrane) of the positive single-charged trace ions appeared to follow the sequence (in decreasing order): $NH_4^+ > Na^+(Na_2SO_4) > Na^+(NaI) \sim K^+(KCl) > Na^+(NaBr) \sim Na^+(NaNO_3)$ inversely in accordance with the positive rejection sequence of their negative trace counterions which was $SO_4^{2-} > I^- > Br^- \sim NO_3^-$ (Figure 4.3b). This finding confirmed that both positive and negative trace ions rejections were strongly controlled by the same magnitude of the electric field which was spontaneously arisen depending on all involved ions in each experimental test.

Results showed that a NF membrane containing negative-charged functional groups (carboxylic groups) at the working solution pH, the substitution of the dominant salt from NaCl to $MgCl_2$ promotes the possibility to remove from feed solutions all the mono-charged trace cations (Na^+, K^+, NH_4^+) present in solution (rejections below 0% along the pressure range evaluated).

4.2.3. $MgSO_4$ as dominant salt

Figure 4.4 shows the observable rejection for the dominant salt $MgSO_4$ in presence of different trace salts (CA) (Figure 4.4a) and for trace ions (Figure 4.4b) as a function of the trans-membrane flux and following the notation described above in section 4.2.1. The symbols represent the experimental points and the lines were derived by the SEDF model. The calculated membrane permeabilities to dominant and trace ions are collected in Table 4.2.

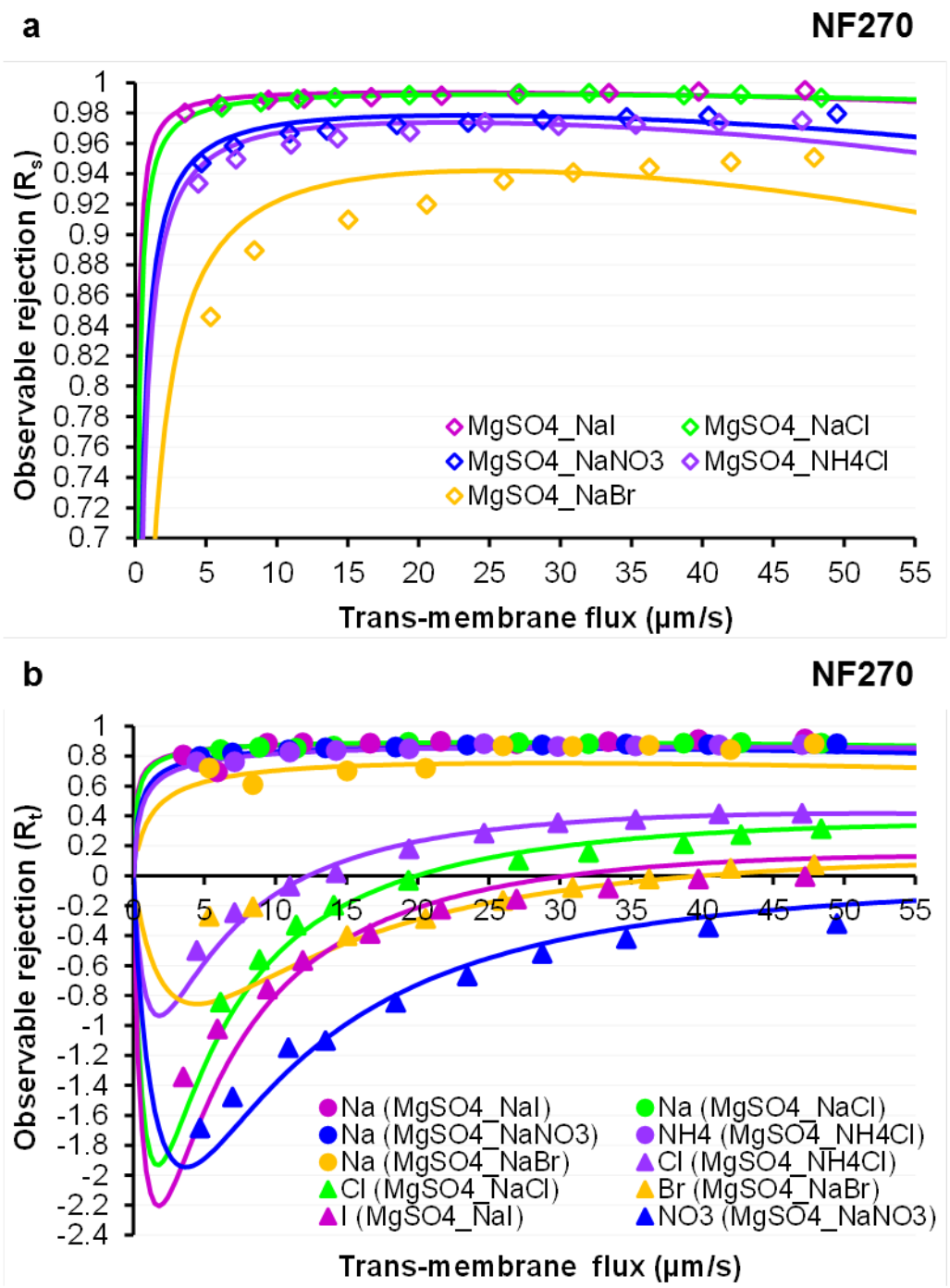

Figure 4.4. Observable rejections for the dominant salt $MgSO_4$ in the presence of trace ions (Figure 4.4a) and for the trace ions (Na^+, NH_4^+, Cl^-, NO_3^-, Br^-, I^-) accompanying the dominant salt (Figure 4.4b) as a function of trans-membrane flux. Lines were obtained by the SEDF model

When dominant $MgSO_4$-based solutions were treated by NF270 membrane, both the dominant $MgSO_4$ (Figure 4.4a) and the single-charged trace cations (Na^+ and NH_4^+) (Figure 4.4b) were very highly rejected over all trans-membrane fluxes (in the removal ranges of 85-99% and 70-90%, respectively). The rejection of Na^+ and NH_4^+ seemed

little influenced by their counter-ion although a subtle rejection sequence depending on their counter-anion was observed as follows: Na^+(NaI) > Na^+(NaCl) > Na^+($NaNO_3$) > NH_4^+(NH_4Cl) > Na^+(NaBr) being in accordance with the dominant salt rejection sequence obtained $MgSO_4$(NaI) ≈ $MgSO_4$(NaCl) > $MgSO_4$($NaNO_3$) ≈ $MgSO_4$(NH_4Cl) > $MgSO_4$(NaBr), that was also dependent on the anions from the trace salts.

The single-charged trace anions were poorly rejected showing a wide range on their rejections and even including negative values (removal percentages between -170% and 40%) over all trans-membrane fluxes (Figure 4.4b). At the highest trans-membrane flux, Cl^- was the most rejected regardless the form in which it was added (40% and 30% when it was added as NH_4Cl and NaCl, respectively), followed by Br^- and I^- (with rejection values lower than 10%) and finally NO_3^-, which was negatively rejected over all trans-membrane flux.

At low trans-membrane flux, the highest negative rejections of the single-charged anion patterns were determined by the following retention sequence: Cl^- (-50% (NH_4Cl)) < Br^- (-65%) < Cl^- (-84% (NaCl)) < I^- (-135%) < NO_3^- (-168%), that was similarly to the retention sequence achieved at highest trans-membrane flux.

As described by Umpuch et al. (Umpuch et al., 2010) the separation factor of mixtures of lactate/glucose was achieved by addition of strong electrolytes (Na_2SO_4 or NaCl) taking benefit of both the power of the dielectric exclusion and the nature of the dominant ions. Then, for example single-charged cations (organic or inorganic) could be removed from an aqueous solution with a membrane having negatively charged functional groups at the pH of the treated solution by using for example a (+2/-1) electrolyte type (e.g. $MgCl_2$, $CaCl_2$ or $BaCl_2$) promoting the permeation of single-charged cations although dominant cations (Mg^{2+}, Ca^{2+} or Ba^{2+}) would be highly rejected.

Figure 4.3 shows that the use of a 0.1 M $MgCl_2$ solution provides a 100% permeation of Na^+ /K^+/NH_4^+ ions. If the desired objective is to hardly permeate single-charged trace anions, a (+2/-2) electrolyte type (e.g. $MgSO_4$) could be used. In Figure 4.2, permeation values for halide ions (Cl^-, Br^- and I^-) and NO_3^- were below 10%, and separation factors close to 1.5 would be achieved.

4.2.4. Membrane permeabilities to dominant salt and trace ions: dependence on electrolyte type

The difference in the rejections of the dominant and the trace ions lies on the membrane permeabilities towards them, which have been calculated by means of the SEDF model as summarized in Table 2.1.

Salt membrane permeabilities decreased from the highest value 20-30 μm/s measured for NaCl (an electrolyte with two single-charged species (1:1, Na^+/Cl^-)) to 1.8-2.8 μm/s for $MgCl_2$ (an electrolyte with one double-charged and two single-charged species (1:2, Mg^{+2}/Cl^-)) and down to 0.1-0.6 μm/s for $MgSO_4$ (an electrolyte with two

double-charged species (1:1, Mg^{2+}/SO_4^{2-})).

Among the different mechanisms used for describing ion rejections by NF membranes, the dielectric exclusion mechanism justified the permeability values measured in this study. Yaroshchuk (Yaroshchuk, 2000) postulated dielectric exclusion as one of separation mechanisms of NF. Dielectric exclusion is caused by the interactions of ions with the boundary electric charges induced by ions at interfaces between media of different dielectric constants or due to the presence of ionizable groups present on the membrane (e.g. carboxylic and amine groups of NF270).

The dielectric exclusion from the polymer network pores of the membranes with closed geometry is shown to be essentially stronger than that from free volume with relatively open geometry. Originally it was common to believe that their main rejection mechanism was the Donnan exclusion caused by a fixed electric charge. That conclusion was based, in fact, on the only observation that double-charged anions were rejected essentially better than single-charged ones. However, that is characteristic of dielectric exclusion too.

According to Kim et al. (Kim et al., 2005) thin film PA layers of RO and NF membranes have a bimodal distribution with sizes (e.g. 2.1-2.4 Å and 3.5-4.5 Å for FT30 RO membrane), which is just the range where the dielectric exclusion can be strong. In principle, that mechanism is more universal than the Donnan exclusion because a membrane may have or may not have a fixed charge (e.g. NF270 as a function of the pH) whereas the existence of a low dielectric constant matrix is beyond any doubt. Thus, due to the dielectric exclusion membranes protect themselves from the intrusion of ions which gives rise to the screening of dielectric exclusion itself.

Both mechanisms, the dielectric and Donnan exclusions, cause a rejection of ions. However, they are far from being simply additive, and the interaction between them is non-trivial. Indeed, it has been shown that a fixed charge makes the screening of interactions with polarization charges stronger thus making the dielectric exclusion weaker (Bandini and Vezzani, 2003; Yaroshchuk, 2000).

At the same time the dielectric exclusion is equivalent to a decrease in the bulk electrolyte concentration. The latter is known to cause an increase in the Donnan exclusion. Thus, the dielectric exclusion makes the Donnan exclusion stronger, whereas the presence of fixed charge makes the dielectric exclusion weaker. That can be illustrated by the effect of dielectric exclusion on the relationship between fixed charge density and Donnan potential. It essentially depends on the pore geometry parameter and the type of electrolyte according to the ions valence.

For instance, for single-charged electrolytes (e.g. NaCl) dielectric exclusion is lower than for electrolytes (e.g. $MgCl_2$) with a double-charged counter-ion, which in turn is lower than for electrolytes containing two double-charged ions (e.g. $MgSO_4$). Therefore in the case of electrolytes with double-charged counter-ions such as $MgSO_4$

a fixed charge of considerable magnitude is likely to cause a decrease in the reflection coefficient. At the same time a fixed charge of moderate magnitude may be beneficial for membrane performance. This behaviour has been extended to other electrolytes data for NF270 reported in the literature and the same trend is reported, as it is the case of $CaCl_2$ and Na_2SO_4 with permeability values of 4.8-5 μm/s, and 0.1-0.2 μm/s, respectively (Pages et al., 2013; Yaroshchuk et al., 2011).

A second phenomenon related to the presence of charges on the membrane structure should be stressed. As previously reported above, the isoelectric point at the solution pH, the free carboxylic groups are ionized. Then, for a given electrolyte, the negative ion (e.g. Cl^- in NaCl and $MgCl_2$ and SO_4^{2-} in $MgSO_4$), will suffer from electrical repulsion, and then rejected in a stronger way than the positively charged ion (e.g. Na^+ in NaCl or Mg^{2+} in $MgCl_2$ and $MgSO_4$). This is in agreement with the measured ion permeabilities, where the most potentially fast ion from this couple (Na^+, Mg^{2+}) is expected to be the Na^+. Na^+ has the largest ion permeability >100 for all the experiments with NaCl as dominant salt higher than Mg^{+2}, affected additionally by the dielectric exclusion effect. With regards to anions, the potentially fastest ion was Cl^- with permeability values of 11-17 μm/s for both NaCl and $MgCl_2$ dominant salts, followed by SO_4^{2-} with permeability values of 0.05-0.1 μm/s for dominant $MgSO_4$, due to the dielectric exclusion effect. Similar values of permeability for SO_4^{2-} were reported by Pages et al. (Pages et al., 2013) for dominant Na_2SO_4 salt experiments.

The influence of the nature of the dominant electrolyte on the membrane permeability to the trace ions was also extracted from experimental data by using the SEDF model. Results, collected in Table 4.2, showed that membrane permeabilities to trace cations (Na^+, Mg^{2+}) were similar as those determined for them in experiments as dominant salt. Then, size exclusion mechanism as it is claiming in some NF models is not having a relevant contribution for Na^+ rejections and solution composition (nature of the dominant electrolyte) and the membrane properties are having a highest contribution.

Membrane permeability values to NH_4^+ were approx. 400 μm/s and 2300 μm/s in NaCl- and $MgCl_2$-dominated solutions, respectively, much higher than the value of 54 μm/s corresponding to a $MgSO_4$-dominated solution. This latter low value is due to the fact that in a solution dominated by a (+2/-2) electrolyte type, the negatively charged ion (SO_4^{2-} in this case) accelerates trace anions permeation while des-accelerates the transport of cations such as NH_4^+. The same explanation as before applies to the permeability values to K^+ (approx. 200 μm/s and 100 μm/s for NaCl- and $MgCl_2$-dominated solutions, respectively) are slightly lower than to NH_4^+.

It is of particular mention the behaviour of ion permeability of Na^+. For dominant NaCl and $MgCl_2$ solutions Na^+ ion is showing the highest ion permeabilities with values higher than 100. However in dominant $MgSO_4$ solutions as trace values of rejection measured range from 0 up to 80% at the maximum linear velocity. For the case of anionic species, sulfate ions as trace component in $MgCl_2$ and NaCl, solutions provided permeability values similar to those for dominant salts as well as chloride

ions in $MgSO_4$ dominant salt concentration. For the case of non-common anions such as Br^-, I^- and NO_3^-, values reported were similar to a monovalent ion as Cl^-. Both Br^- and I^- have similar chemical properties, although different size properties as it is reported by the hydrated radius with values of 330 pm, and 340 pm respectively, and 195 pm for Cl^-. However this has not been traduced in such different ion permeabilities as it is claimed by models considering size exclusion effects. Similarly NO_3^- (340 pm hydrated radius), a single-charged ion, with also similar permeability values to halide anions.

4.3. Conclusions

In order to study the effect of dominant salt concentration on the removal of trace ions (Na^+, K^+, Cl^-, Ca^{2+}, Mg^{2+}, SO_4^{2-}, NO_3^-, NH_4^+, Br^- and I^-) a set of NF experiments with different dominant salts (NaCl, $MgCl_2$, $MgSO_4$) was designed. The rejections of easily-permeating ions such as single-charged inorganic ions in NF membranes containing ionizable free carboxylic and amine groups are controlled to a larger extent by a combination of the electric field, the membrane permeability to them, the membrane properties and the solution composition. The experimental data with various trace ions and dominant salts confirm this hypothesis and can be qualitatively interpreted within the scope of extended SEDF model in the case of feed solutions consisting of one dominant salt and (any number of) trace ions.

The applicability of the SEDF model was confirmed, since it was possible to fit the experimental data by means of the model, even in the case of negative rejections. The successful SEDF model fitting highlighted the importance of the polarization layer and electric-field effects on which the model is based. The study has demonstrated severe changes on the selectivity rejection of inorganic ions as Br^-, I^-, NO_3^-, NH_4^+, K^+ depending on the environment solutions. Although the information on the membrane permeabilities to ions has remained empirical in this study, in principle, it can further be used for the verification of self-consistency of various mechanistic models. The availability of three “measurable” quantities, the membrane permeabilities to the cations and anions of the dominant salt as well as to the trace ions, in contrast to just one permeability to the salt available from conventional measurements with single salts, can make self-consistency checks much more conclusive.

Chapter 5
Ion rejections analogues by NF flat sheet (FS) and spiral wound (SW) configurations

5.1. Materials and methods

5.1.1. Definition of membrane module designs

The module is the main part of any membrane plant. For this reason, some important aspects have to be taken into consideration for its design, such as the membrane packing density, cost-effective manufacture, easy access for cleaning, and cost-effective membrane replacement. According to design considerations, several module configurations have been developed such as the tubular module, the hollow fibre or the capillary module, the FS modules and the SW modules (Pabby et al., 2008).

The filtration process in both FS and SW configurations is carried out in cross-flow mode, so that the feed solution circulates axially across the module while the permeate is tangentially produced due to a positive pressure gradient. FS configuration is commonly used at lab scale due to its overall dimension and low productivity. FS packing densities of about 100-400 m^2/m^3 are achieved. Some FS modules exist at industrial scale but they are not comfortable operated due to bearing a lot of layers and high space requirements. The main benefit of working at lab scale with any membrane configuration is the low installation cost (Giorno and Drioli, 2000).

Essentially, in SW modules two or more membrane pockets are wound around a centrally located permeate collecting tube with a special mesh used as spacer. The membrane pocket consists of two membrane sheets with a highly porous material (the porous-intermediate and the support layers) in-betweens, which are glued together along three edges. The fourth edge of the pocket is connected to the collecting tube. Several such pockets which are SW around the perforated permeate tube have a feed-side spacer placed between them. Usually, several such membrane elements are arranged in one pressure vessel (Pabby et al., 2008). The feed-side flow is strictly axial, while the permeate flows through the porous support inside the pocket, along the spiral pathway to the collecting tube (Hillis, 2000). SW modules are characterized by providing high packing density (>900 m^2/m^3) such being compact modules that are also resistant to fouling at higher pressures. Most of the commercially available NF membranes are made in SW configuration (Schäfer et al., 2005).

Commonly FS configuration is used at lab-scale test membrane to evaluate the ions rejections of interest by the NF process under given conditions whereas SW configuration is used at industrial scale because of the need for a larger active membrane area and space optimization. Ribera et al. (Ribera et al., 2013) have been doing a comparison of both membrane configurations by working at constant TMP and constant J_v .They concluded that the experimentation at lab-scale plant can be useful to design a full scale plant.

In this chapter, a comparison between FS and SW configurations has been performed by varying the TMP and the J_v. A rejection curve has been obtained for each ion and each membrane configuration by using different synthetic mixtures based on a dominant salt combined with a trace salt as feed solution in each experiment. The SEDF model which has been developed by Yaroshchuk et al. (Yaroshchuk et al. 2009, Yaroshchuk et al. 2011) was used to describe the experimental data.

5.1.2. Rejection experiments by FS and SW NF processes

Both FS and SW set-ups were equipped by the same sort of NF membrane (NF270, Dow Chemical) to evaluate the influence of the membrane plant configuration on the ion rejection. The effective membrane area of the SW module (2.6 m^2) was near 190 times larger than FS module's one (0.014 m^2). The main features of NF270 and the operating limits of both pilot plants described by the manufacturer can be found in Table 5.1.

Table 5.1. NF270 specifications and operation limits of the membrane pilot plants

Membrane material	Polyamide thin-film composite
Maximum operating temperature	45 ºC
Maximum operating pressure	41 bar
Maximum feed flow rate	1.4 m^3/h
Maximum pressure drop	1.0 bar
pH Range, continuous operation	2 – 11
pH Range, short-term cleaning (30 min)	1 – 12
Maximum feed silt density index (SDI)	SDI 5
Free chlorine tolerance	< 0.1 ppm

The operating procedure in both FS and SW configurations was nearly the same. The membrane module was previously compacted by distillated water and subsequently, by the working solution at the limiting operating conditions. Then, the experiment was driven at increasing pressure gradients in closed loop by recirculating the permeate and the concentrate streams into the feed tank.

Multi-parameter sensors had been also installed to monitor the process in SW configuration while the TMP set-point was manually fixed along the needle valve settled in the concentrate stream. TMP was varied from the osmotic pressure to 20 bar and the temperature was kept constant (21.5 ± 2.5ºC), although the permeate flow-rate produced by the SW module was ranged between 1 and 3 $L \cdot min^{-1}$.

The main contrast between both configurations is that the minimum volume required to work with a NF SW module of 2.5'' is 100 L while the FS module used 25 L as maximum. Both membrane set-ups which worked under the same operating procedure were depicted by Figure 3.1 whose procedure was described on section 3.1.3

An objective and reliable performance comparison between both configurations was achieved by working with the same based feed solutions made of one dominant salt mixed with one trace salt. A summary of the rejection experiments analogues carried out by both FS and SW configurations is found in Table 5.2.

Table 5.2. Rejection experiments performed with multi-ion solutions by FS and SW NF configurations (NF270)

Dominant salt	Trace salt	Feed concentration		Trans-membrane pressure
		Dominant salt (mol L^{-1})	Trace salt (mol L^{-1})	(bar)
NaCl	$MgSO_4$	0.1	0.002	4.5 - 20
NaCl	NaI	0.1	0.002	4.5 – 20
NaCl	NaBr	0.1	0.002	4.5 - 20
NaCl	$NaNO_3$	0.1	0.002	4.5 – 20
NaCl	NH_4Cl	0.1	0.002	4.5 - 20
NaCl	KCl	0.1	0.002	4.5 – 20
$MgSO_4$	NaI	0.1	0.0005	4.5 – 20
$MgSO_4$	NaBr	0.1	0.0005	4.5 - 20
$MgSO_4$	$NaNO_3$	0.1	0.0005	4.5 – 20
$MgSO_4$	NH_4Cl	0.1	0.0005	4.5 - 20
Na_2SO_4	KCl	0.1	0.0005	7 – 20
$MgCl_2$	NaI	0.1	0.0005	7 – 20
$MgCl_2$	NaBr	0.1	0.0005	7 – 20
$MgCl_2$	$NaNO_3$	0.1	0.0005	7 – 20
$MgCl_2$	NH_4Cl	0.1	0.0005	7 – 20
$MgCl_2$	KCl	0.1	0.0005	7 – 20

5.2. Results and discussion

5.2.1. NaCl dominant

Figure 5.1 shows the experimental rejections of NaCl (used as dominant salt) and Mg^{2+} and SO_4^{2-} (Figure 5.1a) and NO_3^- (Figure 5.1b) as traces for both FS and the SW configurations along different J_v and also the predicted rejections by the SEDF model.

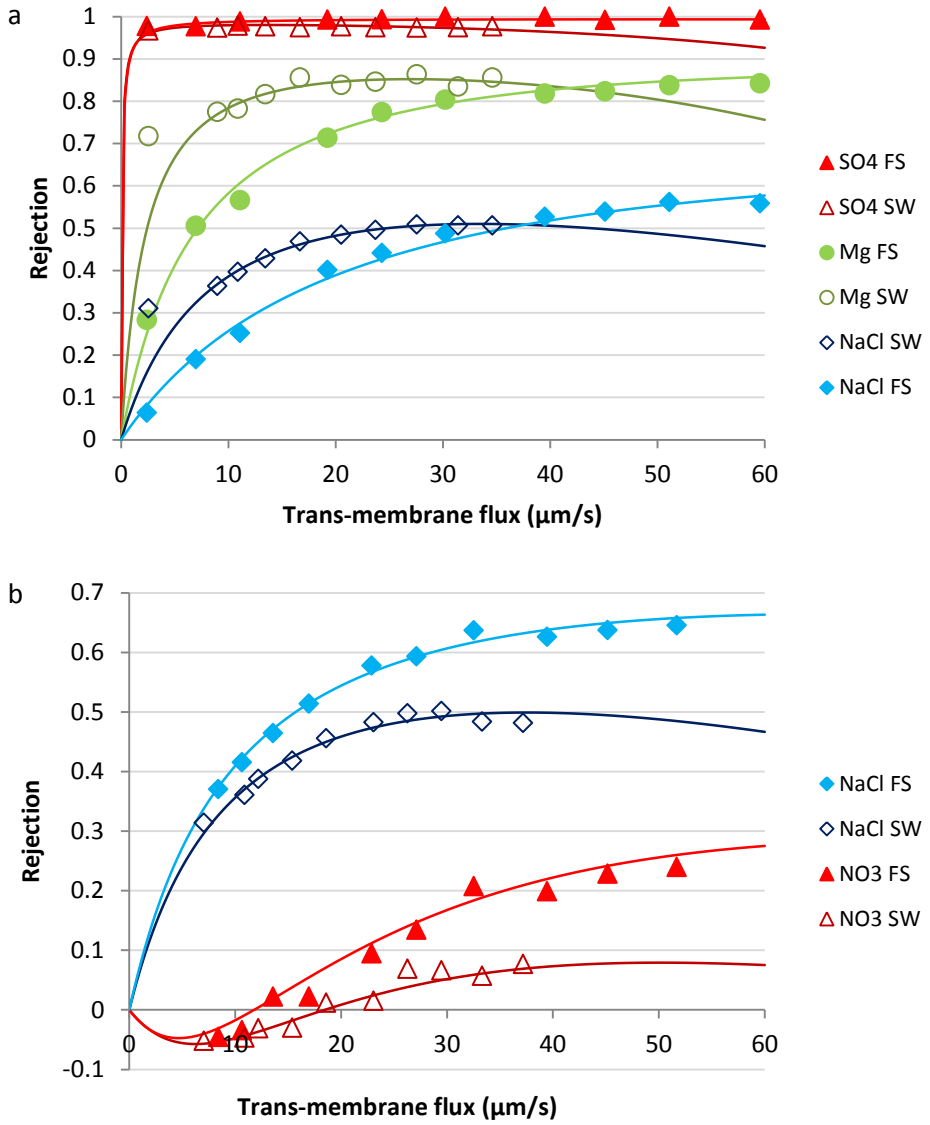

Figure 5.1. Comparison between rejections experimentally obtained and rejections predicted with the SEDF model using a FS and a SW membrane configurations a) NaCl dominant salt and $MgSO_4$ as trace b) NaCl dominant salt and $NaNO_3$ as trace. Solid lines were obtained by SEDF model.

The dominant salt and trace ion rejections are shown in Figure 5.1. Generally, ionic species rejection using NF membranes describes an increasing curve as TMP, and consequently J_v increases until a maximum rejection value where the rejection remains constant although varying the TMP. Figure 5.1 shows that rejection trends under both configurations were similar.

In both cases, NaCl exhibited a moderate stable rejection at around 50%. The dominant salt rejection is independent of the trace salt (with divalent ions $MgSO_4$ or monovalent $NaNO_3$). It is known that NF membranes reject divalent ions better than single charged ones and that trace rejection depends only on the dominant salt rejection. The concentration of the trace is too low to modify the conditions in the

membrane, thus, the use of a divalent (SO_4^{2-}) or monovalent ion (NO_3^-) as part of a trace salt does not represent a substantial effect on the NaCl rejection obtained for both experiments.

When $MgSO_4$ was used as trace salt, SO_4^{2-} and Mg^{2+} were highly rejected with rejections of 99% and around 85%, respectively at J_v around 40 µm/s. The rejection order obtained was R(SO_4^{2-}) > R(Mg^{2+}) > R(NaCl). These patterns are in accordance with results reported in previously NF studies for NaCl (Lee and Lee, 2007; Pontié et al., 2008; Walha et al., 2007), SO_4^{2-} (Bódalo et al., 2004; Galiana-Aleixandre et al., 2011) and Mg^{2+} (Afonso et al., 2004) rejections.

Noteworthy is the rejection pattern of NO_3^- which shows much lower rejection and even negative values at low J_v. Negative rejections can be explained as reported in previous studies (Pages et al., 2013). The magnitude of the electric field depends on the difference between the membrane permeability with respect to dominant salt ions, so that if the membrane permeability with respect to the dominant anion is smaller than to the dominant cation, there is a delay of the trace cation and an acceleration of the trace anion. On the other hand, if the membrane permeability with respect to the dominant cation permeability is lower than to the anion, the trace anion is delayed and the trace cation is accelerated. Briefly, the electric field is capable to attract some ions, accelerating them and making their rejection values negative. Furthermore, the electric field is able to repulse trace ions, delaying them and making their rejections values higher.

5.2.2. $MgSO_4$ dominant

Figure 5.2 shows the experimental rejections and the rejections predicted by the SEDF model with a solution of $MgSO_4$ as a dominant salt and NH_4Cl as trace for both configuration membranes.

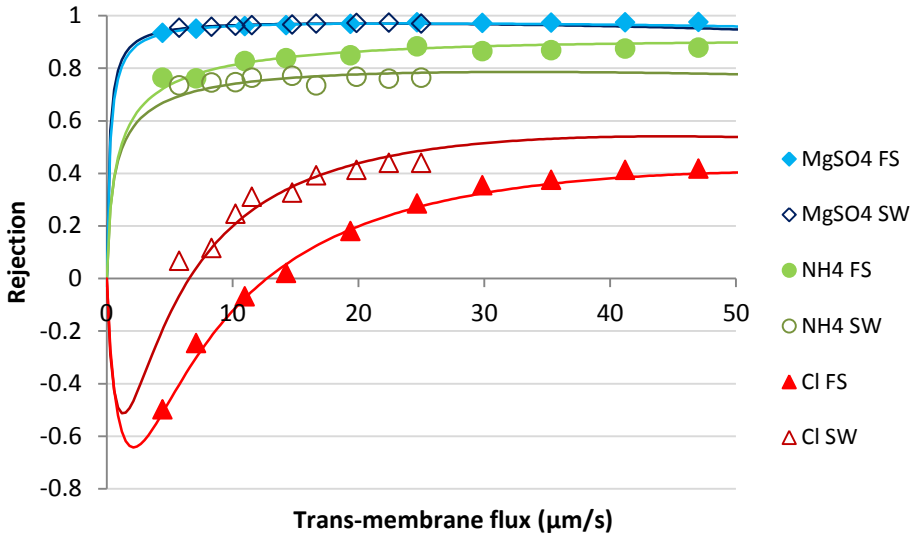

Figure 5.2. Comparison between rejections experimentally obtained and rejections predicted with the SEDF model using a FS and a SW membrane configuration. $MgSO_4$ dominant salt and NH_4Cl as trace. Solid lines were obtained by SEDF model.

Noticeable difference in the rejection patterns was observed with respect to the previous experiments. The dominant salt was highly rejected (almost 100%). The positive trace ion NH_4^+ was also fairly well rejected (around 80%). As it was explained before, the trace rejection strongly depends on the dominant salt. Depending on the difference between the membrane permeabilities with respect to each dominant salt ion, the arisen electric field would be stronger or weaker.

Comparing the current experiment (using magnesium as part of the dominant salt) with the first one showed (using magnesium as trace salt), the rejection of Mg^{2+} as trace ion depending on NaCl as dominant salt was lower. The reason of this behaviour lies in the fact that, using NaCl as dominant salt, the membrane permeability with respect to chloride is much higher than the membrane permeability with respect to sulphate when using $MgSO_4$ as dominant salt, so the arisen electric field in the case of NaCl is weaker and magnesium is less rejected than it is expected. On the other side, using $MgSO_4$ as dominant salt, the electric field strongly retards the cations making their rejections much higher than they are expected.

As before, the rejection pattern of the anion used as trace ion in the experiment, in this case Cl^-, showed much lower rejection and again negative values at low J_v. It can be stated that, $R(MgSO_4) > R(NH_4) > R(Cl)$, which matches previous results reported in the literature (Kurama, 2002). For instance, Häyrynen et al. (Häyrynen et al., 2009) calculated the retention for different ions, such as sulphate, magnesium and ammonium obtaining a rejection of 98.9%, 81.8% and 56.2% for sulphate, magnesium and ammonium, respectively.

It is important to point out that the membrane configuration does not appear to significantly affect the dominant salt or the trace ions rejections.

5.2.3. $MgCl_2$ dominant

Figure 5.3 shows the experimental rejections and the rejections predicted by the SEDF model with a solution of $MgCl_2$ as a dominant salt and KCl as trace for both configuration membranes.

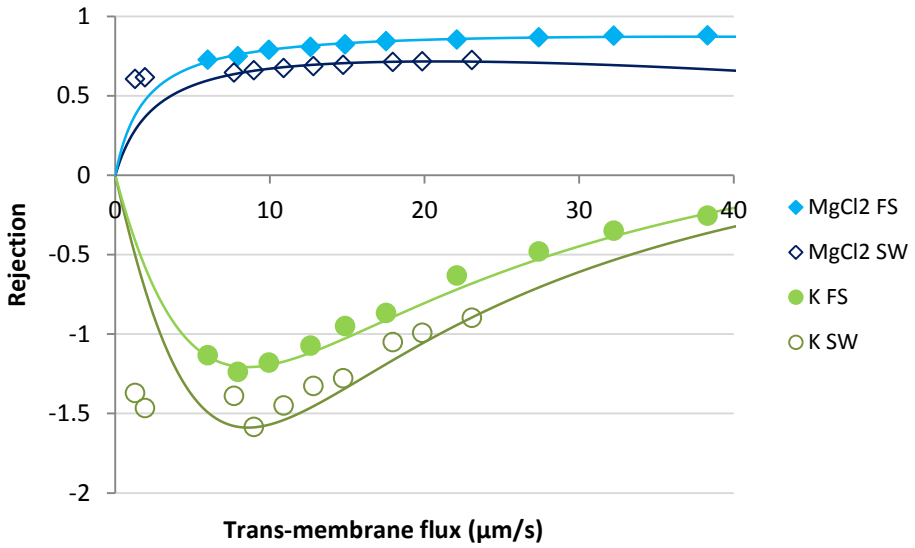

Figure 5.3. Comparison between rejections experimentally obtained and rejections predicted with the SEDF model using a FS and a SW membrane configurations. $MgCl_2$ dominant salt and KCl as trace. Solid lines were obtained by SEDF model.

Using $MgCl_2$ as dominant salt, its rejection with both membrane configurations reported similar results. The monovalent cation rejection behaved similarly in both configurations. Moreover, the single-charged trace cations rejection was always negative. In this case, the negative rejection for the trace cation was related to the membrane permeability with respect to magnesium is always much lower than with respect to the chloride. This fact leads trace cations to be accelerated with the electric field obtaining negative rejections. Thus, R($MgCl_2$) > R(monovalent cations) was the order obtained in this study.

As a general conclusion for all the experiments that were carried out, it can be stated that the J_v obtained in both membrane configurations were quite different. Working with a FS membrane configuration, higher values of J_v were obtained compared to those obtained using the SW configuration working at equal TMP with the same salt feed solution. This fact depends on the polarization layer thickness. At lower polarization layer thickness, higher J_v is obtained. Working at the same conditions, the thickness of the polarization layer was lower working with the FS configuration and, for this reason, the J_v obtained were higher.

5.2.4. Membrane permeability with respect to each ion

Results of membrane permeability with respect to each ion can be obtained by the SEDF model. Their order in each salt mixture allows understanding the electric effects for the ions rejection. Table 5.3, Table 5.4 and Table 5.5 summarize in decreasing order the membrane permeability with respect to each ion obtained for each one of the tests and also its value in both membrane configurations.

Table 5.3. Membrane permeability with respect to each ion for different salt mixtures in both membrane configurations using NaCl as dominant salt

Salt mixture (Dominant salt _Trace salt)	**Membrane permeability with respect to each ion (µm/s)**
NaCl_NaI	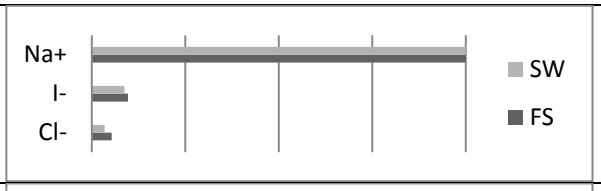
NaCl_NaBr	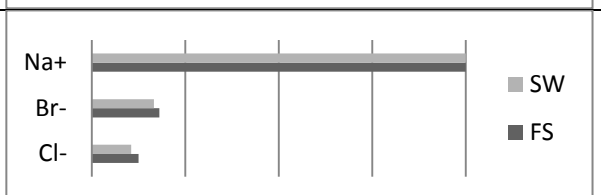
NaCl_$NaNO_3$	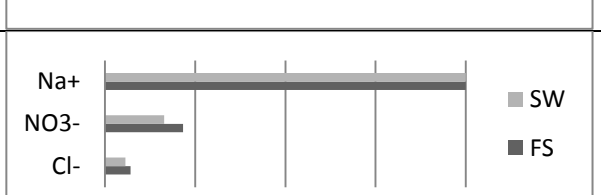
NaCl_NH_4Cl	
NaCl_KCl	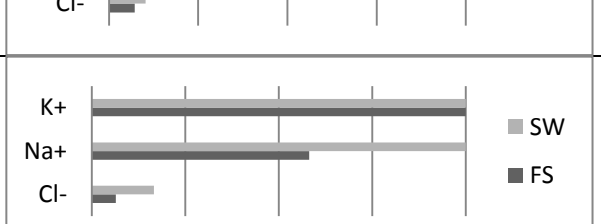
NaCl_$MgSO_4$	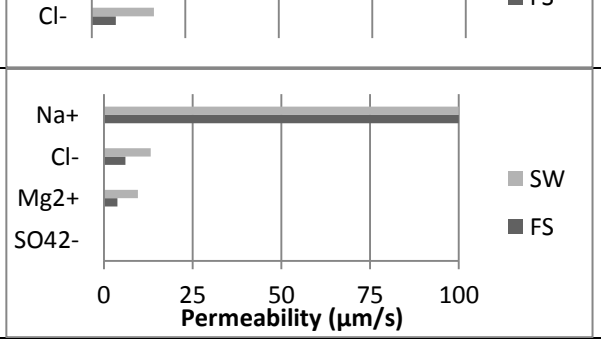

Table 5.4. Membrane permeability with respect to each ion for different salt mixtures in both membrane configurations using $MgSO_4$ or Na_2SO_4 as dominant salt.

Salt mixture (Dominant salt _Trace salt)	**Membrane permeability with respect to each ion (µm/s)**
$MgSO_4$_NaI	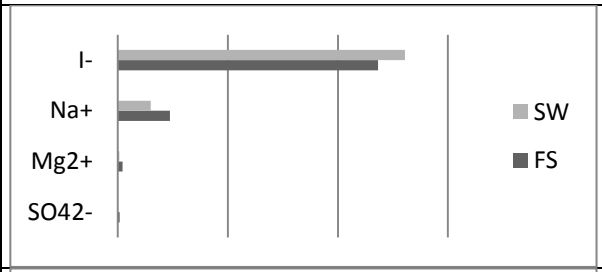
$MgSO_4$_NaBr	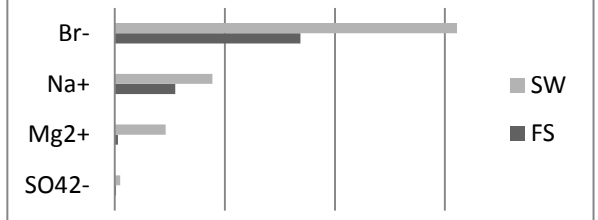
$MgSO_4$_$NaNO_3$	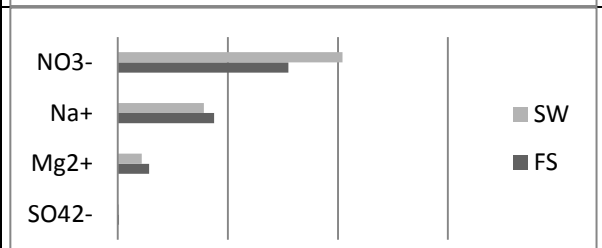
$MgSO_4$_NH_4Cl	
Na_2SO_4_KCl	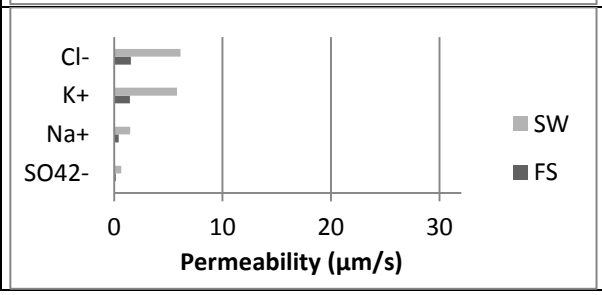

Table 5.5. Membrane permeability with respect to each ion for different salt mixtures in both membrane configurations using $MgCl_2$ as dominant salt.

Salt mixture (Dominant salt _Trace salt)	**Membrane permeability with respect to each ion (µm/s)**
$MgCl_2$_NaI	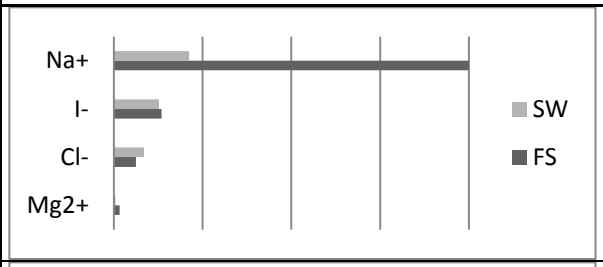
$MgCl_2$_NaBr	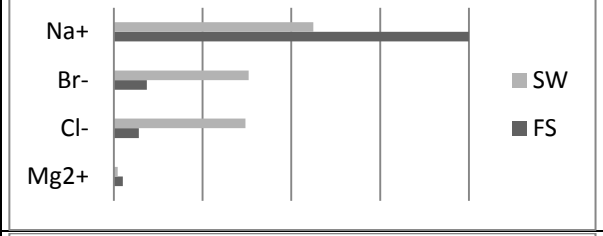
$MgCl_2$_$NaNO_3$	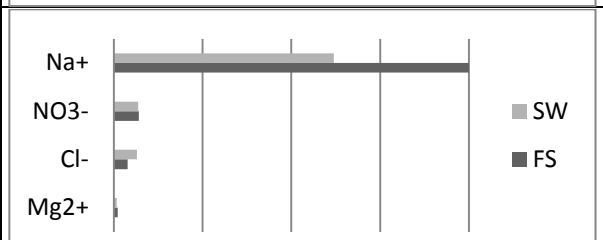
$MgCl_2$_NH_4Cl	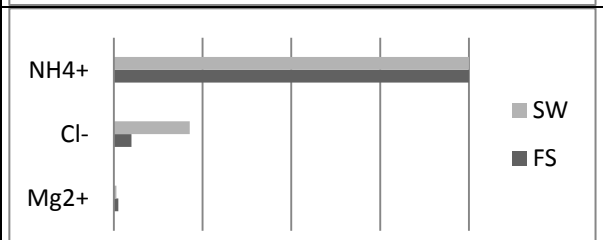
$MgCl_2$_KCl	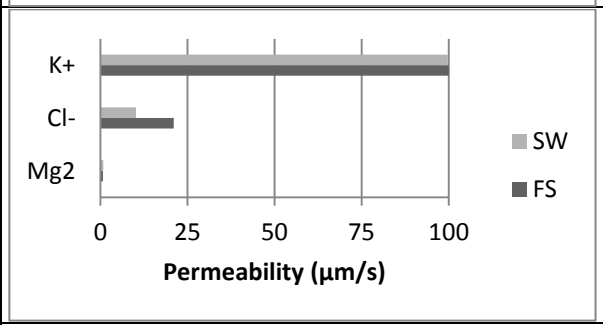

As can be seen in Table 5.3, three trace cases have been studied working with NaCl as a dominant salt in the solution: monovalent anions (I^-, Br^- and NO_3^-), monovalent cations (NH_4^+ and K^+) and divalent trace ions (Mg^{2+} and SO_4^{2-}).

When working with a single-charged anion trace (NO_3^-), the membrane permeability with respect to sodium is the highest one, followed by the membrane permeability with respect to the trace anion and the lowest is reported for chlorine.

By working with a monovalent trace cation (NH_4^+), the membrane permeability with respect to chloride is still the lowest one, although now the membrane permeability with respect to trace cation is as high as that to sodium. Finally, using a divalent salt as a trace ($MgSO_4$), the membrane permeability with respect to the double-charged ions is much lower.

For $MgSO_4$ as dominant salt, two trace cases have been studied: trace monovalent anions (I^-, Br^- and NO_3^-) and trace monovalent cation (NH_4^+ and K^+) (Table 5.4). In the former case, the membrane permeability with respect to the single-charged anion is the highest one, followed by the membrane permeability with respect to sodium, magnesium and finally sulphate. In the case of KCl or NH_4Cl as salt traces, the membrane permeability order with respect to each ion is chloride, monovalent cation, magnesium and the lowest one sulphate again. The same two trace cases have been studied using $MgCl_2$ as dominant salt (Table 5.5). The membrane permeability with respect to each ion was: sodium > single-charged anion > chloride > magnesium and monovalent cation > chloride > magnesium.

The results are consistent with previous studies (Galiana-Aleixandre et al., 2011; Pages et al., 2013; Yaroshchuk et al., 2011, 2009), in which it was observed that the membrane NF270 exhibit less permeability to divalent ions. Besides, membrane permeability with respect to sulphate was lower than to magnesium and the permeability to chloride was lower than the one obtained to sodium.

According to Yaroshchuk et al. (Yaroshchuk et al., 2013), the membrane permeability with respect to each ion of the dominant salt can explain the behaviour of the electric fields which controls the rejections of the trace ions during the experiments. And by means of Table 5.3, Table 5.4 and Table 5.5 it has been shown that they are fairly the same for both membrane configurations, being the permeability number of each ion in the same order of magnitude for each membrane configuration.

5.3. Conclusions

The same NF membrane was used for both configurations: NF270 (Dow Chemical). Comparing both membrane configurations, the trans-membrane flux obtained with the FS configuration was higher than that observed with the SW under the same operating conditions.

In general, it is proved that ion rejection curves for both membrane configurations were fairly similar. Moreover, the membrane permeabilities with respect to each ion in both configurations were quantitatively similar.

Comparing both membrane configurations it can be said that the J_v obtained is higher by using the FS membrane configuration working at the same pressure and salt mixture. The dominant salt rejection seems to be not affected by the membrane configuration, as similar rejection curves were obtained for both configurations. The general trend observed for the trace ion rejection was the same.

SEDF model is a valid model which is capable to fit satisfactorily experimental data of a dominant salt and a trace mixture and determinate the rejection curves for each of the ions versus the J_v produced in each experiment. Moreover, according to the SEDF model the rejection values obtained can be explained with the effect of the spontaneously-arising electric fields.

Membrane permeability with respect to each ion can be calculated with the SEDF model and for both membrane configurations are similar. Furthermore, qualitatively they have the same order of membrane permeability with respect to each ion, as it is shown in Table 5.3, Table 5.4 and Table 5.5.

In general terms, it seems that the two configurations behave in a similar way. This trend is useful implementing NF technology at industrial scale, since SW configuration is used at large scale, representing a larger membrane active area and occupying a small space, whereas the FS configuration is used in test in a lab scale, for its simplicity and its easiest methodology is of great interest in order to obtain experimental data.

Chapter 6
Hybrid Sorption-Ultrafiltration process to reduce DOC and ions contained in brackish waters

One of the major challenges faced by drinking water treatment plants (DWTPs) is the removal of NOM, as NOM induce many adverse effects on the potabilization process. Among these effects are an increased demand of chemicals for coagulation, flocculation and disinfection, the formation of DBPs, the production of unpleasant odours and tastes, and the inducement of bacterial growth within distribution systems with the subsequent increase of chlorine demand (Gibert et al., 2013; Li et al., 2003).

Conventional water potabilization treatments, using coagulation/flocculation, are the most frequent process for drinking water treatment targeting NOM and colour and particle removal. However, aluminium or iron coagulation only removes a portion of NOM (30–80%), especially organic compounds of higher MW, depending on water quality and water treatment conditions (Edzwald, 2011; Matilainen et al., 2010). Then, coagulation/flocculation is not sufficient to achieve dissolved organic matter (DOM) values lower than 2 mg C/l, which is the reference guideline in the EU (Bolto et al., 2002). As a consequence, DWTPs tend to improve or develop new technologies for potabilization of waters with a low DOC content.

Among the possible alternatives to coagulation/flocculation for NOM, removal several studies at the end of the 1970s highlighted the strong potential of anion-exchange resins and found that they outperformed activated carbon (Boening et al., 1980) and non-ionic resins (Anderson and Maier, 1979). IEX is based on the phenomenon of

exchanging ions between a medium (e.g. solid material typically) and electrolytes contained in a solution. The medium is usually made of a complex cross-linked polymer matrix. IEX resins have been widely used for water softening and production of ultrapure water (Zagorodni, 2007). Advantages of IEX include simplicity of operation and the fact that there is no energy need for the exchange phenomenon to occur, while the limitations of IEX resins are restricted resin exchange capacity and consumption of chemicals for regeneration (Neale and Schäfer, 2009).

Nowadays, the availability of advanced technologies (e.g. sorption, IEX, membranes) for removal of pollutants or precursors of DBPs to produce high quality drinking water from low quality surface and groundwater is high (García et al., 2015; Raich-Montiu et al., 2014). Integrating IEX and membrane technologies presents alternative processes to improve organic and inorganic contents in process and surface waters (López-Roldán et al., 2015, 2013b).

In very recent years, IEX processes have received considerable attention with the use of a new magnetic IEX resin developed by Ixom Co.: the MIEX resin (Abdulgader et al., 2013; Allpike et al., 2005; Drikas et al., 2003; Fearing et al., 2004; Humbert et al., 2005; Singer and Bilyk, 2002). MIEX is a strong base anion-exchange resin with quaternary ammonium functional groups counteracted with chloride ions ($R_4N^+Cl^-$) which are supported on a magnetic polyacrylic matrix containing iron oxide inside (Shuang et al., 2012; Singer and Bilyk, 2002; Slunjski et al., 2000). MIEX beads are 2-5 times smaller than traditional ones providing a larger specific surface area and a faster solid-phase mass transfer to remove more efficiently the smallest hydrophilic organic compounds which are usually not quite well separated (Bourke and Arias, 2009). The magnetic component allows the fluidization of MIEX beads at high hydraulic loading rates and also their agglomeration and subsequent quick settling when the regeneration is needed (Kim and Dempsey, 2010; Q. Wang et al., 2012). The small resin beads facilitate rapid reaction whilst the magnetic properties allow separation and reuse of the resin in a continuous process.

The first full scale MIEX plant (1300 m^3/d) was commissioned at Mt Pleasant (Australia) in 2001. The operation showed that the use of MIEX resin as a pre-treatment to MF or conventional coagulation treatment produced water with lower DOC concentration (Mergen et al., 2008). The processes incorporating MIEX also produced more consistent water quality and were less affected by changes in the concentration and composition of the raw water DOC. These facts postulated that the use of MIEX could simplify the operation and maintenance to provide the required water quality even when subjected to large variations in the raw water DOC concentration and character (Drikas et al., 2011; Walker and Boyer, 2011).

The removal of NOM in drinking water treatment by magnetic IEX resins such as MIEX reduced the formation of THMs and HAAs, both which are typical DBPs. Furthermore, the MIEX pre-treatment of drinking water can provide additional benefits such as reducing the coagulant dosage or protecting the membrane from fouling. However, the removal of hydrophobic NOM by MIEX was reported to be

much less efficient than hydrophilic NOM for raw waters. Humic acid (HA), as a hydrophobic fraction of NOM, can cause the anion exchange resin fouling problem (Huber et al., 2011; Kaewsuk and Seo, 2011; Shuang et al., 2012).

In recent years, although the main attention has been allocated to the NOM reduction, an increased interest has been given to other ions found in water (in some case at trace levels) which are poorly removed by conventional water treatment methods (Belgiorno et al., 2007; Murray, 2009). These ions may be responsible for organoleptic problems (sulphate, chloride and phosphate) (Ding et al., 2012b) or associated to human risk due to its toxicity (nitrate, bromate, perchlorate and organic micropollutants) (Johnson and Singer, 2004; Liu et al., 2011; Phetrak et al., 2014; Tang et al., 2014, 2013; Zhang et al., 2014; Zhu et al., 2015) or are involved in the formation of DBPs (bromide, iodide) (Arias-Paic et al., 2016; Watson et al., 2015). Therefore, there is a strong need to develop novel treatment technologies in order to upgrade or improve the conventional treatment processes.

The review of the state of the art indicates that the integration of IEX and adsorption systems with low pressure membrane processes such as MF and UF can be a promising alternative to conventional treatments (Abdulgader et al., 2013; Boyer and Singer, 2005; Stoquart et al., 2012). The potential advantages of these hybrid processes are enhanced produced water quality, better performance of water treatment processes, and/or reduced production cost. In some cases the combination of IEX resins with MF/UF (Huang et al., 2012; Humbert et al., 2007; Kabsch-Korbutowicz et al., 2008; Kim and Dempsey, 2010) and NF/RO (Comstock et al., 2011; Huang et al., 2011) has a pronounced synergetic effect in creation of efficient and cost-effective water treatment technologies.

The interest on hybrid processes in water treatment are mainly stimulated by the need for higher quality of treated water, overall optimization of the treatment process and cost reduction. According to the literature, studies on hybrid IEX-pressure driven membrane processes are focused mainly on prevention of membrane fouling during water treatment, selective removal of targeted pollutants, treatment of wastewaters and desalination of brackish and seawater. The majority of studies on hybrid IEX-MF/UF processes for water treatment have focused on prevention of membrane fouling by NOM and other organic substances (Cornelissen et al., 2009; Galjaard et al., 2004; Kabsch-korbutowicz et al., 2006; Kim and Dempsey, 2010; Son et al., 2005). MIEX has been chosen for this study due to its high capabilities in removing negatively charged NOM, particularly humic acids and fulvic acids (Boyer and Singer, 2008).

In this study, the efficiency of a hybrid MIEX-UF bench-pilot (magnetic IEX resin coupled to a UF capillary membrane) to remove disinfection precursors (DOC and Br^-) and inorganic anions (SO_4^{2-} and NO_3^-) was evaluated. During the operating time the hybrid set-up was continuously fed with sand-filtered water from a DWTP treating surface water and, occasionally, groundwater. The membrane system operated in an inside-out flow filtration mode at variable TMP for the two different MIEX concentrations evaluated (1 and 3 ml/l). Chemical enhanced backwash (CEB) cycles

were regularly performed to control membrane resistance due to fouling.

6.1. Materials and methods

6.1.1. Water quality sources

Experiments were performed at the Sant Joan Despí Drinking Water Potabilization Plant (SJD-DWTP) (Sant Joan Despí (Barcelona, Spain)). The waterworks has as a nominal capacity of 5 m^3/s, supplying a population of over 1.5 million people in the Metropolitan Area of Barcelona. The raw water used by the DWTP comes from a combination of the Llobregat River and, occasionally, its aquifer. River water presents moderately high total organic carbon (TOC) (3.4–4.9 mg/l), high turbidity (70-230 FNU) and high conductivity (1160–1939 µS/cm), while groundwater typically exhibit lower TOC concentrations (1.1–1.4 mg/l) and turbidity (0.2-0.5 FNU), but similar conductivities (1970–2012 µS/cm) (Gibert et al., 2015).

The high salinity of the Llobregat River stems from the brines associated with the important mining activities on the salt deposits located in the upper part of the basin, with a significant presence of chloride, sulphate, sodium, calcium and, to a lower degree of barium, strontium, potassium, bromide and iodide (Fernández-Turiel et al., 2000; López-Roldán et al., 2013a; Raich-Montiu et al., 2014). Furthermore, many problems are associated with the increase in micropollutant and microbiological levels due to both urban and industrial sewage. These problems produce many interruptions in the operation of the SJD-DWTP, some of them lasting many hours.

The treatment train applied in the SJD-DWTP includes a conventional treatment comprised of pre-chlorination, coagulation/flocculation with aluminium based salts, subsequent sedimentation and sand filtration, followed by an advanced treatment comprised of ozonation, granular activated carbon filtration and post-chlorination. Samples of raw water for this study were sampled from both the sand filtration step and the aquifer well. Due to the high levels of TOC, together with the high levels of bromide (ranging between 0.5 and 1.2 mg/l), high concentrations of THMs may be produced after chlorination (Chang et al., 2001; Raich-Montiu et al., 2014). A summary of the composition for these two waters is shown in Table 6.1.

Table 6.1. Composition of different water sources used in the experiments performed by the hybrid MIEX-UF process

Parameter	Units	Sand-filtered water	Groundwater
Suspended solids	mg/l	0.4	-
Turbidity	FNU	0.4	[0.2 – 0.5]
TOC	mg C/l	[2.5 – 4]	[1.1 – 1.4]
Temperature	ºC	18	-
pH	units of pH	7.5	-
Cl^-	mg/l	[238 – 293]	297
Na^+	mg/l	155	-
K^+	mg/l	27.5	-
Ca^{2+}	mg/l	104	-
Mg^{2+}	mg/l	29	-
SO_4^{2-}	mg/l	[152 – 189]	230
HCO_3^-	mg/l	282	-
NH_4^+	mg/l	0.4	-
NO_3^-	mg/l	[11 – 20]	13
Br^-	mg/l	[0.5 – 0.7]	[0.8 – 1.2]
I^-	mg/l	0.06	-

6.1.2. MIEX resin properties

Table 6.2 summarizes the characteristics of MIEX resin sample based on manufacturer data (Ixom Watercare, 2016). Prior to perform the tests, MIEX resin was washed and regenerated to avoid any experimental interference as iron oxide might be present into the carrier water. Then, MIEX concentration was measured in terms of volume of settled resin per volume of raw water.

Table 6.2. Characteristics of strong-base anion magnetic exchanger MIEX (Ixom Watercare, 2016)

Property	Units	Units
Exchange capacity	meq/l	0.5 + 0.02
Water content	%	64 – 66
Structure		Macroporous with iron oxide
Matrix		Polyacrylic
Functional Group	units of pH	Quaternary Ammonium $R(CH_3)_3N^+$
Particle size	µm	150 to 180
Counter ion		Chloride

Taking into account that MIEX resin is a strong base anion exchange resin, the removal process of the evaluated anions can be described by Eq.(12):

$$R_4N^+Cl^- + X^- \Leftrightarrow R_4N^+X^- + Cl^- \quad (12)$$

where $R_4N^+Cl^-$ represents the functional groups of MIEX resin in the chloride form and X^- the anions potentially exchangeable (DOC, NO_3^-, SO_4^{-2}, Br^-).

NOM is defined as a complex matrix of organic materials present in all natural waters. For simplicity, as NOM characterisation was outside the scope of this study, its content was associated to the parameter of DOC, as probably from 90-95% of the total value is associated to NOM. Nowadays, the characterization of the NOM can be made e.g. by high performance size exclusion chromatography (HPSEC) analysis, whereby the molecular weight distribution can be determined (Chow et al., 2008), or by fractionation techniques, whereby organic compounds of NOM are divided into hydrophilic and hydrophobic fractions with resins (Sharp et al., 2006a).

The hydrophilic fractions are composed mostly of aliphatic carbon and nitrogenous compounds, such as carboxylic acids, carbohydrates and proteins. Hydrophobic NOM primarily consists of humic and fulvic acids and is rich in aromatic carbon, phenolic structures and conjugated double bonds (Swietlik et al., 2004). A hypothetical molecular structure of a HA is shown in Figure 6.1 (Duan and Gregory, 2003). Generally, the humic substances account over half of the TOC content.

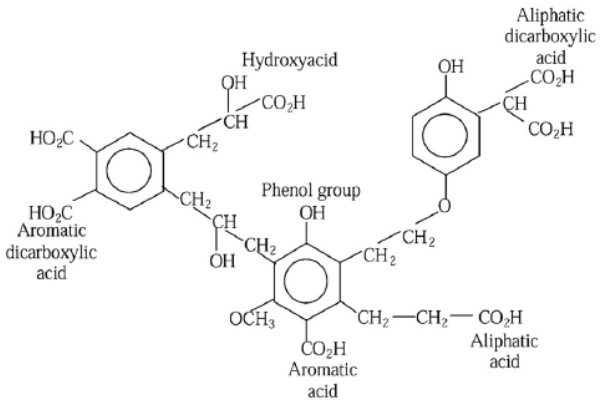

Figure 6.1. Hypothetical molecular structure of a humic acid (HA) (Duan and Gregory, 2003)

Then, according to the proposed structure, humic substances can be regarded as natural anionic polyelectrolytes, with anionic charge at pH values higher than 4. The DOC removal process can thus be described as indicated by Figure 6.2, where R represents the methyl groups of MIEX resin.

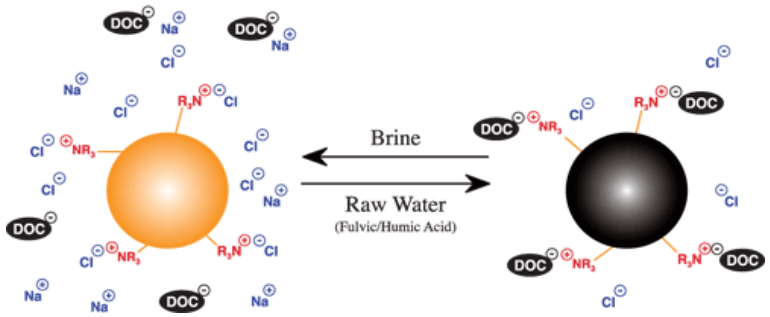

Figure 6.2. Schematic description of DOC removal from aqueous solutions following an anion exchange with chloride ions of MIEX (Ixom Watercare, 2016)

It is difficult to determine a molar ratio of DOC to chloride anions as the molecular weight and the number of potential ionic groups of the DOC involved in the exchange are usually unknown. Indarawis and Boyer (Indarawis and Boyer, 2013) proposed the use of the charge density titration for DOM to determine the concentration of DOM (meq/l) given the pH of that sample if the factor needs to be estimated $K_{DOC/Cl}$.

6.1.3. Batch sorption test

Anions test solutions were prepared by dissolving a weighed amount of the corresponding in water obtained from a Milli-Q-Academic-A10 apparatus (Millipore Co. France). Batch experiments were performed at room temperature (21±1ºC). Samples of MIEX were mechanically mixed in glass stoppered tubes with an aqueous solution at different initial anions concentrations until equilibrium was achieved (24 h). After phase separation with a 0.2-µm syringe filter, the equilibrium pH was measured using a pH electrode (Crison GLP22), and the total anions and TOC concentration was measured as described in section 6.1.6.

6.1.4. Hybrid sorption-membrane pilot set-up

The configuration of the continuous-flow pilot set-up is represented by the scheme shown in Figure 6.3. This hybrid system is composed of a continuous-stirred tank, a high-performance peristaltic pump (Masterflex I/P, Vernon Hills, Illinois, USA), a membrane module of UF capillaries (Pentair X-Flow, The Netherlands) placed in horizontal, two differential digital manometers (LEO3, Keller, Switzerland), several three-way valves (Parker-Legris), polyurethane and silicone tubing and fittings.

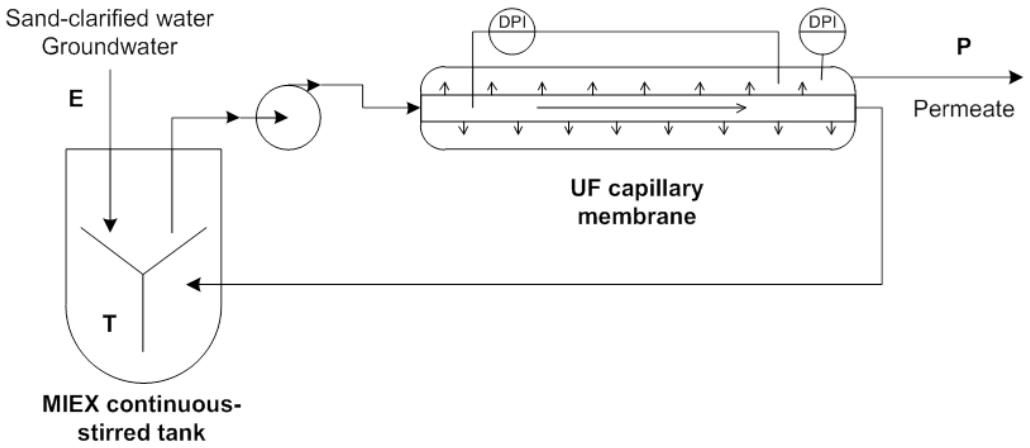

Figure 6.3. Simplified hybrid sorption-membrane process including the main components: a mixed continuous stirred tank and the UF membrane module.

UF polyethersulfone capillary membrane (nominal MWCO of 100 kDa) was supplied by Pentair. The membrane module was filled with an average of 100 capillaries whose hydraulic diameter was 0.8 mm and length 1 m (i.e. providing a membrane filtration area of 0.251 m^2). The main characteristics and the limiting operating parameters of the UF membrane can be found in Table 6.3.

Table 6.3. Characteristics and limiting operating parameters of UF membrane (Pentair X-Flow, 2011)

Membrane properties	Units	Value
Pore structure	-	asymmetric/microporous (< 2 nm)
Average pore size	nm	20
Trans-membrane pressure	bar	[-3 – 3]
Temperature	ºC	[1 – 80]
pH feed	-	[2 – 12]
Chlorine exposure	mg/l (max. at 0-40ºC)	500
Flow filtration mode	-	At pressure, inside-out

The UF membrane was previously washed by filtering tap water to remove the conservative agents. The initial permeability of virgin membrane was determined in the range of 200 – 400 $l/h \cdot m^2 \cdot bar$ provided by the manufacturer at 20ºC.

6.1.5. Experimental tests performed by the hybrid MIEX-UF process

Prior to start the hybrid process, a fluidized bed of MIEX was kept into the stirred tank with sand-filtered water (40 l) during few seconds. Subsequently, the hybrid MIEX-UF process was started-up by circulating the influent (E) (sand-filtered water or groundwater) to the stirred tank (which was approximately level kept) while the permeate (P) was continuously produced by the system (Figure 6.3).

The water/MIEX slurry (T) contained in the stirred tank was circulated as feed to the UF membrane module by the peristaltic pump at approximately constant flow-rate

over the range pointed out on the Table 6.4, which also shows the operating parameters of all experiments performed by the hybrid MIEX-UF system. The produced P was obtained by operating the membrane in an inside-out operation mode in cross-flow configuration, while the retentate containing the MIEX resin was recirculated into the tank (Figure 6.3).

For all trials, the membrane process was operated at variable TMP in the range of 0.1 - 0.8 bar recommended by the manufacturer. Cleaning cycles were alternated with the filtration cycles over the experiments containing MIEX to control UF fouling. The TMP gradients (ΔTMP) and the water composition for the different experiments are collected in Table 6.4.

Table 6.4. Hydraulic operating parameters of the MIEX-UF pilot tests

MIEX resin concentration l/m^3	Kind of Water	Feed flow-rate l/h	TMP bar	ΔTMP bar	Filtration time* h
0	tap water	[31-113]	[0.10-0.30]	0.20	1.5
0	sand-filtered water	[43-62]	[0.11-0.53]	0.42	4.25
1	sand-filtered water groundwater	[34-48]	[0.32-0.84]	0.52	18
3	sand-filtered water	[17-48]	[0.26-0.77]	0.51	18

The TMP was measured by the manometer (DPI) located in feed and permeate sides of membrane capillaries. An initial TMP of ~0.3 bar was especially required in the experiments performed with MIEX to produce a significant permeate flux. In addition to TMP, the level of the stirred tank and the permeate flux were monitored.

CEB cycles were regularly performed during the experiments to control membrane resistance from fouling and recover the hydraulic membrane performance. CEB cycles included a hydraulic cleaning (HC) followed by a chemical cleaning (CC) comprising various chemicals. CEB cycles were performed when the hybrid filtration process worked at minimum flux production (20 $l/m^2 \cdot h$) or at maximum TMP (0.8 bar) to prevent membrane damage.

HC consisted in a back-flushing (BF) of feed water (without MIEX) inside the membrane capillaries by reversing the flow direction at retentate pressure of 1.4 bar to remove any foulant from the surface of the membrane. Then, a backwash (BW) was performed by circulating permeate or tap water in an outside-in mode to remove any remaining foulant from the membrane pores, also from bottom to top module ends. Specifically, the BW was initially started at TMP ~0.4 bar in cross-flow configuration and progressively in dead-end by closing the concentrate valve. Then, the TMP was adjusted by increasing the pump flow-rate to a limiting value (2 bar) kept for 20 seconds. Finally, the TMP was reduced to ~0.4 bar to proceed with the two consecutive chemical cleaning sequences.

Following the HC, a two-step CC was conducted. First, a base solution (pH ≈ 12) of caustic soda with sodium hypochlorite (0.01 mol/l NaOH, 200 mg/l active chlorine) was employed to backwash the membrane up to the limiting TMP (2 bar) during 20 seconds. Then, the TMP was decreased to ~0.4 bars and a subsequent basic soaking step was carried out by closing all UF valves for 15 minutes on standby. After that, the chemical solution was rinsed out of the unit by performing a BW to conclude with the first chemical cleaning sequence. The second sequence was executed in the same way as the first one, but an acid solution (0.01 mol/l HCl) was used instead.

All chemical cleaning procedures aimed to remove different foulants by oxidizing (NaClO, 4% w/w), reducing (NaS_2O_5 0.5% w/w), complexing (0.5 mmol/l $H_2C_2O_4$), basic (0.01 mol/l NaOH), acid (0.1 mol/l HCl) and permeate or tap water. At the end of the CC, the system was brought back into inside-out flow membrane filtration to check the efficiency of the cleaning procedure by recovering the permeate flux.

6.1.6. Samples monitoring and analyses

Samples from the influent (E), the tank feeding the UF module (T) and the permeate (P) (see Figure 6.3) were collected every 5-10 minutes at the beginning of the experiment, and more separately after 30 minutes. Samples collected from the tank were filtered with syringe filters of 0.45 µm to separate the MIEX beads from the aqueous phase to avoid any ion-exchange or adsorption phenomena on MIEX beads during the analysis.

Enough volume (50 ml) was taken to determine the concentration of the TOC using a TOC analyser (TOC-V_{CPH} Shimadzu, Japan) and the targeted ions (Br^-, SO_4^{2-}, NO_3^-, I^- and F^-) by ionic chromatography (IC) (ICS-1000 Dionex, California, USA) in all samples. The samples were filtered with syringe filters of 0.45 µm and 0.22 µm prior to analyse them in order to prevent capillary clogging of TOC and IC analysers, respectively.

6.2. Membrane hydraulic performance evaluation

6.2.1. Determination of the trans-membrane flux and permeability

The trans-membrane flux (J_v) was experimentally determined from Eq.(10) as described in section 2.4. By knowing the dynamic viscosity coefficient (μ) of the bulk solution and the TMP of the UF system, the total membrane resistance (R_{tot}) and the permeability (K_v) could be then calculated from the flux determination by means of the Darcy's equation as follows:

$$J_v(t) \equiv \frac{1}{\mu R_{tot}} TMP \equiv K_v\, TMP \qquad (13)$$

The loss of permeability at a given time of experiment (ΔK_v) caused by membrane fouling can be calculated as follows

$$\Delta K_v(t) = 1 - \frac{K_v}{K_{v_0}} \tag{14}$$

where K_{v_0} is the initial permeability of the membrane before suffering from fouling.

6.2.2. Determination of the solute mass accumulated within the system

A mass balance of each solute 'i' over the hybrid sorption-membrane process allows calculating the mass flux of the solute 'i' accumulated within the system at any time $\left(\frac{dm^i(t)}{dt}\right)$ using the following equation:

$$\frac{dm^i(t)}{dt} = Q_E(t)C_E^i(t) - Q_P(t)C_P^i(t) \tag{15}$$

where $Q_E(t)$ and $C_E^i(t)$ are the flow-rate and the concentration of solute "i" in the influent stream, respectively, and $Q_P(t)$ and $C_P^i(t)$ are the flow-rate and the concentration of the solute 'i' in the permeate stream, respectively. It is worth noting that the permeate stream is exempt of MIEX beads, and therefore all MIEX beads pumped from the tank are retained by the UF membrane and recirculated back to the tank with the retentate.

The term $\left(\frac{dm^i(t)}{dt}\right)$ specifically accounts for the mass of solute 'i' accumulated inside the system either dissolved in water phase $\left(\frac{d(V_{tank}(t)\cdot C_{tank}^i(t))}{dt}\right)$ or exchanged onto MIEX $\left(\frac{dm_{MIEX}^i(t)}{dt}\right)$. Since the concentration of 'i' in the tank was periodically monitored, the latter can be calculated as follows:

$$\frac{dm_{MIEX}^i(t)}{dt} = \frac{dm^i(t)}{dt} - \frac{d(V_{tank}(t)C_{tank}^i(t))}{dt} \tag{16}$$

By numerically integrating Eq.(16) the mass of solute 'i' accumulated on MIEX at time t, $m_{MIEX}^i(t)$ was quantified as Eq.(17) shows.

$$m_{MIEX}^i(t) = \int_0^t \frac{dm_{MIEX}^i(t)}{dt}dt \approx \sum_{n=0}^{N} \frac{1}{2}\left(\frac{m_{MIEX}^i(t_n)}{dt} + \frac{m_{MIEX}^i(t_{n-1})}{dt}\right)(t_n - t_{n-1}) \tag{17}$$

In addition, the uptake of solute 'i' at time t, $q_{MIEX}^i(t)$ in $\frac{mol\ solute\ i}{L\ MIEX}$ was calculated using the following equations.

$$q_{MIEX}^i(t) = \frac{m_{MIEX}^i(t)}{V_{dried\ MIEX}\ MW_{solute}} \tag{18}$$

where the volume of resin ($V_{dried\ MIEX}$) was calculated from both apparent ($\rho_{wet\ MIEX}$) and solid-phase densities ($\rho_{dried\ MIEX}$) as it is described by Eq.(19).

$$V_{dried\ MIEX} = V_{wet\ settled\ MIEX} \frac{\rho_{wet\ MIEX}}{\rho_{dried\ MIEX}} \quad (19)$$

MIEX wet is considered the solid-phase filled up with water over its surface/porosity while in the MIEX dried only its solid-phase is considered.

6.3. Results and discussion

6.3.1. DOC and anions removal by MIEX batch and preliminary hybrid MIEX-UF kinetic tests

DOC removal from sand-filtered water at SJD-DWTP was evaluated by the hybrid MIEX-UF process at four different MIEX concentrations of 0.6, 1, 1.7 and 2.5 ml/l as function of the filtration time (Figure 6.4). All MIEX concentrations provided a fast and efficient removal of DOC. The higher the MIEX concentration, the higher the sorption rate and the higher the TOC removal. For a resin concentration of 2.5 ml/l, the DOC content of the sand-filtered water, was reduced from 2.9 mg/l to a minimum of 1.6 mg/l after less than 5 min of filtration time. Similar values on sorption rate were observed for the other resin concentrations. Due to the complex nature of the DOC, although the interaction of the positively charged groups of MIEX are involved for simplicity the removal process is considered as sorption.

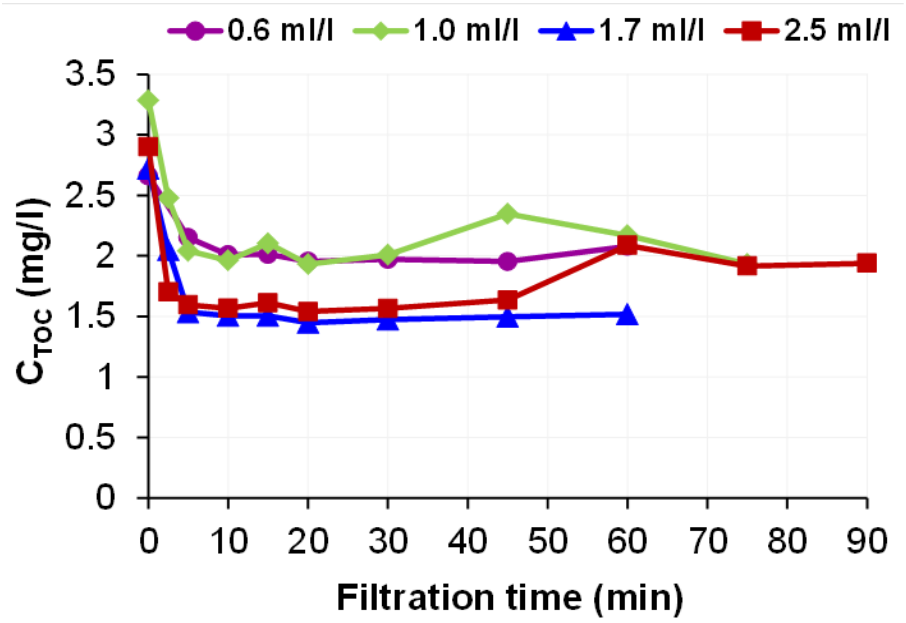

Figure 6.4. TOC removal from sand-filtered water at Sant Joan Despí DWTP by four MIEX concentrations of 0.6, 1, 1.7 and 2.5 ml/l evaluated in the hybrid MIEX-UF process as a function of the filtration time

Measured removals were similar to values reported by different studies using MIEX for DOC removal in DWTPs (Boyer and Singer, 2006; Boyer et al., 2008b; Humbert et al., 2012). The removal rate of an ion onto IEX resins can be limited either by diffusion or by chemical reactions at the IEX sites. Although, removal onto IEX resins was mainly diffusion controlled (Helfferich, 1962). Two types of diffusion rate-limiting step may occur: (i) diffusion through the film boundary layer surrounding the resin bead (film diffusion) and (ii) diffusion within the resin particle (intraparticle diffusion). As the rate of the film diffusion mechanism is a function of (1/r) (where r is the IEX resin bead radius) and intraparticle diffusion is a function of ($1/r^2$) (Liberti and Passino, 1977; Schmuckler and Golstein, 1977), whatever the diffusion rate-limiting step involved, reducing resin bead size results in improving resin sorption rates. Anyway, the removal rate in IEX resins is mainly determined by the slower of these two processes.

The development of MIEX was directed in the direction of improving the IEX rate by reducing the particle size as this is translated into short times (between 5 – 10 minutes) needed to reach equilibrium in comparison with standard IEX resins with radius in the mm size for which equilibration time required are in the order of 20 to 60 minutes (Liberti,1982, 1983).

Boyer et al. (Boyer et al., 2008a) demonstrated that DOC removal by MIEX in a completely mixed flow reactor with resin recycle and partial resin regeneration could be described by DOC transport via intraparticle pore diffusion. Values of the DOC intraparticle diffusion coefficient $\left(D_{p,e}^{DOC}\right)$ ranged between 0.4 to 3.4 $x10^{-10}$ m^2/s depending on the type of surface water used and then, the composition of DOM. The measured $D_{p,e}^{DOC}$ are between 1 to 2 orders of magnitude higher than those determined by anion-exchange resins using standard IEX resins (Boyer and Singer, 2006).

Results of batch kinetic removal of SO_4^{2-}, NO_3^-, Br^-, I^-, F^- and DOC with ultra-filtered doped (Br^-: 5 mg/l, I^-: 5 mg/l and F: 5 mg/l) water from SJD-DWTP at two different MIEX concentrations of 0.7 and 1.5 ml/l are collected in Figure 6.5. The set of anions was selected taking into account the average composition of the Llobregat River water and their interest as pollutants or responsible for DBPs formation (López-Roldán et al., 2015, 2013a). Both MIEX concentrations provided a fast and efficient removal of the evaluated anionic species and comparable to those for DOC measured indirectly as UV254 (Boyer, 2013). The higher the MIEX concentration, the higher the rate of sorption and the higher the anions removal. For a resin concentration of 1.5 ml/l, the UV254 of the ultra-filtered doped water was reduced up to a maximum of 60% for the higher dose, after less than 5 min of filtration time. Similar values on sorption rate were observed for the other anions.

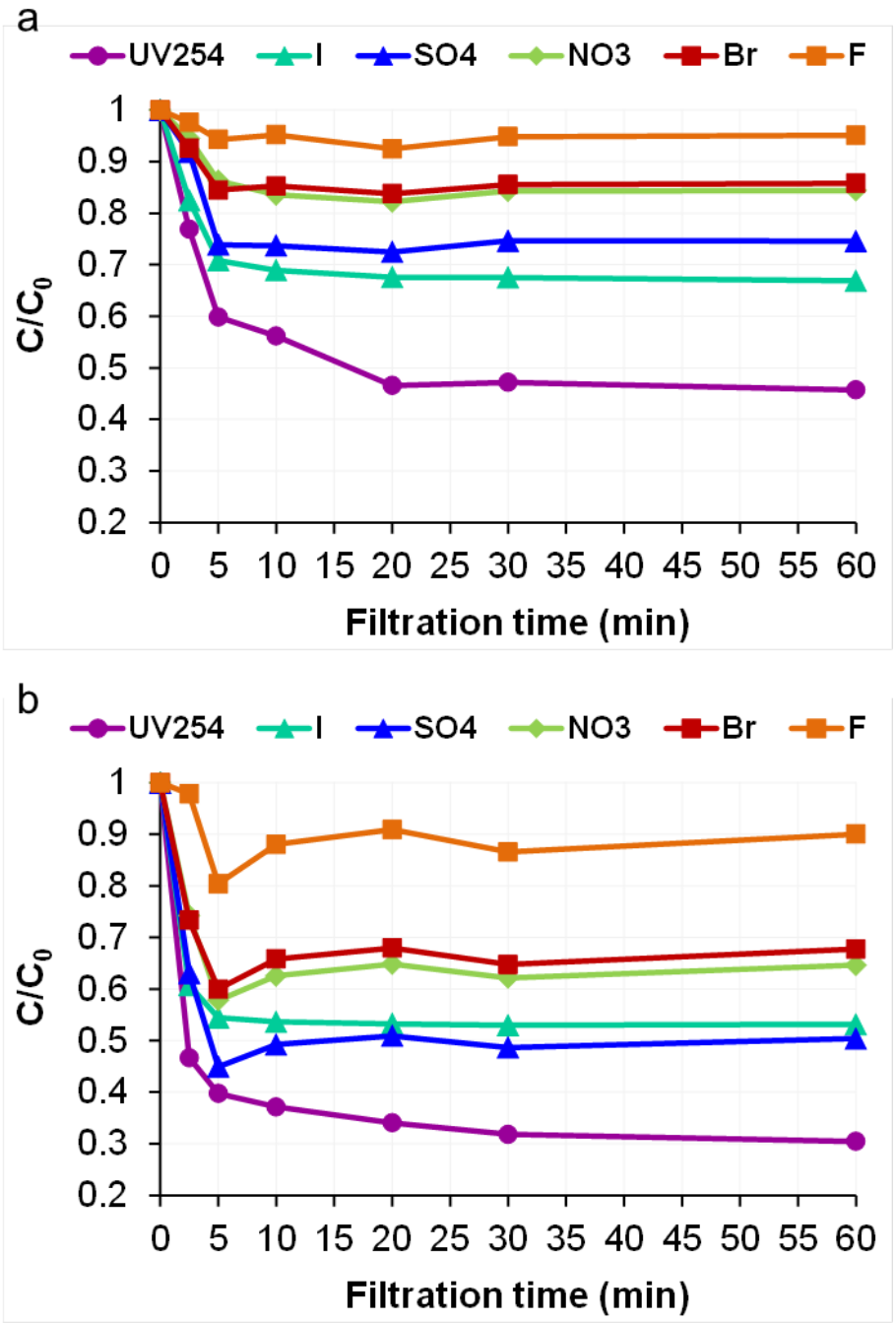

Figure 6.5. Anions removal from ultra-filtered doped water of Sant Joan Despí DWTP at two MIEX concentrations of 0.7 and 1.5 ml/l evaluated in the batch process as a function of the filtration time.

From the measured removal ratios at equilibrium (e.g. at 60 minutes), a selectivity sequence could be defined for the set of anions selected as follows $F^- < Br^- \approx NO_3^- < I^- \approx SO_4^{2-} <$ DOM for both MIEX concentrations.

A comparison between the reduction of DOC for the various MIEX concentrations evaluated, regardless the kind of water used as a feed (sand-filtered water or ultra-filtered water) and the integrated process carried out (MIEX batch or hybrid MIEX-UF process) can be observed in Figure 6.6. For instance, a MIEX concentration of 1.7 ml/l provides TOC values below 1.5 mg/l. Such values are not typically achieved by conventional water potabilization treatments using coagulation/flocculation targeting NOM, colour and particle removals as it is the case of the SJD-DWTP where the TOC values are typically higher than 3 mg /l (Gibert et al., 2015).

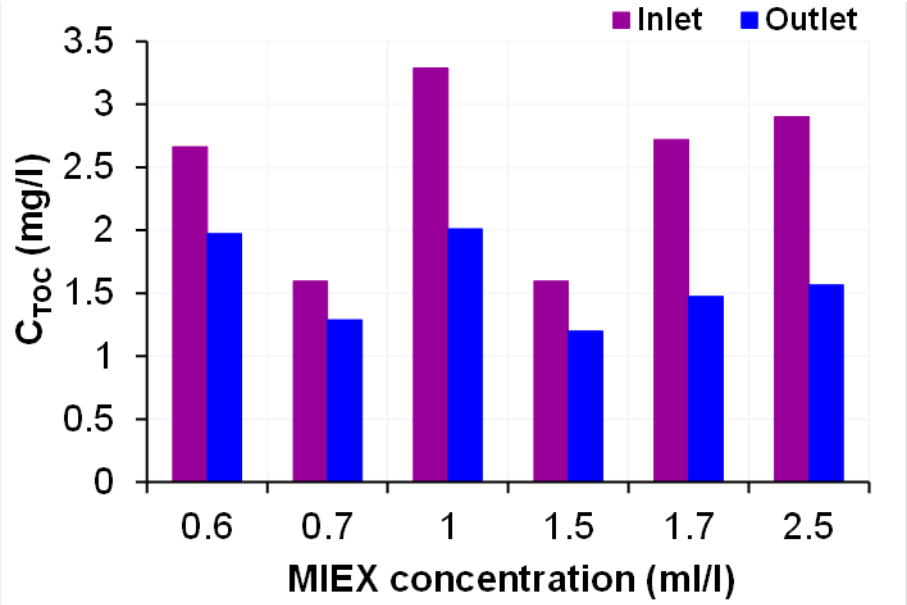

Figure 6.6. Removal of DOC from sand-filtered waters by the hybrid MIEX-UF and the MIEX batch processes for the MIEX concentrations of 0.6, 0.7, 1, 1.5, 1.7 and 2.5 ml/l evaluated after 30 minutes of filtration time

Then, for systems where coagulation/flocculation is not sufficient to achieve DOM values lower than 2 mg C/l, which is the reference guideline in the EU (Council Directive 98/83/EC, 1998), the use of MIEX could provide a new solution to achieve this standard as it has been demonstrated.

6.3.2. Membrane hydraulic performance

The effect of 1) water quality (tap and sand-filtered were used) and 2) the presence/absence of MIEX on the UF membrane hydraulic performance is shown in Figure 6.7.

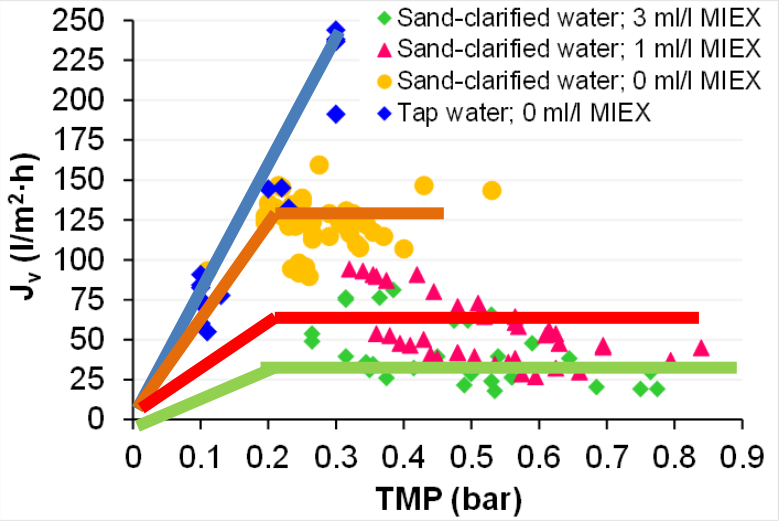

Figure 6.7. Permeate flux (J_v) produced by the hybrid MIEX-UF process (100 kDa capillary membrane) using different quality waters in absence/presence of MIEX (at MIEX concentrations of 0 ml/l, 1 ml/l and 3 ml/l)

In the absence of MIEX, and regardless the feed water quality (tap water or sand-filtered water), the J_v increased with TMP by obeying Darcy's law (Eq.(13)), with tap water showing a more pronounced slope (i.e. higher values of permeability K_v) than sand-filtered water (679 l/m^2 h bar and 500 l/m^2 h bar respectively). This was due to the expected higher values of DOM in sand-filtered water, which results in a more severe formation of a cake layer and the subsequent decrease of flux followed by a stabilization.

In the presence of MIEX two differences in the membrane hydraulic performance were observed in comparison with the findings described above. First, lower J_v were obtained for a given TMP, suggesting that MIEX beads added an additional resistance to the membrane due to the accumulation on the membrane surface and the formation of a MIEX layer. For instance, with sand-filtered water at a TMP of 0.35 bar the J_v exceeded 120 (l/m^2·h) while in the presence of MIEX it ranged between 25 and 80 (l/m^2·h). This finding is expected as although the removal of DOM will favour the reduction of membrane fouling it could not be avoided the formation of the MIEX cake layer as it has been reported in the literature for MF and UF membranes.

On one hand, Kim et al. (Kim and Dempsey, 2010) report that MIEX pre-treatment of a tertiary-treated wastewater effluent removed in fact almost all tendency to foul a polyethersulfone (PES) UF membrane. In line with this finding, Humbert et al. (Humbert et al., 2007) observed that the treatment of MIEX of a clarified-water caused, though very slightly, a decrease of flux in a subsequent UF membrane. Partially in agreement with those findings, Huang et al. (Huang et al., 2012) reported moderate decreases of fouling of a PES UF membrane after MIEX pre-treatment of natural surface water, but not for polyvinylidene (PVDF) UF membrane.

In contrast, Fabris et al. (Fabris et al., 2007), when treating surface water with MIEX followed by a PDVF MF membrane, observed that the presence of MIEX could lead to an increase of the membrane fouling. The authors hypothesised that this detrimental effect of MIEX was due to the abrasion of MIEX resin beads, resulting in an increase of fine material that contributed to the fouling of the membrane.

6.3.2.2. *Flux decline*

Plotted in Figure 6.8 are a) the progress of the normalised permeated flux (J_{v_0}/J_v) and b) the loss of hydraulic permeability over the filtration experiments carried out with sand-filtered water at MIEX concentrations of 1 ml/l and 3 ml/l. It can be seen that the progress consists of a succession of cycles each comprising a filtration step (in which permeated flux gradually decreased and the loss of hydraulic permeability increased) and a CEB step (after which the permeate flux and the hydraulic permeability were restored).

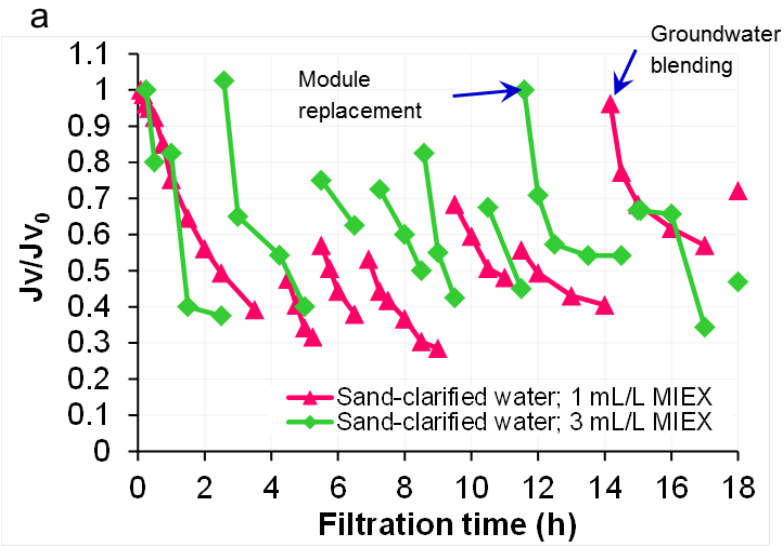

Figure 6.8. Progress of normalised permeate flux (J_v/J_{v_0}) by the hybrid MIEX-UF process upon 18 hours of sand-filtered water filtration at various MIEX concentrations (1 ml/l and 3 ml/l)

For both experiments the same amount of CEB cycles (7-9) were performed during the whole operating time of 18 hours, which corresponded to a permeate volume accumulated of 230 l and 190 l for the MIEX concentrations of 1 ml/l and 3 ml/l, respectively.

As it can be seen in Figure 6.8, the larger flux decline was observed mainly at the beginning of both experiments as well when the membrane module was replaced and when groundwater was blended with sand filtered water (50%/50% volume) in the experiments at MIEX concentrations of 3 ml/l and 1 ml/l, respectively. This decline

was mostly caused due to the thin layer of MIEX suspended next to the membrane surface.

For the experiment at MIEX concentration of 3 ml/l the membrane module was replaced after 12 hours of operation because neither the permeate flux nor the hydraulic permeability could be recovered. In contrast, over the whole experiment at MIEX concentration of 1 ml/l no gain of hydraulic permeability was observed, but the permeate flux was recovered twice. Also, when groundwater was blended into the system from 14 hours to the end of the experiment, the flux was recovered almost up to 100% being the loss of hydraulic permeability smaller since the beginning of the experiment. It might be as groundwater had 3 times less organic content and more sulphate (1.3 times) than sand-clarified water whose two facts could assist on the permeate production.

6.3.3. Efficiency on the removal of negatively charged species

The removal of anion species (DOC, NO_3^-, SO_4^{2-}, Br^- and Cl^-) from sand-filtered water by the hybrid MIEX-UF process at two different MIEX concentrations (1 ml/l and 3 ml/l) is depicted in Figure 6.9.

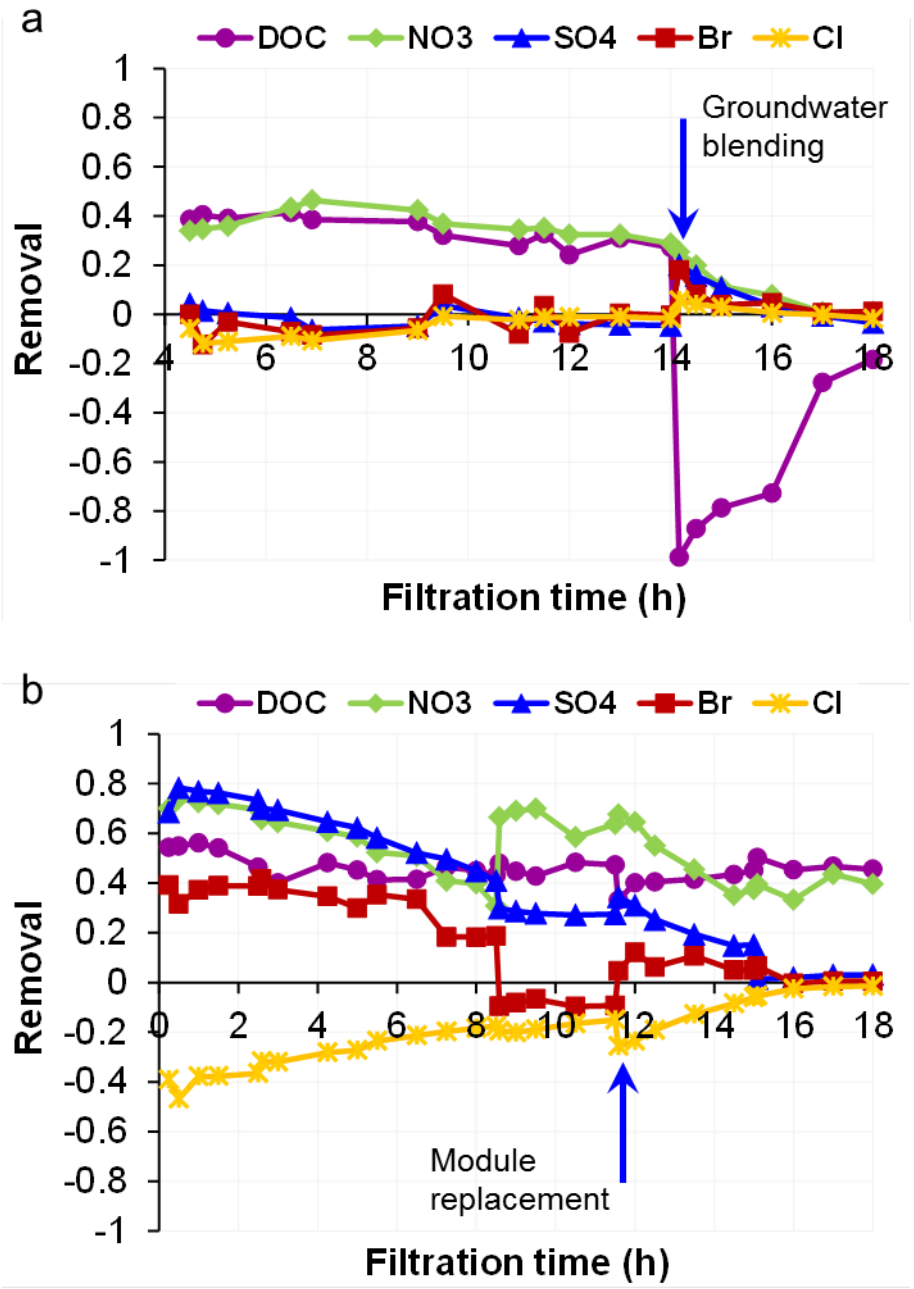

Figure 6.9. Removals of DOC, NO_3^-, SO_4^{2-}, Br^- and Cl^- from sand-filtered water by the hybrid MIEX-UF process at two different MIEX concentrations: a) 1 ml/l and b) 3 ml/l) with respect to the operating time.

Under the MIEX concentration of 1 ml/l while the system only received sand-filtered water (up to 14 h of operating time), the removals of DOC and NO_3^- were indistinctly between 30-40% whereas SO_4^{2-} and Br^- were not even removed (Figure 6.9a). It is known that DOC and NO_3^- are selectively removed by exchanging them in chloride sites of MIEX. Zhou et al. (Zhou et al., 2012) compared the efficiency of nitrate removal by two magnetic anion exchange resins (NDM-1 and MIEX) and attributed its high removal selectivity factor due to their longer alkyl chains of exchange sites.

When groundwater was fed into the system after 14 h of experiment, the removal profiles of all involved species changed their tendencies. Because these two waters differed in their composition (sand-filtered water was richer in TOC but poorer in SO_4^{2-}) (Table 6.1), this change of feed water resulted in differences in the removal extent of solutes. The high concentration of SO_4^{2-} in the new feed water (230 mg/l) caused an increase of its removal (from -5% to 20%), which was accompanied, however, by an abrupt depletion on the removal of DOC (from 27% to -99%) and, to a much lesser extent, of NO_3^- (from 29% to 25%). Boyer et al. (Boyer and Singer, 2006) also observed that working with waters with high content resulted on a decrease of DOC removal.

SO_4^{2-}/NO_3^- selectivity has been largely studied as it is an important factor in the design of an IEX process for NO_3^- removal from potable water. The expected dilute-solution selectivity sequence for the common ions is: $SO_4^{2-} > NO_3^- > Cl^- > HCO_3^-$ (Helfferich, 1962). The causes for this selectivity in anion resins was studied by Clifford and Weber (Clifford and Weber, 1983), for acrylics and epoxies, with closely spaced N-containing (amine) functional groups. It was concluded that nature of both functional groups and matrix are the most important parameters to explain divalent/monovalent selectivity factors. Rokicki and Boyer (Rokicki and Boyer, 2011), explored the efficacy of using anion exchange resin with bicarbonate as counter ion, which will produce a non-chloride treated effluent. The affinity sequence for MIEX resin was UV254-absorbing substances > DOC > $SO_4^{2-} > NO_3^- > Cl^- - HCO_3^-$.

At a MIEX concentration of 3 ml/l, DOC, NO_3^-, SO_4^{2-} and Br^- were continuously removed by the system from the start of the experiment. However, only DOC and, to a lesser extent, NO_3^- removals persisted over time until the end of the experiment (averaged removal percentages of ca 40%), while the removal of SO_4^{2-} and Br^- gradually decreased down to undetectable removals by the end of the experiment. The extraction process is accompanied by a constant increase of the chloride concentration in solution as consequence of the anion exchange reactions described by Eq.(12).

Specifically, at the beginning of the experiment at MIEX concentration of 3 ml/l (Figure 6.9b), SO_4^{2-} and NO_3^- removals were quite similar and higher than DOC and Br^- ones. Nevertheless, Br^- was suddenly released when DOC and NO_3^- were better removed than SO_4^{2-} in the middle of the experiment (~ 8.5 h). Steady removals either of both DOC or NO_3^- were obtained achieved from 16 h onwards once SO_4^{2-}, Br^- and Cl^- were entirely released out the system.

6.3.4. Uptakes of negatively charged species by MIEX

Anions uptakes by MIEX resin were determined by means of the mass balances described in section 6.2. The progression of the solute accumulated into the system for the two evaluated MIEX concentrations (1 ml/l and 3 ml/l) are shown in Figure 6.10 and Figure 6.11, respectively.

For the hybrid experiment at MIEX concentration of 1 ml/l (Figure 6.10), NO_3^- and DOC uptakes progressively increased. At the end of the experiment, NO_3^- uptaken by MIEX amounted 2.5 mol/l MIEX, five times higher than that of DOC (0.5 ml/l MIEX) (Figure 6.10a). On the contrary, SO_4^{2-} was hardly uptaken by the MIEX system (in agreement with the negligible removal shown in Figure 6.9) until 14 h of experiment, when groundwater rich in SO_4^{2-} (230 mg/l) was introduced. From this moment onwards, the SO_4^{2-} uptake increased (always in accordance with the removal discussed in Figure 6.9) up to 1 mol/l MIEX at the end of the experiment. Br^- was also removed from liquid-phase as well as SO_4^{2-} (20%) and better than Cl^- (10%), but neither Br^- nor Cl^- had not ever been uptaken by MIEX (Figure 6.10a and Figure 6.10b, respectively) as their concentrations marginally decreased from liquid-phase. Finally, the measured Cl^- (the resin counter-ion) concentration on the liquid-phase accumulated into the system was up to 7 times higher than SO_4^{2-} and up to 600 times higher than Br^-.

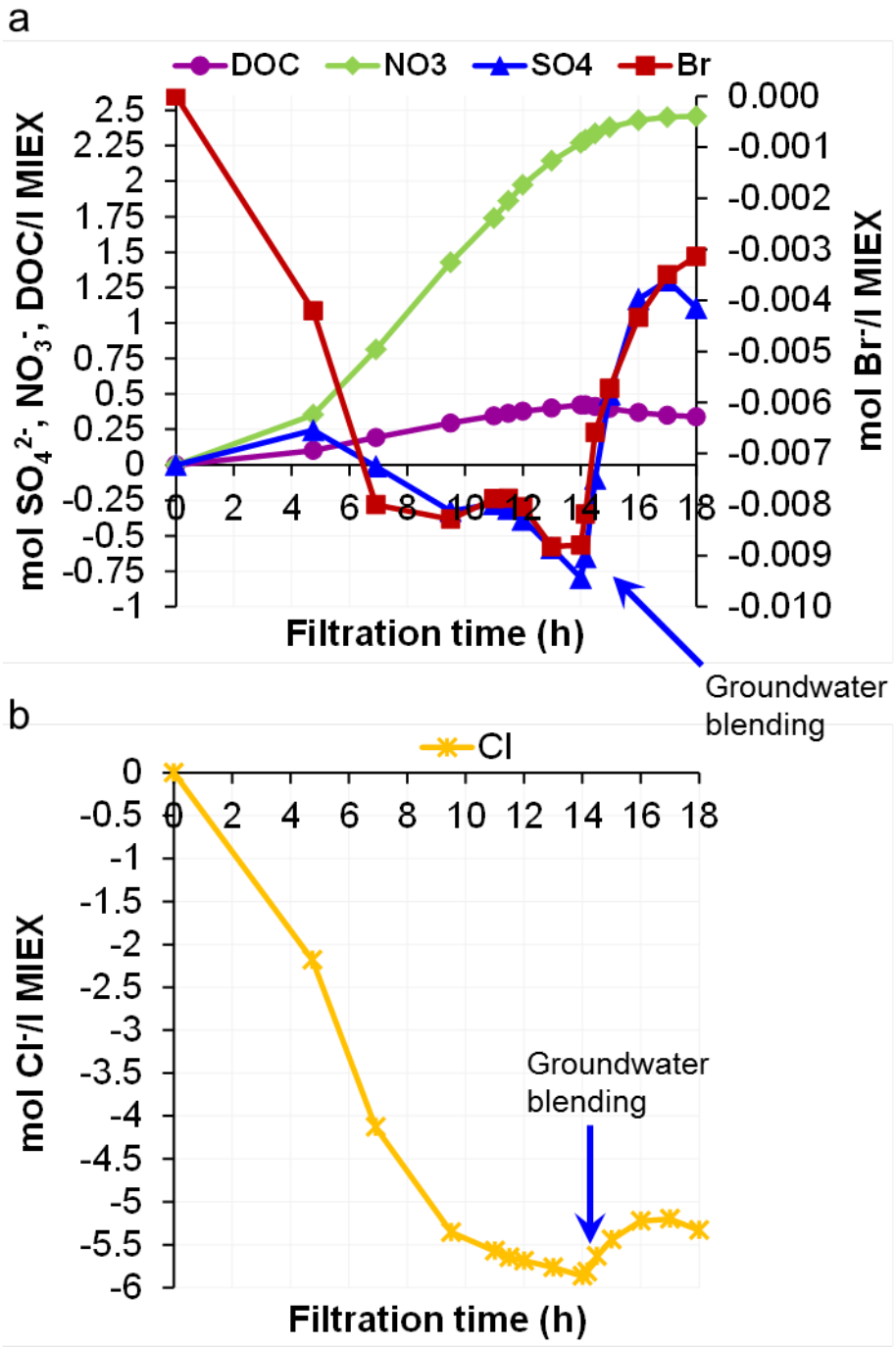

Figure 6.10. Uptakes of SO_4^{2-}, NO_3^-, DOC, Br^- and Cl^- from sand-filtered water by the hybrid MIEX-UF process at MIEX concentration of 1 ml/l.

Since organic compounds were still uptaken at lower sorption rates than SO_4^{2-}, a slight DOC uptake declining was observed (Figure 6.10a) while NO_3^- uptake remained constant. Then, the corresponding uptakes of the involved anions (Figure 6.10) were not in accordance with their removals (Figure 6.9) by the system, as for instance DOC removal dropped whereas NO_3^- removal faintly decreased.

Ates and Incetan (Ates and Incetan, 2013) investigated the affinity and efficiency of two anion exchange resins (MIEX and DOWEX11) on NOM removal in waters with low UV absorbance and high SO_4^{2-} concentration. Two low-UVA surface waters with different SO_4^{2-} concentrations were used. Batch experiments showed NOM removals by both resins, which were higher in low-SO_4^{2-}-content than in high-SO_4^{2-}-content waters. A decrease in NOM removal from 60% to 20% observed with increasing influent SO_4^{2-} concentration indicated that SO_4^{2-} content was a more important parameter influencing DOC removal than the content of other anions such as HCO_3^-, NO_3^- and Br^-.

By using the hybrid MIEX-UF process with sand-filtered water at MIEX concentration of 3 ml/l (Figure 6.11), the solute uptake profiles were quite different in comparison to those obtained at MIEX concentration of 1 ml/l (Figure 6.10). SO_4^{2-} was the best selectively uptaken with respect to the other solutes present in the feed solution. Indeed, SO_4^{2-} was better uptaken than DOC which was thought to have the greatest affinity for MIEX. Even technically working at the largest MIEX concentration, the maximum Cl^- release (2 mol/l MIEX) was three times smaller than the measured in the experiment at MIEX concentration of 1ml/l (6 mol/l MIEX).

As a result for MIEX concentration of 3 ml/l, SO_4^{2-} uptake (0.96 mol/l MIEX) was at least five times higher than DOC uptake (0.19 mol C/l MIEX) over the whole operating time. DOC and NO_3^- showed similar uptake profiles pointing out almost the same affinity for MIEX. Br^- was near five hundred times worse uptaken (0.002 mol/l MIEX) than SO_4^{2-}, although they could seem to follow an equal uptake profile. DOC was also hundred times better uptaken than Br^- and thus, these DBP precursors would have fewer chances to react in order to avoid the undesirable THM formation (Kingsbury and Singer, 2013).

A review of the literature reveals that most of the work done on Br^- removal from water has been carried out with membrane filtration, such as NF, UF and RO, but is not a cost effective method because of expensive membrane (Chellam, 2000). Boyer and Singer (Boyer and Singer, 2008) found that MIEX resin could remove Br^- from raw water to a certain extent, as well as dissolved organic compounds. Ding et al. (Ding et al., 2012a) studied the adsorption characteristics of Br^- by MIEX resin in a batch mode. The high removal efficiency of Br^- (11.51 mg/ml for 1ml/l of MIEX) in comparison with other sorbents (Sánchez-Polo et al., 2007) is obtained at the pH range of 4–9. The uptake of Br^- was shown to decrease with increasing temperature of solution and the coexistent anions have significant effect on Br^- removal following the sequence $SO_4^{2-} > CO_3^{2-} > Cl^-$.

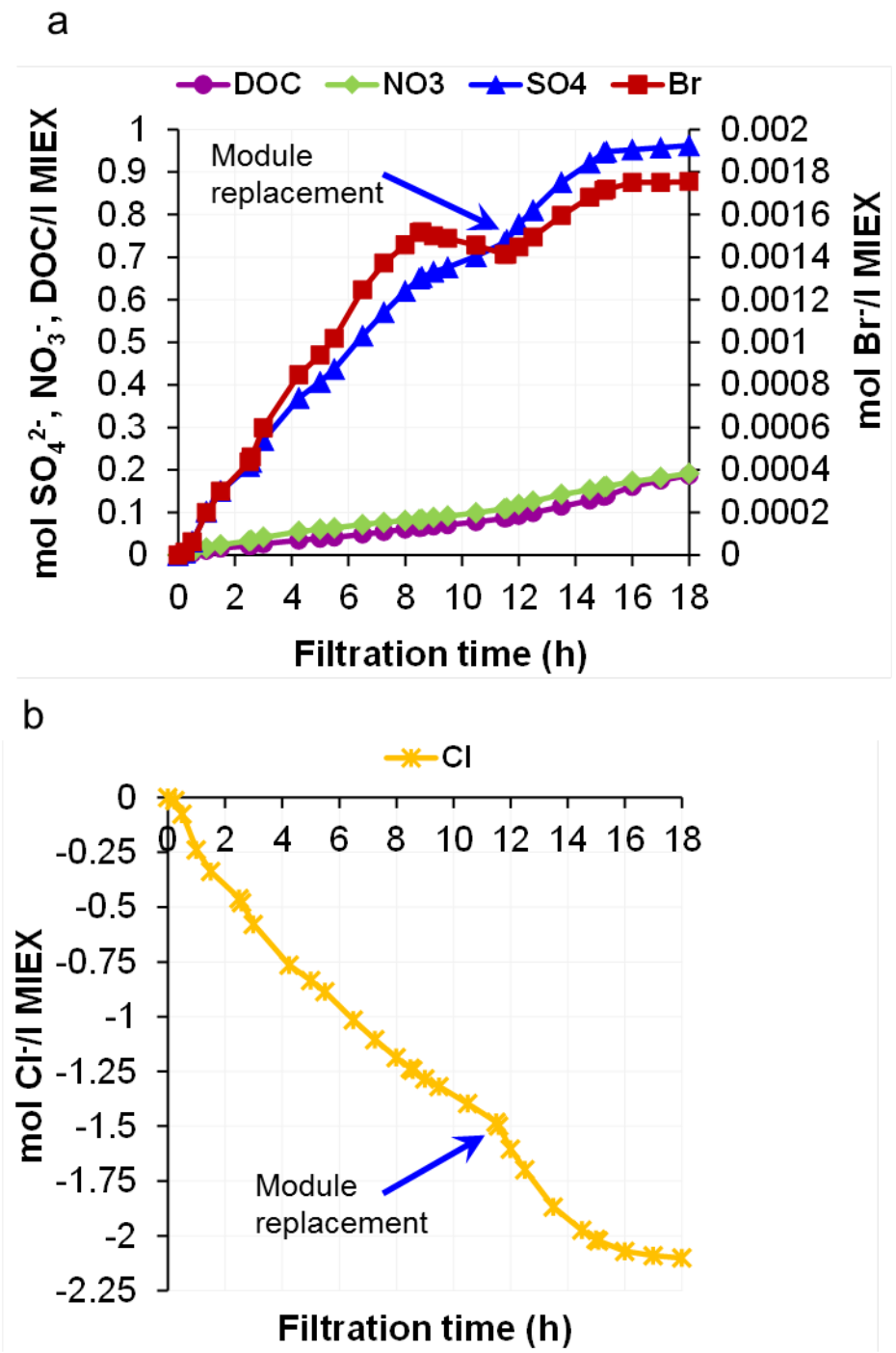

Figure 6.11. Uptakes of SO_4^{2-}, NO_3^-, DOC, Cl^- and Br^- from sand-filtered water by the hybrid MIEX-UF process at MIEX concentration of 3 ml/l.

Solute uptake profiles were not in accordance with their respective solute removals as, for instance, SO_4^{2-} which was the highest uptaken by MIEX (Figure 6.11a) showed a descending removal over the whole operating time (Figure 6.10).

6.3.5. Performance of the hybrid process for DOC, nitrate, sulphate and bromide removal for improving drinking water quality

DOC, SO_4^{2-}, NO_3^- and Br^- concentrations in the UF permeate measured throughout the filtration experiment at 3 ml MIEX/l of sand-filtered water with continuous introduction of raw water are depicted by Figure 6.12. Results show that DOC and by the hybrid MIEX-UF process was much higher than UF alone (data not shown). Residual DOC was kept constant from 1.5 to 2 mg/l over the 18 hours of the experiment.

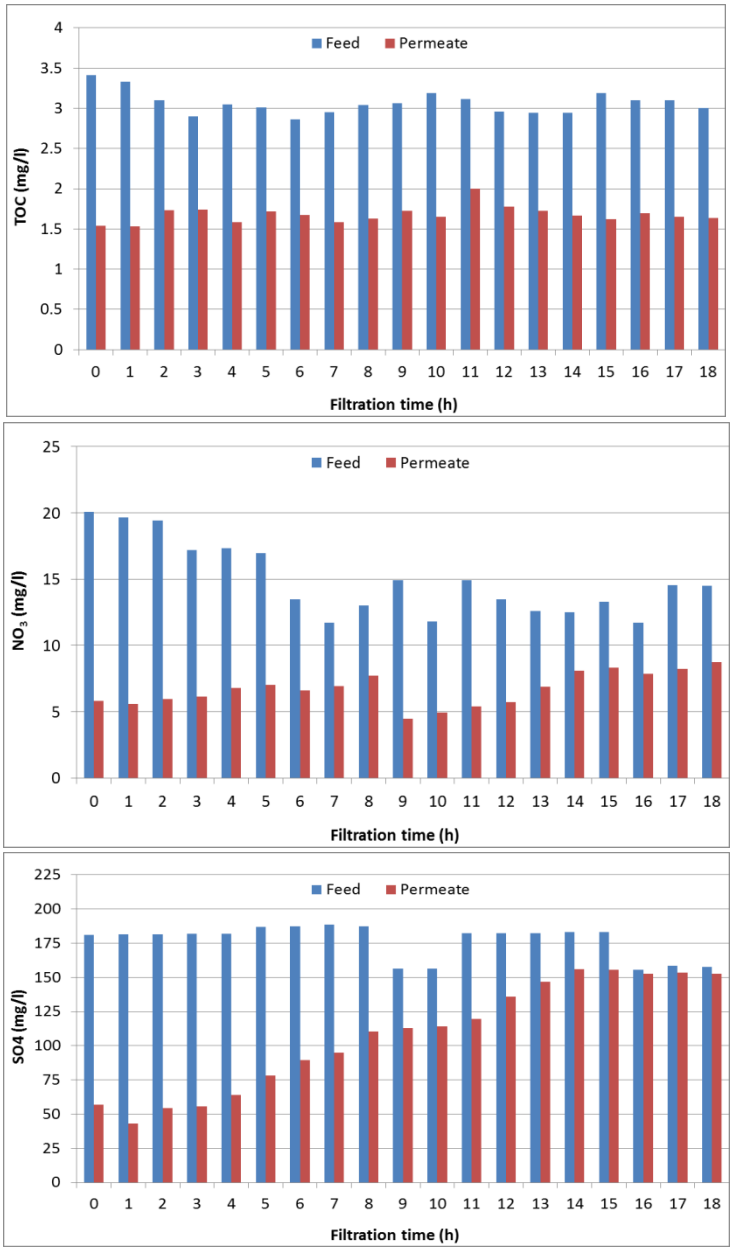

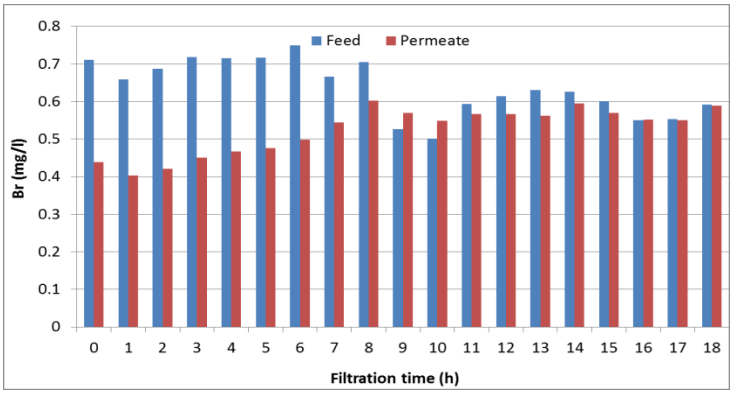

Figure 6.12. (a) DOC (b) NO_3^- (c) SO_4^{2-} (d) Br^- concentrations of sand-filtered water (feed) and UF permeate as a function of filtration time during the experiment conducted at MIEX concentration of 3 ml/l.

After 15 h of filtration, the system reached a stationary profile where the DOC content of the sand-filtered water was reduced from 3.4 to 1.6 mg C/l corresponding to a 50% removal yield. Slightly lower DOC removal values (45%) were obtained for sand-filtered water treated by the hybrid MIEX-UF process at MIEX concentration of 2.5 ml/l (Figure 6.4). Although the DOM was better removed up to 70% when the ultra-filtered doped water was treated by the MIEX batch process at lower MIEX concentration of 1.5 ml/l (Figure 6.5).

It should be indicated that the mean hydraulic residence time was about 20 minutes for the tested pilot configuration, which is very high compared to the fast DOC sorption observed for MIEX. In other words, the contact time is not the limiting factor for DOC sorption. The volume of the MIEX contactor can be reduced without impact on DOC removal. These first results show that MIEX/UF hybrid processes are probably a promising polishing technology for DOC removal.

Results on SO_4^{2-}, NO_3^- and Br^- indicate that the hybrid MIEX-UF process show a high efficiency on the removal of the undesired anions with different organoleptic and human health implications. In the case of NO_3^-, although values found in the raw water, between 20-30 mg NO_3^-/l, are below the regulated value 50 mg NO_3/l (Council Directive 98/83/EC, 1998) a reduction of the concentration between 75% at the initial stages of the filtration cycle, values of 45% were also measured at the end of the filtration cycle. Similar results were measured for SO_4^{2-} with concentration reduction up to 65% at the initial stages of the filtration stage, and not eliminated at the end of the filtration experiment where the system seemed to be saturated by SO_4^{2-}.

Although the Br^- itself is not regulated in EU drinking water regulation (Council Directive 98/83/EC, 1998), the presence of Br^- in water sources potentially endangers the security of drinking water distribution supplies due to the occurrence of brominated DBPs (USEPA, 2006). During the process of chlorination carried out at SJD-DWTP, bromide can be oxidized to HBrO which can react with NOM to form brominated organic DBPs (Bond et al., 2010). Then, and taking into account that

brominated organic DBPs are more harmful to human health than conventional chlorinated organic DBPs (Gan et al., 2013; Richardson, 2003) reduction of Br^- is of key interest (Phetrak et al., 2016).

Removal of Br^- reached up to 40-45% at the initial stages although it is completely accumulated into the system after 8 hours of experiment. These results, are more promising that the reported attempts on Br^- removal, including the use of Ag-doped carbon aerogels (Echigo et al., 2007; Sánchez-Polo et al., 2007); enhanced coagulation by aluminium chloride (Ge and Zhu, 2008; Ge et al., 2007). The main limitation of these removal technologies is the cost associated to the disposal of the wastes generated (Lv et al., 2008) similarly as when NF and RO have been used to reduce Br^- (Chellam, 2000).

Analysis of UF data along the filtration experiments showed a breakthrough profile defined by the selectivity data of the main anion-exchange reactions involved described by Eq.(20) to (23):

$$nP - R_3N^+Cl^- + DOC^{-n} + \Leftrightarrow (P - R_3N^+)_n DOC^{-n} + Cl^- \quad K_{Cl^-/DOC^{-n}} \tag{20}$$

$$P - R_3N^+Cl^- + NO_3^- + \Leftrightarrow P - R_3N^+NO_3^- + Cl^- \quad K_{Cl^-/NO_3^-} \tag{21}$$

$$2P - R_3N^+Cl^- + SO_4^{-2} + \Leftrightarrow (P - R_3N^+)_2\, SO_4^{-2} + 2Cl^- \quad K_{Cl^-/SO_4^{-2}} \tag{22}$$

$$P - R_3N^+Cl^- + Br^- + \Leftrightarrow P - R_3N^+Br^- + Cl^- \quad K_{Cl^-/Br^-} \tag{23}$$

From the measured breakthrough profiles (Figure 6.10 and Figure 6.11) the anion-exchange constants of the set anion-exchange reactions followed different sequences respectively: $K_{Cl-/NO3-} > K_{Cl-/DOC} > K_{Cl-/SO4-2} > K_{Cl-/Br-}$ and $K_{Cl-/SO4-2} > K_{Cl-/NO3-} > K_{Cl-/DOC} > K_{Cl-/Br-}$. IEX equilibrium studies for MIEX are lacking on the literature and only data on single solute sorption experiments could be found (Boyer et al., 2008b; Ding et al., 2012a, 2012b; Graf et al., 2014; Hsu and Singer, 2010; Sánchez-Polo et al., 2007; Willison and Boyer, 2012). Analysis of isotherms data from conventional granular anion-exchange resins (Dron and Dodi, 2011a, 2011b) indicated that similar trends on selectivity factors have been reported and only higher selectivity for sulphate over nitrate were reported by Ates and Incetan (Ates and Incetan, 2013). However, it should be mention that both sulphate and chloride concentration of the evaluated water is much higher than the surface waters reported on these studies.

For multi-solutes systems (e.g. complex surface waters), Apell and Boyer (Apell and Boyer, 2010) explored sequential IEX (anion-exchange followed by cation-exchange and cation-exchange followed by anion-exchange) selectivity factors for MIEX resins. In this studies hardness cations, DOM, and sulphate were shown to interact differently in separate anion and cation exchange processes when treated sequentially compared to the combined IEX process. More recently, Indarawis and Boyer (Indarawis and Boyer, 2013) studied the superposition of anion and cation exchange for removal of anions and DOC from natural waters using MIEX. Because, not enough information is known regarding DOM to calculate a selectivity coefficient, separation factors were used to evaluate the changes in affinity for various ions during combined IEX

compared to conventional IEX. Using charge density titrations of DOM the concentration of DOM (meq/l) was determined. Table 6.5 lists the separation factor calculated for each pair of ions for combined IEX and separate IEX process.

Table 6.5. Calculated $SUVA_{254}$, ionic strength, and separation factors for anion-exchange (AEX), cation-exchange (CEX) and combined IEX (CIEX). Test waters: Cedar Key (CK), Ca hardness (Ca), Mg hardness (Mg), Ca/Mg hardness (Ca/Mg), no hardness (No) (Indarawis and Boyer, 2013)

Resin – water	$SUVA_{254}$	Ionic strength	Separation factors (resin-phase ion/aqueous-phase ion)		
	l/mg m	mol/l	Cl^-/HCO_3^-	Cl^-/SO_4^{2-}	Cl^-/DOC
CIEX-Ca	1.2	0.011	0.44	6.9	32
AEX-Ca	1.1	0.013	1.5	9.4	47
CEX-Ca	4.3	0.011	-	-	-
Control-Ca	4.2	0.014	-	-	-
CIEX-Ca/Mg	1.2	0.011	0.53	6.8	32
AEX-Ca/Mg	1.2	0.014	0.47	9.2	49
CEX-Ca/Mg	4.2	0.011	-	-	-
Control-Ca/Mg	4.4	0.014	-	-	-
CIEX-Mg	1.3	0.011	0.47	6.5	33
AEX-Mg	1.2	0.014	0.33	8.4	40
CEX-Mg	4.2	0.011	-	-	-
Control-Mg	4.3	0.014	-	-	-
CIEX-No	0.9	0.006	0.08	1.8	6
AEX-No	0.9	0.006	0.05	1.9	7
CEX-No	4.2	0.006	-	-	-
Control-No	4.2	0.006	-	-	-
CIEX-CK	1.1	0.005	0.22	0.9	6
AEX-CK	1.1	0.006	0.57	-*	7
CEX-CK	3.0	0.005	-	-	-
Control-CK	2.8	0.007	-	-	-

*No SO_4^{2-} in solution at equilibrium

The trend of lower separation factors for sulphate and DOM during combined IEX than separate anion exchange held true for all experimental waters. During both separate anion-exchange and combined IEX processes, with chloride as the pre-saturation ion, the MIEX resin selectivity sequence was: $HCO_3^- < SO_4^{2-} <$ DOM for two different types of surface water. These results follow general trends in selectivity expected for anion and cation exchange, however information on MIEX selectivity factors for nitrate are lacking.

Because the saturation of MIEX respect of target solutes occurs at different filtration times regeneration of MIEX should be conducted once the first breakthrough point appears (e.g. permeate concentration is 50% of the feed concentration). In our study, as it is shown in Figure 6.12, Br^- reaches the breakthrough point after approximately 9 hours of filtration. Much before than SO_4^{2-} (ca. 16 h) and NO_3^- and DOC which did not reach saturation after 18 h.

Then an additional effort, outside the scope of the present study, is to quantify the potential benefit of increasing the MIEX regeneration frequency to have an improvement on water quality. Measured removal factors approach to those reported by Valero and Arbós (Valero and Arbós, 2010) for water from the Llobregat River at the Abrera DWTP using EDR with values of 75% for bromide and nitrate, 70% for sulphate and 30% for TOC.

6.4. Conclusions

The hybrid process combining magnetic IEX resins and ultrafiltration could be a promising technology after conventional clarification because it could increase the quality of water in terms of DOC and inorganic species.

The use of MIEX resin allowed a rapid sorption of DOC in less than 10 min with about 40 and 60% removal yields on DOC for sand-clarified water.

The reduction of DOC, for doses higher than 6 ml/l provides TOC values below 2 mg C/l. Such values are not typically achieved by conventional water potabilization treatments, using coagulation/flocculation targeting NOM and colour and particle removal, as it is the case of the Sant Joan Despí DWTP where values are typically higher than 3 mg C/l. Then, for systems where coagulation/flocculation is not sufficient to achieve DOM values lower than 2 mg C/l, which is the reference guideline in the EU, the use of MIEX could provide a new solution to achieve this standard as it has been demonstrated.

The capacity of MIEX resin to reduce the levels of non-desired ions in drinking water as SO_4^{2-}, NO_3^- and Br^- under partial saturation is of mention (values from 40 to 75%) and the process implementation should consider operation criteria to avoid resin capacity saturation.

If objective of the application to surface water of low quality should be not only the reduction of DOC content and the reduction of the nitrate, sulphate and bromide concentrations it should be avoided to reach the MIEX saturation on organic matter.

The removal factor measured for bromide, nitrate, sulphate and TOC are similar to those obtained by EDR.

Chapter 7
Conclusions

On the application of a NF membrane to reduce salinity (e.g. hardness and inorganic pollutants) in brackish waters and in the effort to characterize and identify the mechanisms of rejection of ionic species under different solution compositions (e.g. dominant salts nature), the following research conclusions have been achieved:

a) The effect of the dominant salt (NaCl, $MgCl_2$, $MgSO_4$) concentration on the rejection of trace ions (Na^+, K^+, Cl^-, Ca^{2+}, Mg^{2+}, SO_4^{2-}, NO_3^-, NH_4^+, Br^- and I^-) have shown that the transport of easily-permeating ions such as single-charged inorganic ions through NF270 membrane containing ionizable free carboxylic and amine groups is controlled to a larger extent by a combination of the electric field, the membrane permeability to them, the membrane properties and the solution composition.

b) The experimental salt and ions rejection data with various trace ions and dominant salts confirm this hypothesis and can be qualitatively interpreted within the scope of the extended SEDF model in the case of feed solutions consisting of one dominant salt and (any number of) trace ions.

c) The use of two trace ions at the same time rejections can simultaneously be fitted by using the same dominant-salt-controlled parameters of the model.

d) The rejection of a trace ion depends decisively on its environment and its dependence is explained by the spontaneously arising electric fields generated in the membrane phase. The electric field gives rise to negative rejections of singly charged inorganic ions present as small additions to well-rejected dominant salts.

e) The application of the SEDF model to relate the intrinsic rejections to the observable ones provides a theoretical interpretation of the intrinsic membrane permeabilities. This approach allows determining the membrane permeabilities to cations and anions of dominant salts as well as to the trace ions, in comparison to conventional measurements with single salts where only the salt permeability could be determined.
f) Severe changes on the selectivity rejection of inorganic ions as Br^-, I^-, NO_3^-, NH_4^+, K^+ depend on the environment solutions. Although the information on the membrane permeabilities to ions has remained empirical in this study, in principle, it can further be used for the verification of self-consistency of various mechanistic models. The availability of three "measurable" quantities, the membrane permeabilities to the cations and anions of the dominant salt as well as to the trace ions, in contrast to just one permeability to the salt available from conventional measurements with single salts, can make self-consistency checks much more conclusive.
g) Comparing rejection data from both membrane configurations, flat sheet and spiral wound, it can be said that the water flux obtained is higher by using the flat sheet membrane configuration working at the same pressure and salt mixture.
h) The dominant salt rejection seems to be not affected by the membrane configuration, as similar rejection curves were obtained for both configurations. The general trend observed for the trace ion rejection is the same.
i) SEDF model is also a valid model which is capable to fit satisfactorily experimental data of a dominant salt and a trace mixture for both membrane configurations and similar membrane permeabilities with respect to each ion were measured.
j) In general terms, it seems that the two configurations behave in a similar way. This trend is useful when implementing NF technology at industrial scale, since SW configuration is used at large scale, representing a larger membrane active area and occupying a small space, whereas the flat sheet configuration is used in test in a lab scale, for its simplicity and its easier operation.

On the evaluation of the suitability of Magnetic Ion Exchangers (MIEX), in base of a quaternary functional group, for water quality improvement, the following conclusions could be drawn:

k) The use of MIEX resin allows a rapid sorption of DOC in less than 10 min with about 40 and 60% removal yields on DOC for sand-clarified water.
l) The reduction of DOC, for doses of MIEX higher than 6 ml/l, provides TOC values below 2 mgC/l. Such values are not typically achieved by conventional water potabilization treatments using coagulation/flocculation targeting NOM and colour and particle removal, as it is the case of the Sant Joan Despí DWTP where values are typically higher than 3 mgC/l. Then, for systems where coagulation/flocculation is not sufficient to achieve DOC values lower than 2 mgC/l, which is the reference guideline in the EU, the use of MIEX could provide a new solution to achieve this standard as it has been

demonstrated.

m) The capacity of MIEX resin to reduce the levels of non-desired ions in drinking water as SO_4^{2-}, NO_3^- and Br^- under partial saturation is of mention (values from 40 to 75%) and the process implementation should consider operation criteria to avoid resin capacity saturation.

n) If the objective of the application of MIEX to surface water of low quality is not only the reduction of DOC content but also the reduction of the NO_3^-, SO_4^{2-} and Br^- concentrations, MIEX saturation on organic matter should be avoided. The removal factor measured for NO_3^-, SO_4^{2-}, Br^- and TOC are similar to those obtained by electrodialysis reversal.

o) The hybrid process combining MIEX and ultrafiltration could be a promising technology after conventional clarification because it could increase the quality of water in terms of DOC and inorganic species.

References

Abdulgader, H. Al, Kochkodan, V., Hilal, N., 2013. Hybrid ion exchange - Pressure driven membrane processes in water treatment: A review. Sep. Purif. Technol. 116, 253–264.

Afonso, M.D., Hagmeyer, G., Gimbel, R., 2001. Streaming potential measurements to assess the variation of nanofiltration membranes surface charge with the concentration of salt solutions. Sep. Purif. Technol. 23, 529–541.

Afonso, M.D., Jaber, J.O., Mohsen, M.S., 2004. Brackish groundwater treatment by reverse osmosis in Jordan. Desalination 164, 157–171.

Afonso, M.D., Pinho, M.N. De, 2000. Transport of MgSO4, MgCl2, and Na2SO4 across an amphoteric nanofiltration membrane. J. Memb. Sci. 179, 137–154.

Al-Amoudi, A.S., 2010. Factors affecting natural organic matter (NOM) and scaling fouling in NF membranes: A review. Desalination 259, 1–10.

Alghoul, M.A., Poovanaesvaran, P., Sopian, K., Sulaiman, M.Y., 2009. Review of brackish water reverse osmosis (BWRO) system designs. Renew. Sustain. Energy Rev. 13, 2661–2667.

Allpike, B.P., Heitz, A., Joll, C. a, Kagi, R.I., Abbt-Braun, G., Frimmel, F.H., Brinkmann, T., Her, N., Amy, G., 2005. Size exclusion chromatography to characterize DOC removal in drinking water treatment. Environ. Sci. Technol. 39, 2334–2342.

Al-Zoubi, H., Hilal, N., Darwish, N. a., Mohammad, A.W., 2007. Rejection and modelling of sulphate and potassium salts by nanofiltration membranes: neural network and Spiegler–Kedem model. Desalination 206, 42–60.

Anderson, C.T., Maier, W.J., 1979. Trace organics removal by anion exchange resins.

J. Am. Water Work. Assoc. 71, 278–283.

Apell, J.N., Boyer, T.H., 2010. Combined ion exchange treatment for removal of dissolved organic matter and hardness. Water Res. 44, 2419–2430.

Arias-Paic, M., Cawley, K.M., Byg, S., Rosario-Ortiz, F.L., 2016. Enhanced DOC removal using anion and cation ion exchange resins. Water Res. 88, 981–989.

Ates, N., Incetan, F.B., 2013. Competition impact of sulfate on NOM removal by anion-exchange resins in high-sulfate and low-SUVA waters. Ind. Eng. Chem. Res. 52, 14261–14269.

Bae, B.-U., Jung, Y.-H., Han, W.-W., Shin, H.-S., 2002. Improved brine recycling during nitrate removal using ion exchange. Water Res. 36, 3330–3340.

Baker, R.W., 2012. Membrane Technology and Applications, 3rd ed. ed. Wiley editions, Chichester.

Bandini, S., Vezzani, D., 2003. Nanofiltration modeling: the role of dielectric exclusion in membrane characterization. Chem. Eng. Sci. 58, 3303–3326.

Bason, S., Freger, V., 2010. Phenomenological analysis of transport of mono- and divalent ions in nanofiltration. J. Memb. Sci. 360, 389–396.

Bason, S., Kaufman, Y., Freger, V., 2010. Analysis of Ion Transport in Nanofiltration Using Phenomenological Coefficients and Structural Characteristics. J. Phys. Chem. B 114, 3510–3517.

Bason, S., Kedem, O., Freger, V., 2009. Determination of concentration-dependent transport coefficients in nanofiltration: Experimental evaluation of coefficients. J. Memb. Sci. 326, 197–204.

Bason, S., Oren, Y., Freger, V., 2011. Ion transport in the polyamide layer of RO membranes: Composite membranes and free-standing films. J. Memb. Sci. 367, 119–126.

Bason, S., Oren, Y., Freger, V., 2007. Characterization of ion transport in thin films using electrochemical impedance spectroscopy. II: Examination of the polyamide layer of RO membranes. J. Memb. Sci. 302, 10–19.

Becker, N.S.C., Bennett, D.M., Bolto, B.A., Dixon, D.R., Eldridge, R.J., Le, N.P., Rye, C.S., 2004. Detection of polyelectrolytes at trace levels in water by fluorescent tagging. React. Funct. Polym. 60, 183–193.

Belgiorno, V., Rizzo, L., Fatta, D., Della Rocca, C., Lofrano, G., Nikolaou, A., Naddeo, V., Meric, S., 2007. Review on endocrine disrupting-emerging compounds in urban wastewater: occurrence and removal by photocatalysis and ultrasonic irradiation for wastewater reuse. Desalination 215, 166–176.

Blaney, L.M., Cinar, S., SenGupta, A.K., 2007. Hybrid anion exchanger for trace phosphate removal from water and wastewater. Water Res. 41, 1603–1613.

Blankert, B., Betlem, B.H.L., Roffel, B., 2007. Development of a control system for in-line coagulation in an ultrafiltration process. J. Memb. Sci. 301, 39–45.

Bódalo, A., Gómez, J.-L., Gómez, E., León, G., Tejera, M., 2005. Ammonium removal from aqueous solutions by reverse osmosis using cellulose acetate membranes. Desalination 184, 149–155.

Bódalo, A., Gómez, J.-L., Gómez, E., León, G., Tejera, M., 2004. Reduction of

sulphate content in aqueous solutions by reverse osmosis using cellulose acetate membranes. Deasalination 162, 55–60.

Boening, P.H., Beckmann, D.D., Snoeyink, V.L., 1980. Activated carbon versus resin adsorption of humic substances. J. Am. Water Work. Assoc. 72, 54–59.

Bolto, B., Dixon, D., Eldridge, R., 2004. Ion exchange for the removal of natural organic matter. React. Funct. Polym. 60, 171–182.

Bolto, B., Dixon, D., Eldridge, R., King, S., 2002. Removal of THM precursors by coagulation or ion exchange. Water Res. 36, 5066–5073.

Bond, T., Goslan, E.H., Parsons, S. a., Jefferson, B., 2010. Disinfection by-product formation of natural organic matter surrogates and treatment by coagulation, MIEX and nanofiltration. Water Res. 44, 1645–1653.

Bourke, M., Arias, M., 2009. Ion Exchange for NOM Removal Prior to Membranes, Orica Watercare.

Bourke, M., Harrison, S., Long, B., Lebeau, T., 2001. MIEX® resin pretreatment followed by microfiltration as an alternative to nanofiltration for DBP precursor removal, in: AWWA Membrane Technology Conference Proceedings. pp. 1–10.

Boussu, K., De Baerdemaeker, J., Dauwe, C., Weber, M., Lynn, K.G., Depla, D., Aldea, S., Vankelecom, I.F.J., Vandecasteele, C., Van der Bruggen, B., 2007. Physico-chemical characterization of nanofiltration membranes. Chemphyschem 8, 370–379.

Bowen, W.R., Cassey, B., Jones, P., Oatley, D.L., 2004. Modelling the performance of membrane nanofiltration—application to an industrially relevant separation. J. Memb. Sci. 242, 211–220.

Bowen, W.R., Mohammad, A.W., Hilal, N., 1997. Characterisation of nanofiltration membranes for predictive purposes - use of salts , uncharged solutes and atomic force microscopy. J. Memb. Sci. 126, 91–105.

Bowen, W.R., Mukhtar, H., 1996. Characterisation and prediction of separation performance of nanofiltration membranes. J. Memb. Sci. 112, 263–274.

Bowen, W.R., Welfoot, J.S., 2002. Modelling the performance of membrane nanofiltration — critical assessment and model development. Chem. Eng. Sci. 57, 1121–1137.

Bowen, W.R., Welfoot, J.S., Williams, P.M., 2002. Linearized transport model for nanofiltration: Development and assessment. AIChE J. 48, 760–773.

Boyer, T.H., Miller, C.T., Singer, P.C., 2008a. Modeling the removal of dissolved organic carbon by ion exchange in a completely mixed flow reactor. Water Res. 42, 1897–1906.

Boyer, T.H., Singer, P.C., 2008. Stoichiometry of removal of natural organic matter by ion exchange. Environ. Sci. Technol. 42, 608–613.

Boyer, T.H., Singer, P.C., 2006. A pilot-scale evaluation of magnetic ion exchange treatment for removal of natural organic material and inorganic anions. Water Res. 40, 2865–2876.

Boyer, T.H., Singer, P.C., 2005. Bench-scale testing of a magnetic ion exchange resin for removal of disinfection by-product precursors. Water Res. 39, 1265–1276.

Boyer, T.H., Singer, P.C., Aiken, G.R., 2008b. Removal of dissolved organic matter by anion exchange: effect of dissolved organic matter properties. Environ. Sci. Technol. 42, 7431–7437.

Bruni, L., Bandini, S., 2009. Studies on the role of site-binding and competitive adsorption in determining the charge of nanofiltration membranes. Desalination 241, 315–330.

Cai, Z., Kim, J., Benjamin, M.M., 2008. NOM removal by adsorption and membrane filtration using heated aluminum oxide particles. Environ. Sci. Technol. 42, 619–623.

Chang, E.E., Lin, Y.P., Chiang, P.C., 2001. Effects of bromide on the formation of THMs and HAAs. Chemosphere 43, 1029–1034.

Chellam, S., 2000. Effects of nanofiltration on trihalomethane and haloacetic acid precursors removal and speciation in waters containing low concentrations of bromide ion. Environ. Sci. Technol. 34, 1813–1820.

Chen, Y., Dong, B.Z., Gao, N.Y., Fan, J.C., 2007. Effect of coagulation pretreatment on the fouling of ultrafiltration membrane. Desalination 204, 181–188.

Childress, A.E., Elimelech, M., 1996. Effect of solution chemistry on the surface charge of polymeric reverse osmosis and nanofiltration membranes. J. Memb. Sci. 119, 253–268.

Cho, M.H., Lee, C.H., Lee, S., 2006. Effect of flocculation conditions on membrane permeability in coagulation-microfiltration. Desalination 191, 386–396.

Choi, Y.H., Kim, H.S., Kweon, J.H., 2008. Role of hydrophobic natural organic matter flocs on the fouling in coagulation-membrane processes. Sep. Purif. Technol. 62, 529–534.

Chow, C.W.K., Fabris, R., Van Leeuwen, J., Wang, D., Drikas, M., 2008. Assessing natural organic matter treatability using high performance size exclusion chromatography. Environ. Sci. Technol. 42, 6683–6689.

Clifford, D., Weber, W.J., 1983. The determinants of divalent/monovalent selectivity in anion exchangers. React. Polym. Ion Exch. Sorbents 1, 77–89.

Comstock, S.E.H., Boyer, T.H., Graf, K.C., 2011. Treatment of nanofiltration and reverse osmosis concentrates: Comparison of precipitative softening, coagulation, and anion exchange. Water Res. 45, 4855–4865.

Cornelissen, E.R., Beerendonk, E.F., Nederlof, M.N., van der Hoek, J.P., Wessels, L.P., 2009. Fluidized ion exchange (FIX) to control NOM fouling in ultrafiltration. Desalination 236, 334–341.

Coronell, O., González, M.I., Mariñas, B.J., Cahill, D.G., 2010. Ionization behavior, stoichiometry of association, and accessibility of functional groups in the active layers of reverse osmosis and nanofiltration membranes. Environ. Sci. Technol. 44, 6808–6814.

Coronell, O., Mariñas, B.J., Cahill, D.G., 2011. Depth heterogeneity of fully aromatic polyamide active layers in reverse osmosis and nanofiltration membranes. Environ. Sci. Technol. 45, 4513–4520.

Coronell, O., Mariñas, B.J., Zhang, X., Cahill, D.G., 2007. Quantification of functional groups in the active layer of nanofiltration (NF) and reverse osmosis

(RO) membranes.

Council Directive 98/83/EC, 1998. , of 3 November 1998 on the quality of water intended for human consumption.

Darvishmanesh, S., Robberecht, T., Luis, P., Degrève, J., Van der Bruggen, B., 2011. Performance of Nanofiltration Membranes for Solvent Purification in the Oil Industry. J. Am. Oil Chem. Soc. 88, 1255–1261.

Delpla, I., Jung, A. V., Baures, E., Clement, M., Thomas, O., 2009. Impacts of climate change on surface water quality in relation to drinking water production. Environ. Int. 35, 1225–1233.

Déon, S., Dutournié, P., Limousy, L., Bourseau, P., 2011. The Two-Dimensional Pore and Polarization Transport Model to Describe Mixtures Separation by Nanofiltration: Model Validation. AIChE J. 57, 985–995.

Déon, S., Escoda, A., Fievet, P., Dutournié, P., Bourseau, P., 2012. How to use a multi-ionic transport model to fully predict rejection of mineral salts by nanofiltration membranes. Chem. Eng. J. 189-190, 24–31.

Ding, L., Deng, H., Wu, C., Han, X., 2012a. Affecting factors, equilibrium, kinetics and thermodynamics of bromide removal from aqueous solutions by MIEX resin. Chem. Eng. J. 181-182, 360–370.

Ding, L., Wu, C., Deng, H., Zhang, X., 2012b. Adsorptive characteristics of phosphate from aqueous solutions by MIEX resin. J. Colloid Interface Sci. 376, 224–232.

Dong, B.Z., Chen, Y., Gao, N.Y., Fan, J.C., 2007. Effect of coagulation pretreatment on the fouling of ultrafiltration membrane. J. Environ. Sci. 19, 278–283.

Donnan, F.G., 1995. Theory of membrane equilibria and membrane potentials in the presence of non-dialysing electrolytes. A contribution to physical-chemical physiology. J. Memb. Sci. 100, 45–55.

Drikas, M., Chow, C.W.K., Cook, D., 2003. The impact of recalcitrant organic character on disinfection stability, trihalomethane formation and bacterial regrowth: An evaluation of magnetic ion exchange resin (MIEX®) and alum coagulation. J. Water Supply Res. Technol. - AQUA 52, 475–487.

Drikas, M., Dixon, M., Morran, J., 2011. Long term case study of MIEX pre-treatment in drinking water; understanding NOM removal. Water Res. 45, 1539–1548.

Dron, J., Dodi, A., 2011a. Comparison of adsorption equilibrium models for the study of CL-, NO3- and SO4(2-) removal from aqueous solutions by an anion exchange resin. J. Hazard. Mater. 190, 300–307.

Dron, J., Dodi, A., 2011b. Thermodynamic Modeling of Cl - , NO 3 - and SO 42 - Removal by an Anion Exchange Resin and Comparison with Dubinin - Astakhov Isotherms 2625–2633.

Duan, J., Gregory, J., 2003. Coagulation by hydrolysing metal salts. Adv. Colloid Interface Sci. 100-102, 475–502.

Echigo, S., Itoh, S., Kuwahara, M., Echigo, S., 2007. Bromide removal by hydrotalcite-like compounds in a continuous system. Water Sci. Technol. 56, 117–122.

Edzwald, J.K., 2011. Water Quality & Treatment A Handbook on Drinking Water, Sixth Edit. ed. Mc Graw Hill.

Eikebrokk, B., Vogt, R.D., Liltved, H., 2004. NOM increase in Northern European source waters: Discussion of possible causes and impacts on coagulation/contact filtration processes. Water Sci. Technol. Water Supply 4, 47–54.

El-Manharawy, S., Hafez, A., 2001. Water type and guidelines for RO system design. Desalination 139, 97–113.

EPA, 1998. Stage 1 Disinfectants and Disinfection Byproducts Rule.

Ernst, M., Bismarck, A., Springer, J., Jekel, M., 2000. Zeta-potential and rejection rates of a polyethersulfone nanofiltration membrane in single salt solutions. J. Memb. Sci. 165, 251–259.

Escoda, A., Déon, S., Fievet, P., 2011. Assessment of dielectric contribution in the modeling of multi-ionic transport through nanofiltration membranes. J. Memb. Sci. 378, 214–223.

Evans, C.D., Monteith, D.T., Cooper, D.M., 2005. Long-term increases in surface water dissolved organic carbon: Observations, possible causes and environmental impacts. Environ. Pollut. 137, 55–71.

Fabris, R., Chow, C.W.K., Drikas, M., Eikebrokk, B., 2008. Comparison of NOM character in selected Australian and Norwegian drinking waters. Water Res. 42, 4188–4196.

Fabris, R., Lee, E.K., Chow, C.W.K., Chen, V., Drikas, M., 2007. Pre-treatments to reduce fouling of low pressure micro-filtration (MF) membranes. J. Memb. Sci. 289, 231–240.

Fearing, D.A., Banks, J., Guyetand, S., Eroles, C.M., Jefferson, B., Wilson, D., Hillis, P., Campbell, A.T., Parsons, S.A., 2004. Combination of ferric and MIEX® for the treatment of a humic rich water. Water Res. 38, 2551–2558.

Fernández-Turiel, J.L., Llorens, J.F., Roig, A., Carnicero, M., Valero, F., 2000. Monitoring of drinking water treatment plants using ICP-MS. Toxicol. Environ. Chem. 74, 87–103.

Freger, V., 2004. Swelling and morphology of the skin layer of polyamide composite membranes: An atomic force microscopy study. Environ. Sci. Technol. 38, 3168–3175.

Freger, V., 2003. Nanoscale heterogeneity of polyamide membranes formed by interfacial polymerization. Langmuir 19, 4791–4797.

Freger, V., Srebnik, S., 2003. Mathematical model of charge and density distributions in interfacial polymerization of thin films. J. Appl. Polym. Sci. 88, 1162–1169.

Fritzmann, C., Löwenberg, J., Wintgens, T., Melin, T., 2007. State-of-the-art of reverse osmosis desalination. Desalination 216, 1–76.

Galiana-Aleixandre, M.-V., Mendoza-Roca, J.-A., Bes-Piá, A., 2011. Reducing sulfates concentration in the tannery effluent by applying pollution prevention techniques and nanofiltration. J. Clean. Prod. 19, 91–98.

Galjaard, G., Kruithof, J., Kamp, P.C., Raspati, G., 2004. Influence of NOM and Membrane Surface Charge on UF-membrane fouling, in: 2nd IWA Leading-Edge Conference on Water and Wastewater Treatment.

Gan, X., Karanfil, T., Kaplan Bekaroglu, S.S., Shan, J., 2013. The control of N-DBP and C-DBP precursors with MIEX®. Water Res. 47, 1344–1352.

García, V., Fenández, A.R., Medina, M.E., Ferrer, O., Cortina, J.L., Valero, F., Devesa, R., 2015. Flavour assessment of blends between desalinated and conventionally treated sources. Desalin. Water Treat. 53, 3466–3474.

Garcia-Aleman, J., Dickson, J.M., 2004. Mathematical modeling of nanofiltration membranes with mixed electrolyte solutions. J. Memb. Sci. 235, 1–13.

Ge, F., Shu, H., Dai, Y., 2007. Removal of bromide by aluminium chloride coagulant in the presence of humic acid. J. Hazard. Mater. 147, 457–462.

Ge, F., Zhu, L., 2008. Effects of coexisting anions on removal of bromide in drinking water by coagulation. J. Hazard. Mater. 151, 676–681.

Gibert, O., de Pablo, J., Cortina, J.L., Ayora, C., 2008. Evaluation of a Sheep Manure/Limestone Mixture for In Situ Acid Mine Drainage Treatment. Environ. Eng. Sci. 25, 43–52.

Gibert, O., Lefèvre, B., Fernández, M., Bernat, X., Paraira, M., Pons, M., 2013. Fractionation and removal of dissolved organic carbon in a full-scale granular activated carbon filter used for drinking water production. Water Res. 47, 2821–2829.

Gibert, O., Lefèvre, B., Teuler, A., Bernat, X., Tobella, J., 2015. Distribution of dissolved organic matter fractions along several stages of a drinking water treatment plant. J. Water Process Eng. 6, 64–71.

Giorno, L., Drioli, E., 2000. Biocatalytic membrane reactors: applications and perspectives. Trends Biotechnol. 18, 339–349.

Graf, K.C., Cornwell, D. a., Boyer, T.H., 2014. Removal of dissolved organic carbon from surface water by anion exchange and adsorption: Bench-scale testing to simulate a two-stage countercurrent process. Sep. Purif. Technol. 122, 523–532.

Grakist, G., Maas, K., Rosbergen, W., Kappelhof, J., 2002. Keeping our wells fresh, in: 17th Salt Water Intrusion Meeting, Delft, The Netherlands. pp. 337–340.

Hagmeyer, G., Gimbel, R., 1998. Modelling the salt rejection of nanofiltration membranes for ternary ion mixtures and for single salts at different pH values. Des 117, 247–256.

Hall, M.S., Lloyd, D.R., Starov, V.M., 1997. Reverse osmosis of multicomponent electrolyte solutions Part II. Experimental verification. J. Memb. Sci. 128, 39–53.

Häyrynen, K., Pongrácz, E., Väisänen, V., Pap, N., Mänttäri, M., Langwaldt, J., Keiski, R.L., 2009. Concentration of ammonium and nitrate from mine water by reverse osmosis and nanofiltration. Desalination 240, 280–289.

Helfferich, F., 1962. Ion exchange, McGraw-Hil. ed. New York.

Her, N., Amy, G., Chung, J., Yoon, J., Yoon, Y., 2008. Characterizing dissolved organic matter and evaluating associated nanofiltration membrane fouling. Chemosphere 70, 495–502. doi:10.1016/j.chemosphere.2007.06.025

Hilal, N., Al-Zoubi, H., Darwish, N.A., Mohammad, A.W., 2005a. Characterisation of nanofiltration membranes using atomic force microscopy. Desalination 177, 187–199.

Hilal, N., Al-Zoubi, H., Darwish, N.A., Mohammad, A.W., Abu Arabi, M., 2004. A comprehensive review of nanofiltration membranes: Treatment, pretreatment,

modelling, and atomic force microscopy. Desalination 170, 281–308.

Hilal, N., Al-Zoubi, H., Mohammad, A.W., Darwish, N. a., 2005b. Nanofiltration of highly concentrated salt solutions up to seawater salinity. Desalination 184, 315–326.

Hillis, P., 2000. Membrane Technology in Water and Wastewater Treatment. Royal Society of Chemistry, UK.

Howe, K.J., Marwah, A., Chiu, K.P., Adham, S.S., 2006. Effect of coagulation on the size of MF and UF membrane foulants. Environ. Sci. Technol. 40, 7908–7913.

Hsu, S., Singer, P.C., 2010. Removal of bromide and natural organic matter by anion exchange. Water Res. 44, 2133–2140.

Huang, H., Cho, H., Schwab, K., Jacangelo, J.G., 2011. Effects of feedwater pretreatment on the removal of organic microconstituents by a low fouling reverse osmosis membrane. Desalination 281, 446–454.

Huang, H., Cho, H.H., Schwab, K.J., Jacangelo, J.G., 2012. Effects of magnetic ion exchange pretreatment on low pressure membrane filtration of natural surface water. Water Res. 46, 5483–5490.

Huber, S.A., Balz, A., Abert, M., Pronk, W., 2011. Characterisation of aquatic humic and non-humic matter with size-exclusion chromatography - organic carbon detection - organic nitrogen detection (LC-OCD-OND). Water Res. 45, 879–885.

Humbert, H., Gallard, H., Croué, J.P., 2012. A polishing hybrid AER/UF membrane process for the treatment of a high DOC content surface water. Water Res. 46, 1093–1100.

Humbert, H., Gallard, H., Jacquemet, V., Croué, J.P., 2007. Combination of coagulation and ion exchange for the reduction of UF fouling properties of a high DOC content surface water. Water Res. 41, 3803–3811.

Humbert, H., Gallard, H., Suty, H., Croué, J.P., 2005. Performance of selected anion exchange resins for the treatment of a high DOC content surface water. Water Res. 39, 1699–1708.

Humbert, H., Gallard, H., Suty, H., Croué, J.-P., 2008. Natural organic matter (NOM) and pesticides removal using a combination of ion exchange resin and powdered activated carbon (PAC). Water Res. 42, 1635–1643.

Hung, P.V.X., Cho, S.-H., Moon, S.-H., 2009. Prediction of boron transport through seawater reverse osmosis membranes using solution–diffusion model. Desalination 247, 33–44.

Hung, W.-S., De Guzman, M., Huang, S.-H., Lee, K.-R., Jean, Y.C., Lai, J.-Y., 2010. Characterizing free volumes and layer structures in asymmetric thin-film polymeric membranes in the wet condition using the variable monoenergy slow positron beam. Macromolecules 43, 6127–6134.

Indarawis, K.A., Boyer, T.H., 2013. Superposition of anion and cation exchange for removal of natural water ions. Sep. Purif. Technol. 118, 112–119.

IPCC, 2014. Climate Change 2014 Impacts, Adaptation, and Vulnerability, Part A: Global and Sectoral Aspects, Working Group II Contribution to the Fifth Assessment Report of the Intergovernmental Panel on Climate Change. Cambridge University Press.

Ixom Watercare, 2016. www.miexresin.com.

Jagur-Grodzinski, J., Kedem, O., 1966. Transport coefficients and salt rejection in unchanged hyperfiltration membranes. Desalination 1, 327–341.

Jarvis, P., Mergen, M., Banks, J., Mcintosh, B., Parsons, S.A., Jefferson, B., 2008. Pilot scale comparison of enhanced coagulation with magnetic resin plus coagulation systems. Environ. Sci. Technol. 42, 1276–1282.

Johnson, C.J., Singer, P.C., 2004. Impact of a magnetic ion exchange resin on ozone demand and bromate formation during drinking water treatment. Water Res. 38, 3738–3750.

Jonsson, G., 1983. Concentration profiles retention—flux curves for composite membranes in reverse osmosis. J. Memb. Sci. 14, 211–227.

Jung, C.W., Son, H.J., Kang, L.S., 2006. Effects of membrane material and pretreatment coagulation on membrane fouling: fouling mechanism and NOM removal. Desalination 197, 154–164.

Kabsch-korbutowicz, M., Biłyk, A., Mołczan, M., 2006. The Effect of Feed Water Pretreatment on Ultrafiltration Membrane Performance. Polish J. Environ. Stud. 15, 719–725.

Kabsch-Korbutowicz, M., Majewska-Nowak, K., Winnicki, T., 2008. Water treatment using MIEX®DOC/ultrafiltration process. Desalination 221, 338–344.

Kaewsuk, J., Seo, G.T., 2011. Verification of NOM removal in MIEX-NF system for advanced water treatment. Sep. Purif. Technol. 80, 11–19.

Kedem, O., Freger, V., 2008. Determination of concentration-dependent transport coefficients in nanofiltration: Defining an optimal set of coefficients. J. Memb. Sci. 310, 586–593.

Kedem, O., Katchalsky, A., 1958. Thermodynamic analysis of the permeability of biological membranes to non-electrolytes. Biochim. Biophys. Acta 27, 229 – 246.

Kesting, R.E., 1990. The Four Tiers of Structure in Integrally Skinned Phase Inversion Membranes and Their Relevance to the Various Separation Regimes. J. Appl. Polym. Sci. 41, 2739–2752.

Kim, H.C., Dempsey, B.A., 2010. Removal of organic acids from EfOM using anion exchange resins and consequent reduction of fouling in UF and MF. J. Memb. Sci. 364, 325–330.

Kim, H.C., Hong, J.H., Lee, S., 2006. Fouling of microfiltration membranes by natural organic matter after coagulation treatment: A comparison of different initial mixing conditions. J. Memb. Sci. 283, 266–272.

Kim, S.H., Kwak, S.-Y., Suzuki, T., 2005. Positron Annihilation Spectroscopic Evidence to Demonstrate the Flux-Enhancement Mechanism in Morphology-Controlled Thin-Film-Composite (TFC) Membrane. Environ. Sci. Technol. 39, 1764–1770.

Kingsbury, R.S., Singer, P.C., 2013. Effect of magnetic ion exchange and ozonation on disinfection by-product formation. Water Res. 47, 1060–1072.

Kitis, M., Kilduff, J.E., Karanfil, T., 2001. Isolation of Dissolved Organic Matter (Dom) From Surface Waters Using Reverse Osmosis and Its Impact on the

Reactivity of Dom To Formation and Speciation of Disinfection By-Products 35, 2225–2234.

Konieczny, K., Sąkol, D., Płonka, J., Rajca, M., Bodzek, M., 2009. Coagulation—ultrafiltration system for river water treatment. Desalination 240, 151–159.

Kooiman, I.J.W., Stuyfzand, P.J., Maas, C., Kappelhof, J.W.N.M., 2004. Pumping brackish groundwater to prepare drinking water and keep salinizing wells fresh: A feasibility study, in: 18th Salt Water Intrusion Meeting, Cartagena, Spain. pp. 625–635.

Koros, W.J., Fleming, G.K., Jordan, S.M., Kim, T.H., Hoehn, H.H., 1988. Polymeric membrane materials for solution-diffusion based permeation separations. Prog. Polym. Sci. 13, 339–401.

Korth, A., Fiebiger, C., Bornmann, K., Schmidt, W., 2004. NOM increase in drinking water reservoirs - Relevance for drinking water production. Water Sci. Technol. Water Supply 4, 55–60.

Kurama, H., 2002. The application of membrane filtration for the removal of ammonium ions from potable water. Water Res. 36, 2905–2909.

Lau, W.-J., Ismail, A.F., 2009. Polymeric nanofiltration membranes for textile dye wastewater treatment: Preparation, performance evaluation, transport modelling, and fouling control - a review. Desalination 245, 321–348.

Lee, S., Lee, C., 2007. Effect of membrane properties and pretreatment on flux and NOM rejection in surface water nanofiltration. Sep. Purif. Technol. 56, 1–8.

Leiknes, T., 2009. The effect of coupling coagulation and flocculation with membrane filtration in water treatment: A review. J. Environ. Sci. 21, 8–12.

Levenstein, R., Hasson, D., Semiat, R., 1996. Utilization of the Donnan effect for improving electrolyte separation with nanofiltration membranes. J. Memb. Sci. 116, 77–92.

Li, F., Yuasa, A., Ebie, K., Azuma, Y., 2003. Microcolumn test and model analysis of activated carbon adsorption of dissolved organic matter after precoagulation: Effects of pH and pore size distribution. J. Colloid Interface Sci. 262, 331–341.

Liberti, L., Passino, R., 1977. Chapter 3, in: Ion Exchange and Solvent Extraction. New York.

Liberti, L., Passino, R., Petruzzelli, D., 1983. Chloride-sulphate exchange on anion resins. Kinetic investigation, IX. Direct, isotopic and reverse exchange. Desalination 48, 55–66.

Liberti, L., Passino, R., Petruzzelli, D., 1982. Chloride/sulphate exchange on anion resins. Kinetic investigation, VIII. Influence of some physico-chemical properties of the resins. Desalination 41, 199–207.

Litter, M.I., Morgada, M.E., Bundschuh, J., 2010. Possible treatments for arsenic removal in Latin American waters for human consumption. Environ. Pollut. 158, 1105–1118.

Liu, Z., Yan, X., Drikas, M., Zhou, D., Wang, D., Yang, M., Qu, J., 2011. Removal of bentazone from micro-polluted water using MIEX resin: Kinetics, equilibrium, and mechanism. J. Environ. Sci. 23, 381–387.

Loeb, S., Sourirajan, S., 1964. High flow porous membranes for separating water from

saline solutions. 3133132.

Loi-Brügger, A., Panglisch, S., Buchta, P., Hattori, K., Yonekawa, H., Tomita, Y., Gimbel, R., 2006. Ceramic membranes for direct river water treatment applying coagulation and microfiltration. Water Sci. Technol. Water Supply 6, 89–98.

López-Roldán, R., Gonzalez, S., Pelayo, S., Piña, B., Platikanov, S., Tauler, R., De La Cal, A., Boleda, M.R., Cortina, J.L., 2013a. Integration of on-line and off-line methodologies for the assessment of river water quality. Water Sci. Technol. Water Supply 13, 1340–1347.

López-Roldán, R., Jubany, I., Martí, V., González, S., Cortina, J.L., 2013b. Ecological screening indicators of stress and risk for the Llobregat river water. J. Hazard. Mater. 263, 239–247.

López-Roldán, R., Platikanov, S., Martín-Alonso, J., Tauler, R., González, S., Luis Cortina, J., 2016. Integration of UltravioleteVisible spectral and physicochemical data in chemometrics analysis for improved discrimination of water sources and blends for application to the complex drinking water distribution network of Barcelona. J. Clean. Prod. 112, 4789–4798.

López-Roldán, R., Rubalcaba, A., Martin-Alonso, J., González, S., Martí, V., Cortina, J.L., 2015. Assessment of the water chemical quality improvement based on human health risk indexes: Application to a drinking water treatment plant incorporating membrane technologies. Sci. Total Environ. 540, 334–343.

Luo, J., Wan, Y., 2013. Effects of pH and salt on nanofiltration - a critical review. J. Memb. Sci. 438, 18–28.

Lv, L., Wang, Y., Wei, M., Cheng, J., 2008. Bromide ion removal from contaminated water by calcined and uncalcined MgAl-CO3 layered double hydroxides. J. Hazard. Mater. 152, 1130–1137.

Malek, A., Hawlader, M.N.A., Ho, J.C., 1994. A lumped transport parameter approach in predicting B10 RO permeator performance. Desalination 99, 19–38.

Marque, S., Jacqmin-Gadda, H., Dartigues, J.-F., Commenges, D., 2003. Cardiovascular mortality and calcium and magnesium in drinking water: an ecological study in elderly people. Eur. J. Epidemiol. 18, 305–9.

Martínez Beltrán, J., Koo-Oshima, S., 2006. Water desalination for agricultural applications. FAO L. water Discuss. Pap. 5, 48.

Matilainen, A., Vepsäläinen, M., Sillanpää, M., 2010. Natural organic matter removal by coagulation during drinking water treatment: A review. Adv. Colloid Interface Sci. 159, 189–197.

Meerganz von Medeazza, G., Moreau, V., 2007. Modelling of water-energy systems. The case of desalination. Energy 32, 1024–1031.

Mergen, M.R.D., Adams, B.J., Vero, G.M., Price, T.A., Parsons, S.A., Jefferson, B., Jarvis, P., 2009. Characterisation of natural organic matter (NOM) removed by magnetic ion exchange resin (MIEX resin). Water Sci. Technol. Water Supply 9, 199–205.

Mergen, M.R.D., Jefferson, B., Parsons, S.A., Jarvis, P., 2008. Magnetic ion-exchange resin treatment: Impact of water type and resin use. Water Res. 42, 1977–1988.

Mi, B., Coronell, O., Mariñas, B.J., Watanabe, F., Cahill, D.G., Petrov, I., 2006.

Physico-chemical characterization of NF/RO membrane active layers by Rutherford backscattering spectrometry. J. Memb. Sci. 282, 71–81.

Mohammad, A.W., Hilal, N., Al-Zoubi, H., Darwish, N.A., 2007. Prediction of permeate fluxes and rejections of highly concentrated salts in nanofiltration membranes. J. Memb. Sci. 289, 40–50.

Mohammad, A.W., Teow, Y.H., Ang, W.L., Chung, Y.T., Oatley-Radcliffe, D.L., Hilal, N., 2015. Nanofiltration membranes review: Recent advances and future prospects. Desalination 356, 226–254.

Morran, J.Y., Drikas, M., Cook, D., Bursill, D.B., 2004. Comparison of MIEX® treatment and coagulation on NOM character. Water Sci. Technol. Water Supply 4, 129–137.

Mouhoumed, E.I., Szymczyk, A., Schäfer, A., Paugam, L., La, Y.H., 2014. Physico-chemical characterization of polyamide NF/RO membranes: Insight from streaming current measurements. J. Memb. Sci. 461, 130–138.

Mulder, M.H.V., 1996. Basic Principles of Membrane Technology, Journal of Chemical Information and Modeling. Kluwer Academic Publishers, Dordrecht, The Netherlands.

Murray, B., 2009. MIEX jar testing method for potable water.

Nassar, N.N., 2010. Rapid removal and recovery of Pb(II) from wastewater by magnetic nanoadsorbents. J. Hazard. Mater. 184, 538–546.

Neale, P.A., Schäfer, A.I., 2009. Magnetic ion exchange: Is there potential for international development? Desalination 248, 160–168.

Nielsen, D.W., Jonsson, G., 1994. Bulk-phase criteria for negative ion rejection in nanofiltration of multicomponent salt solutions. Sep. Sci. Technol. 29, 1165–1182.

Oatley, D.L., Llenas, L., Pérez, R., Williams, P.M., Martínez-Lladó, X., Rovira, M., 2012. Review of the dielectric properties of nanofiltration membranes and verification of the single oriented layer approximation. Adv. Colloid Interface Sci. 173, 1–11.

Oatley-Radcliffe, D.L., Williams, S.R., Barrow, M.S., Williams, P.M., 2014. Critical appraisal of current nanofiltration modelling strategies for seawater desalination and further insights on dielectric exclusion. Desalination 343, 154–161.

Oh, H.-J., Hwang, T.-M., Lee, S., 2009. A simplified simulation model of RO systems for seawater desalination. Desalination 238, 128–139.

Oki, T., Kanae, S., 2006. Global hydrological cycles and world water resources. Science (80-.). 313, 1068–1072.

Olsthoorn, T.N., 2008. Brackish Groundwater as a New Resource for Drinking Water, Specific Consequences of Density Dependent Flow, and Positive Environmental Consequences, in: 20th Salt Water Intrusion Meeting, 23-28 June Naples, FL, USA. pp. 174–177.

Pabby, A.K., Rizvi, S.S.H., Sastre, A.M., 2008. Handbook of Membrane Separations: Chemical, Pharmaceutical, Food, and Biotechnological Applications. CRC Press, Florida.

Pacheco, F.A., Pinnau, I., Reinhard, M., Leckie, J.O., 2010. Characterization of

isolated polyamide thin films of RO and NF membranes using novel TEM techniques. J. Memb. Sci. 358, 51–59.

Pages, N., Yaroshchuk, A., Gibert, O., Cortina, J.L., 2013. Rejection of trace ionic solutes in nanofiltration: Influence of aqueous phase composition. Chem. Eng. Sci. 104, 1107–1115.

Paul, D.R., 2004. Reformulation of the solution-diffusion theory of reverse osmosis. J. Memb. Sci. 241, 371–386.

Peeters, J.M.M., Boom, J.P., Mulder, M.H. V, Strathmann, H., 1998. Retention measurements of nanofiltration membranes with electrolyte solutions. J. Memb. Sci. 145, 199–209.

Pendergast, M.M., Hoek, E.M.V., 2011. A review of water treatment membrane nanotechnologies. Energy Environ. Sci. 4, 1946.

Pendergast, M.T.M., Nygaard, J.M., Ghosh, A.K., Hoek, E.M. V, 2010. Using nanocomposite materials technology to understand and control reverse osmosis membrane compaction. Desalination 261, 255–263.

Pentair X-Flow, 2011. Ufc M5. Enschede, The Netherlands.

Pereira, S., Peinemann, K.-V., 2006. Membrane Technology in the Chemical Industry, 2nd ed. 2nd Edition. WILEY-VCH Verlag GmbH & Co. KGaA,Weinheim, Germany, Weinheim, Germany.

Pérez-González, A., Urtiaga, A.M., Ibáñez, R., Ortiz, I., 2012. State of the art and review on the treatment technologies of water reverse osmosis concentrates. Water Res. 46, 267–283.

Phetrak, A., Lohwacharin, J., Sakai, H., Murakami, M., Oguma, K., Takizawa, S., 2014. Simultaneous removal of dissolved organic matter and bromide from drinking water source by anion exchange resins for controlling disinfection by-products. J. Environ. Sci. (China) 26, 1294–1300.

Phetrak, A., Lohwacharin, J., Takizawa, S., 2016. Analysis of trihalomethane precursor removal from sub-tropical reservoir waters by a magnetic ion exchange resin using a combined method of chloride concentration variation and surrogate organic molecules. Sci. Total Environ. 539, 165–174.

Pontié, M., Dach, H., Leparc, J., Hafsi, M., Lhassani, A., 2008. Novel approach combining physico-chemical characterizations and mass transfer modelling of nanofiltration and low pressure reverse osmosis membranes for brackish water desalination intensification. Desalination 221, 174–191.

Post, V.E.A., 2004. Groundwater salinization processes in the coastal area of the Netherlands due to transgressions during the Holocene. Vrije Universiteit Amsterdam.

Puigdomènech, I., 2001. Chemical Equilibrium Software Hydra and Medusa.

Raich-Montiu, J., Barios, J., Garcia, V., Medina, M.E., Valero, F., Devesa, R., Cortina, J.L., 2014. Integrating membrane technologies and blending options in water production and distribution systems to improve organoleptic properties. The case of the Barcelona Metropolitan Area. J. Clean. Prod. 69, 250–259.

Ramon, G.Z., Wong, M.C.. Y., Hoek, E.M. V., 2012. Transport through composite membrane, Part 1: Is there an optimal support membrane? J. Memb. Sci. 415-

416, 298–305.

Reig, M., Casas, S., Aladjem, C., Valderrama, C., Gibert, O., Valero, F., Centeno, C.M., Larrotcha, E., Cortina, J.L., 2014. Concentration of NaCl from seawater reverse osmosis brines for the chlor-alkali industry by electrodialysis. Desalination.

Ribera, G., Llenas, L., Martínez, X., Rovira, M., de Pablo, J., 2013. Comparison of nanofiltration membranes' performance in flat sheet and spiral wound configurations: a scale-up study. Desalin. Water Treat. 51, 458–468.

Richards, L.A., Vuachère, M., Schäfer, A.I., 2010. Impact of pH on the removal of fluoride, nitrate and boron by nanofiltration/reverse osmosis. Desalination 261, 331–337.

Richardson, S.D., 2003. Disinfection by-products and other emerging contaminants in drinking water. TrAC - Trends Anal. Chem. 22, 666–684.

Rietveld, L.C., Norton-Brandao, D., Shang, R., Van Agtmaal, J., Van Lier, J.B., 2011. Possibilities for reuse of treated domestic wastewater in The Netherlands. Water Sci. Technol. 64, 1540–1546.

Robinson, R.A., Stokes, R.H., 2002. Electrolyte Solutions, Second Rev. ed, Dover Publications. Dover Publications, Mineola, NY.

Rokicki, C.A., Boyer, T.H., 2011. Bicarbonate-form anion exchange: Affinity, regeneration, and stoichiometry. Water Res. 45, 1329–1337.

Rouquerol, J., Avnir, D., Fairbridge, C., Everett, D., Haynes, J., Pernicone, N., Ramsay, J., Sing, K., Unger, K., 1994. Recommendations for the characterization of porous solids. IUPAC Handbook.

Sánchez-Polo, M., Rivera-Utrilla, J., Salhi, E., von Gunten, U., 2007. Ag-doped carbon aerogels for removing halide ions in water treatment. Water Res. 41, 1031–1037.

Sani, B., Basile, E., Rossi, L., Lubello, C., 2008. Effects of pre-treatment with magnetic ion exchange resins on coagulation/flocculation process. Water Sci. Technol. 57, 57–64.

Sasidhar, V., Ruckenstein, E., 1982. Anomalous effects during electrolyte osmosis across charged porous membranes. J. Colloid Interface Sci.

Schaep, J., Van der Bruggen, B., Vandecasteele, C., Wilms, D., 1998. Influence of ion size and charge in nanofiltration. Sep. Purif. Technol. 14, 155–162.

Schaep, J., Vandecasteele, C., 2001. Evaluating the charge of nanofiltration membranes. J. Memb. Sci. 188, 129–136.

Schäfer, A.I., Fane, A.., Waite, T.D., 1998. Nanofiltration of natural organic matter : Removal , fouling and the influence of multivalent ions. Desalination 118, 109–122.

Schäfer, A.I., Fane, A.G., Waite, T.D., 2005. Nanofiltration: Principles and Applications. Oxford.

Schlögl, R., Helfferich, F., 1952. Zur Theorie des Potentials von Austauscher-Membranen. Zeitschrift für Elektrochemie, Berichte der Bunsengesellschaft für Phys. Chemie 644–647.

Schmuckler, G., Golstein, S., 1977. Chapter 1, in: Ion Exchange and Solvent Extraction. New York.

Sharp, E.L., Parsons, S.A., Jefferson, B., 2006a. Seasonal variations in natural organic matter and its impact on coagulation in water treatment. Sci. Total Environ. 363, 183–194.

Sharp, E.L., Parsons, S.A., Jefferson, B., 2006b. The impact of seasonal variations in DOC arising from a moorland peat catchment on coagulation with iron and aluminium salts. Environ. Pollut. 140, 436–443.

Shiklomanov, I., 1993. Chapter 2: World fresh water resources, in: Gleick, P. (Ed.), Water in Crisis: A Guide to the World's Fresh Water. Oxford University Press.

Shorrock, K., Drage, B., 2006. A pilot plant evaluation of the magnetic ion exchange process for the removal of dissolved organic carbon at Draycote water treatment works. Water Environ. J. 20, 65–70.

Shrivastava, A., Kumar, S., Cussler, E., 2008. Predicting the effect of membrane spacers on mass transfer. J. Memb. Sci. 323, 247–256.

Shuang, C., Pan, F., Zhou, Q., Li, A., Li, P., Yang, W., 2012. Magnetic polyacrylic anion exchange resin: Preparation, characterization and adsorption behavior of humic acid. Ind. Eng. Chem. Res. 51, 4380–4387.

Singer, P.C., Bilyk, K., 2002. Enhanced coagulation using a magnetic ion exchange resin. Water Res. 36, 4009–4022.

Singer, P.C., Boyer, T., Holmquist, A., Morran, J., Bourke, M., 2009. Integrated analysis of NOM removal by magnetic ion exchange. J. / Am. Water Work. Assoc. 101, 65–73.

Singer, P.C., Schneider, M., Edwards-Brandt, J., Budd, G.C., 2007. MIEX for removal of DBP precursors: Pilot-plant findings. J. / Am. Water Work. Assoc. 99, 128–139.

Slunjski, M., Bourke, M., Leary, B.O., 2000. MIEX-DOC Process for Removal of Humics in Water Treatment, in: IHSS – Australian Chapter Seminar. pp. 1–6.

Smith, E., 2001. Pollutant concentrations of stormwater and captured sediment in flood control sumps draining an urban watershed. Water Res. 35, 3117–3126.

Smith, E., Kamal, Y., 2009. Optimizing treatment for reduction of disinfection by-product (DBP) formation. Water Sci. Technol. Water Supply 9, 191–198.

Son, H.J., Hwang, Y.D., Roh, J.S., Ji, K.W., Sin, P.S., Jung, C., Kang, L., 2005. Application of MIEX® pre-treatment for ultrafiltration membrane process for NOM removal and fouling reduction. Water Sci. Technol. Water Supply 5, 15–24.

Sotto, A., 2008. Aplicación de la tecnologia de membranas de Nanofiltración y ósmosis inversa para el tratamiento de disoluciones acuosas de compuestos fenólicos y ácidos carboxílicos. Universidad Rey Juan Carlos.

Sotto, A., Arsuaga, J.M., Van der Bruggen, B., 2013. Sorption of phenolic compounds on NF/RO membrane surfaces: Influence on membrane performance. Desalination 309, 64–73.

Spiegler, K.S., Kedem, O., 1966. Thermodynamics of hyperfiltration (reverse osmosis): criteria for efficient membranes. Desalination 1, 311–326.

Stawikowska, J., Livingston, A.G., 2012. Nanoprobe imaging molecular scale pores in polymeric membranes. J. Memb. Sci. 413-414, 1–16.

Stoquart, C., Servais, P., Bérubé, P.R., Barbeau, B., 2012. Hybrid Membrane Processes using activated carbon treatment for drinking water: A review. J. Memb. Sci. 411-412, 1–12.

Stuyfzand, P.J., Raat, K.J., 2010. Benefits and hurdles of using brackish groundwater as a drinking water source in the Netherlands. Hydrogeol. J. 18, 117–130.

Stylianou, S.K., Szymanska, K., Katsoyiannis, I.A., Zouboulis, A.I., Stylianou, S.K., Szymanska, K., Katsoyiannis, I.A., Zouboulis, A.I., 2015. Novel Water Treatment Processes Based on Hybrid Membrane-Ozonation Systems: A Novel Ceramic Membrane Contactor for Bubbleless Ozonation of Emerging Micropollutants. J. Chem. 2015, 1–12.

Swietlik, J., Dabrowska, A., Raczyk-Stanisławiak, U., Nawrocki, J., 2004. Reactivity of natural organic matter fractions with chlorine dioxide and ozone. Water Res. 38, 547–58.

Szymczyk, a, Fatinrouge, N., Fievet, P., Ramseyer, C., Vidonne, A., 2007. Identification of dielectric effects in nanofiltration of metallic salts. J. Memb. Sci. 287, 102–110.

Szymczyk, A., Fievet, P., 2005. Investigating transport properties of nanofiltration membranes by means of a steric, electric and dielectric exclusion model. J. Memb. Sci. 252, 77–88.

Tang, C.Y., Chong, T.H., Fane, A.G., 2011. Colloidal interactions and fouling of NF and RO membranes: a review. Adv. Colloid Interface Sci. 164, 126–143.

Tang, Y., Li, S., Zhang, Y., Yu, S., Martikka, M., 2014. Sorption of tetrabromobisphenol A from solution onto MIEX resin: Batch and column test. J. Taiwan Inst. Chem. Eng. 45, 2411–2417.

Tang, Y., Liang, S., Guo, H., You, H., Gao, N., Yu, S., 2013. Adsorptive characteristics of perchlorate from aqueous solutions by MIEX resin. Colloids Surfaces A Physicochem. Eng. Asp. 417, 26–31.

Tian, J.Y., Liang, H., Li, X., You, S.J., Tian, S., Li, G.B., 2008. Membrane coagulation bioreactor (MCBR) for drinking water treatment. Water Res. 42, 3910–3920.

Tran, T., Gray, S., Naughton, R., Bolto, B., 2006. Polysilicato-iron for improved NOM removal and membrane performance. J. Memb. Sci. 280, 560–571.

Tsuru, T., Nakao, S., Kimura, S., 1991. Calculation of ion rejection by extended Nernst-Planck equation with charged reverse osmosis membranes for single and mixed electrolyte solutions. J. Chem. Eng. Japan 24, 511–517.

Tung, K.-L., Jean, Y.-C., Nanda, D., Lee, K.-R., Hung, W.-S., Lo, C.-H., Lai, J.-Y., 2009. Characterization of fouled nanofiltration membranes using positron annihilation spectroscopy. J. Memb. Sci. 343, 147–156.

Umpuch, C., Galier, S., Kanchanatawee, S., Roux-De Balmann, H., 2010. Nanofiltration as a purification step in production process of organic acids: Selectivity improvement by addition of an inorganic salt. Process Biochem. 45, 1763–1768.

USEPA, 2006. , (US Environmental Protection Agency) Stage 2 Disinfectants and Disinfection Byproducts Rule, 40 CFR, Parts 9, 141 and 142, Fed. Reg. 71.

Valero, F., Arbós, R., 2010. Desalination of brackish river water using Electrodialysis Reversal (EDR). Control of the THMs formation in the Barcelona (NE Spain) area. Desalination 253, 170–174.

Van der Bruggen, B., 2009. Chemical Modification of Polyethersulfone Nanofiltration Membranes: A Review. J. Appl. Polym. Sci. 114, 630–642.

Van Der Bruggen, B., Everaert, K., Wilms, D., Vandecasteele, C., 2001. Application of nanofiltration for removal of pesticides, nitrate and hardness from ground water: Rejection properties and economic evaluation. J. Memb. Sci. 193, 239–248.

Van der Bruggen, B., Kim, J., 2012. Nanofiltration of aqueous solutions: Recent developments and progresses, in: Advanced Materials for Membrane Preparation. pp. 228 – 247.

Van Der Bruggen, B., Koninckx, A., Vandecasteele, C., 2004. Separation of monovalent and divalent ions from aqueous solution by electrodialysis and nanofiltration. Water Res. 38, 1347–1353.

Van der Bruggen, B., Mänttäri, M., Nyström, M., 2008. Drawbacks of applying nanofiltration and how to avoid them: A review. Sep. Purif. Technol. 63, 251–263.

Vázquez-Suñé, E., Abarca, E., Carrera, J., Capino, B., Gámez, D., Pool, M., Simó, T., Batlle, F., Niñerola, J.M., Ibáñez, X., 2006. Groundwater modelling as a tool for the European Water Framework Directive (WFD) application: The Llobregat case. Phys. Chem. Earth 31, 1015–1029.

Vonk, M.W., Smit, J.A.M., 1984. Application of generalized Nernst-Planck equations to the description of ion retention in the hyperfiltration of mixed electrolyte solutions through a neutral membrane. Berichte der Bunsengesellschaft/Physical Chem. Chem. Phys. 88, 724–732.

Vonk, M.W., Smit, J.A.M., 1983. Positive and negative ion retention curves of mixed electrolytes in reverse osmosis with a cellulose acetate membrane. An analysis on the basis of the generalized Nernst-Planck equation. J. Colloid Interface Sci. 96, 121–134.

Voutchkov, N., 2011. Overview of seawater concentrate disposal alternatives. Desalination 273, 205–219.

Walha, K., Amar, R. Ben, Firdaous, L., Quéméneur, F., Jaouen, P., 2007. Brackish groundwater treatment by nanofiltration, reverse osmosis and electrodialysis in Tunisia: performance and cost comparison. Desalination 207, 95–106.

Walker, K.M., Boyer, T.H., 2011. Long-term performance of bicarbonate-form anion exchange: Removal of dissolved organic matter and bromide from the St. Johns River, FL, USA. Water Res. 45, 2875–2886.

Wang, J., Dlamini, D.S., Mishra, A.K., Pendergast, M.T.M., Wong, M.C.Y., Mamba, B.B., Freger, V., Verliefde, A.R.D., Hoek, E.M. V, 2014. A critical review of transport through osmotic membranes. J. Memb. Sci. 454, 516–537.

Wang, Q., Li, A., Wang, J., Shuang, C., 2012. Selection of magnetic anion exchange resins for the removal of dissolved organic and inorganic matters. J. Environ.

Sci. (China) 24, 1891–1899.

Wang, X.L., Fang, Y.Y., Tu, C.H., Van der Bruggen, B., 2012. Modelling of the separation performance and electrokinetic properties of nanofiltration membranes. Int. Rev. Phys. Chem. 31, 111–130.

Wang, X.-L., Tsuru, T., Nakao, S., Kimura, S., 1995. Electrolyte transport through nanofiltration membranes by the space-charge model and the comparison with Teorell-Meyer-Sievers model. J. Memb. Sci. 103, 117–133.

Watson, K., Farré, M.J., Knight, N., 2015. Enhanced coagulation with powdered activated carbon or MIEX secondary treatment: A comparison of disinfection by-product formation and precursor removal. Water Res. 68, 454–466.

Weber, W.J.T.C., Van Vliet, B.M., 1981. Synthetic adsorbents and activated carbons for water treatment: Overview and experimental comparisons. J. / Am. Water Work. Assoc. 73, 420–426.

WHO, 2008. Guidelines for Drinking-water Quality. World Heal. Organ. 1, 1–668.

Wijmans, J.G., 2004. The role of permeant molar volume in the solution-diffusion model transport equations. J. Memb. Sci. 237, 39–50.

Wijmans, J.G., Baker, R.W., 1995. The solution-diffusion model: a review. J. Memb. Sci. 107, 1–21.

Willison, H., Boyer, T.H., 2012. Secondary effects of anion exchange on chloride, sulfate, and lead release: Systems approach to corrosion control. Water Res. 46, 2385–2394.

Wolthek, N., Raat, K., de Ruijter, J.A., Kemperman, A., Oosterhof, A., 2013. Desalination of brackish groundwater and concentrate disposal by deep well injection. Desalin. Water Treat. 51, 1131–1136.

Worrall, F., Burt, T.P., 2009. Changes in DOC treatability: Indications of compositional changes in DOC trends. J. Hydrol. 366, 1–8.

Worrall, F., Burt, T.P., 2007. Trends in DOC concentration in Great Britain. J. Hydrol. 346, 81–92.

Xiangli, Q., Zhenjia, Z., Nongcun, W., Wee, V., Low, M., Loh, C.S., Hing, N.T., 2008. Coagulation pretreatment for a large-scale ultrafiltration process treating water from the Taihu River. Desalination 230, 305–313.

Yaroshchuk, A., Bruening, M.L., Licón Bernal, E.E., 2013. Solution-Diffusion-Electro-Migration model and its uses for analysis of nanofiltration, pressure-retarded osmosis and forward osmosis in multi-ionic solutions. J. Memb. Sci. 447, 463–476.

Yaroshchuk, A., Martínez-Lladó, X., Llenas, L., Rovira, M., de Pablo, J., 2011. Solution-diffusion-film model for the description of pressure-driven trans-membrane transfer of electrolyte mixtures: One dominant salt and trace ions. J. Memb. Sci. 368, 192–201.

Yaroshchuk, A., Martínez-Lladó, X., Llenas, L., Rovira, M., de Pablo, J., Flores, J., Rubio, P., 2009. Mechanisms of transfer of ionic solutes through composite polymer nano-filtration membranes in view of their high sulfate/chloride selectivities. Desalin. Water Treat. 6, 48–53. doi:10.5004/dwt.2009.642

Yaroshchuk, A.E., 2008. Negative rejection of ions in pressure-driven membrane

processes. Adv. Colloid Interface Sci. 139, 150–173.

Yaroshchuk, A.E., 2002. Rejection of single salts versus transmembrane volume flow in RO/NF: Thermodynamic properties, model of constant coefficients, and its modification. J. Memb. Sci. 198, 285–297.

Yaroshchuk, A.E., 2000. Dielectric exclusion of ions from membranes. Adv. Colloid Interface Sci. 85, 193–230.

Yaroshchuk, A.E., 1998. Rejection mechanisms of NF membranes. Membr. Technol. 9–12.

Yaroshchuk, A.E., Ribitsch, V., 2002. The use of trace ions for advanced characterisation of transport properties of NF membranes in electrolyte solutions: Theoretical analysis. J. Memb. Sci. 201, 85–94.

Yermiyahu, U., Tal, A., Ben-Gal, A., Bar-Tal, A., Tarchitzky, J., Lahav, O., 2007. Rethinking Desalinated Water Quality and Agriculture. Science (80-.). 318, 920–921.

Yoon, Y., Lueptow, R., 2005. Removal of organic contaminants by RO and NF membranes. J. Memb. Sci. 261, 76–86.

Zagorodni, A.A., 2007. Ion Exchange Materials: Properties and Applications. Elsevier Science.

Zhang, X., Lu, X., Li, S., Zhong, M., Shi, X., Luo, G., Ding, L., 2014. Investigation of 2,4-dichlorophenoxyacetic acid adsorption onto MIEX resin: Optimization using response surface methodology. J. Taiwan Inst. Chem. Eng. 45, 1835–1841.

Zhou, Y., Shuang, C., Zhou, Q., Zhang, M., Li, P., Li, A., 2012. Preparation and application of a novel magnetic anion exchange resin for selective nitrate removal. Chinese Chem. Lett. 23, 813–816.

Zhu, H., Szymczyk, A., Balannec, B., 2011. On the salt rejection properties of nanofiltration polyamide membranes formed by interfacial polymerization. J. Memb. Sci. 379, 215–223.

Zhu, Y., Gao, N., Wang, Q., Wei, X., 2015. Adsorption of perchlorate from aqueous solutions by anion exchange resins: Effects of resin properties and solution chemistry. Colloids Surfaces A Physicochem. Eng. Asp. 468, 114–121.

Zularisam, A.W., Ismail, A.F., Salim, M.R., Sakinah, M., Matsuura, T., 2009. Application of coagulation-ultrafiltration hybrid process for drinking water treatment: Optimization of operating conditions using experimental design. Sep. Purif. Technol. 65, 193–210.

Zularisam, A.W., Ismail, A.F., Salim, R., 2006. Behaviours of natural organic matter in membrane filtration for surface water treatment - a review. Desalination 194, 211–231.

1
2